The Dissertation Committee for Joon Hee Cho Certifies that this is the approved version of the following dissertation:

Bioinspired Catecholic Polymers for Functional Materials Design

Committee:

Christopher J. Ellison, Supervisor

Carlton Grant Willson

Benny D. Freeman

Wei Li

Joseph H. Koo

Bioinspired Catecholic Polymers for Functional Materials Design

by

Joon Hee Cho, B.E. ; M.E.

Dissertation

Presented to the Faculty of the Graduate School of

The University of Texas at Austin

in Partial Fulfillment

of the Requirements

for the Degree of

Doctor of Philosophy

The University of Texas at Austin

August, 2015

Dedication

Dedicated to Binna and my parents.

Acknowledgements

I would like to give special thanks to Professor Christopher J. Ellison for his great support and invaluable guidance during my doctoral course. I would also like to thank and give my best wishes to the talented members of the Ellison group and the many graduate students that I have worked with over the last five years. Special appreciation goes as well to the people at Austin Korean Presbyterian Church. They have always been there as my friends and even as my family as I have gone through the ups and downs of my research and life in the U.S. I also wish to express my special gratitude to Dr. Ki-Soo Lee for his unwavering personal support. Now, I am grateful for this chance to go back to home sweet home where my wife, parents, and family are living. I could not have done this without them.

Bioinspired Catecholic Polymers for Functional Materials Design

Joon Hee Cho, Ph.D.

The University of Texas at Austin, 2015

Supervisor: Christopher J. Ellison

Melanins and Polydopamine (PDA) are bioinspired catecholic polymers that are well known for their intriguing chemical structure and physiological functions. Indeed, PDA has a suite of properties that are uncommon to many known organic materials and over the last decade researchers have endeavored to exploit those properties in technologically relevant materials. Those efforts notwithstanding, PDAs' chemical structures have yet to be revealed in their entirety and their useful properties yet to be fully explored. In addition, given the natural presence of melanins and dopamine in many animals (including humans), along with their versatile functional features, these materials can serve as non-toxic additives to common polymers and thereby enhance their properties. Or they could, on their own, serve as eco-friendly functional organic films to be used in a variety of useful applications.

To this end, we suggest first the potential of melanins as thermal stabilizers for common polymers by evaluating the addition of melanin to several model polymers with well-known degradation pathways. Small loadings of natural and synthetic melanins significantly alter the radical-initiated chain scission behavior of conventional polymers. Such loadings cause a dramatic increase in its onset decomposition temperature, indicating potential benefits for high temperature processing or increasing their upper use temperature

in demanding applications. Second, we suggest thin films of synthetic melanin and poly(allylamine hydrochloride) be deposited layer-by-layer from dilute aqueous solutions in ambient conditions. The multilayer films show superior UV-protection performance and substantially extend the useful life of a conductive polymer film under UV light, demonstrating the utility of melanin films in high-tech applications. Third, we establish a synthetic approach to prepare block copolymers of poly(methyl methacrylate) (PMMA) and PDA using a modified atom transfer radical polymerization (ATRP) technique. These copolymers display very good solubility in a range of organic solvents and the spin cast thin films of the copolymers show a sharp reduction (by up to 50%) in protein adsorption compared to those of neat PMMA. The enhanced solvent processability, thermal stability, and low protein adsorption characteristics of this copolymer make it an attractive choice for antifouling coatings on large surfaces. Fourth, we exploit PDA to achieve block copolymer (BCP) lithography on a variety of soft-material surfaces. This biomimetic film serves as a reactive platform for subsequently grafting a surface neutral layer to chemically guide the perpendicular orientation of BCP lamellae. BCP nanopatterning may now be achieved over a large area on cheap, rough, and commercially available roll-to-roll flexible polymer substrates having a wide range of surface energies, surfaces that are of interest to be adapted for patterning. Fifth, we develop an efficient, environmentally friendly, and water-based flame-retardant surface nanocoating for highly flammable foamed materials such as flexible polyurethane (PU) foams. Upon exposure to flame, a PDA coating remains intact on the surface, completely stopping the melting and interrupting foam collapse. In addition, given the reported radical-scavenging capability of catechols, the PDA layer is hypothesized to remove flammable radicals which further retards flame spread during a fire. From cone calorimeter data, peak heat release rate of PDA-coated foams shows a sharp reduction, of up to 67%, relative to a control foam. This represents much better

performance than many conventional additives for flexible PU foams that have been reported in the literature. We additionally investigated the effect of catechol functionality on the flammability of PU foams through the comparison of cone calorimetric analysis between PDA-coated flexible PU foams with pristine catechol functionality and LD-containing rigid PU foams with mostly depleted catechols. This new knowledge will be potentially useful in the design of flame-resistant foams and surface coatings.

Table of Contents

List of Tables

List of Figures

List of Schemes

Chapter 1: Bioinspired Catecholic Polymers

1.1 Introduction - Bioinspired Catecholic Chemistry and Its Applications

Catechols, which occur ubiquitously in nature, are benzene derivatives with two neighboring (*ortho*-) hydroxyl groups.[1-2] In industrial settings, mass production of catechols and a variety of catecholic compounds have been derived from petroleum through traditional chemical processes.[3-4] Synthetic catechols are reactive small molecules widely used as starting materials for insecticides, perfumes, drugs, and stabilizing additives.[5] In organic chemistry, scientists have for decades been interested in catechols and their derivatives. Indeed, catechols can act as antioxidant agents, as chelating agents in coordination chemistry, or can trap radicals.[1] For instance, 4-*tert*-pyrobutylcatechol is a small-molecule organic compound employed largely as a polymerization inhibitor.[1] Unfortunately, if released to the environment, it is very toxic to aquatic life and can have long-lasting effects.[4] Despite the diverse industrial uses of petroleum-based catechol derivatives, many of them are known to be toxic to human health and the environment.[6]

Yet nature has engineered nontoxic and useful catecholic derivatives. Researchers have of course tried to mimic their chemistries.[1-2, 7-8] The catechol group is a typical structural feature in natural melanins, derived from the oxidative polymerization of 5, 6-dihydroxyindole (DHI) and 5, 6-dihydroxyindole-2-carboxylic acid (DHICA).[9-10] Besides its natural presence in many animals (including humans), melanin is also commonly consumed by humans in soups, sauces, and pastas and is widely available in large quantities from abundant natural sources such as cuttlefish (*Sepia officinalis*),[11-12] chicken feathers,[13-14] bacteria,[15] and so forth. In addition, recent reports[16] on mussel adhesive proteins postulate a significant role of another catechol, L-3-(3,4-dihydroxyphenyl)-alanine (L-

dopa). This is a substance present in significant quantities in the feet of *Mytilus edulis*, accounting for the ability of mussels to strongly tether to various surfaces.

This discovery has stimulated great interest in using other catechol molecules like dopamine in surface immobilization schemes and antifouling.[17] Dopamine has been identified as a simple structural mimic of the mussel's foot protein,[16] and is the most widely distributed catecholic compound, commonly as a hormone and neurotransmitter.[8] Inspired by natural melanins and mussel adhesive proteins, scientists have devised synthetic pathways to make biopolymers[18] from different precursors like L-dopa, dopamine, and others (**Scheme 1.1**). These bioinspired catecholic polymers have been proven to be biocompatible and extensively exploited in various biomedical studies such as biosensing, imaging, drug delivery, diagnosis, and others.[19-21] In addition, melanins constitute a fascinating class of biopolymers, which are found in the hair, skin, inner ear, eye and brain of living animals[9] and have been attributed to several different functions in the human body that includes photoprotection, photosensitization, metal-ion chelation, thermoregulation, antimicrobial and free-radical quenching.[18] Interestingly, they have also been found to conduct electricity and switch between low- and high-conductivity states.[22]

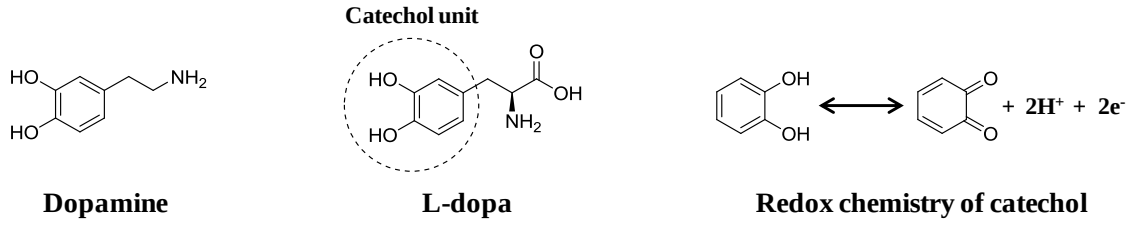

Scheme 1.1: Chemical formula of dopamine and L-dopa and the redox chemistry of catechol.

1.2 PROPERTIES OF MELANIN AND POLYDOPAMINE

1.2.1 CHEMICAL STRUCTURES

Melanins have a suite of properties that are uncommon to many known organic materials. Efforts to exploit those properties in technologically relevant materials have been few compared to other biopolymers such as cellulose, chitin or collagen. Among the different types of melanins, the most widely studied forms are eumelanins and pheomelanins. Both of these pigments are derived from the common precursor dopaquinone formed via the oxidation of L-tyrosine by tyrosinase.[23] Eumelanins are brown and black pigments derived from oxidative polymerization of DHI and DHICA, while pheomelanins are red and yellow pigments derived from cysteinyl dopa units (**Scheme 1.2**).[24-25]

All these reaction traits in **Scheme 1.2** are shared by melanins and polydopamines (PDAs) where coupling reactions among cyclized intermediates result in covalent bonding among monomers. This synthetic route has been used to suggest structural models based on the covalent linkage of subunits (**Scheme 1.3a**).[26-27] Alternative models have also been suggested based on the involvement of hydrogen bonding and π-stacking rather than C-C linkages (**Scheme 1.3b)**. Several analytical methods like solid state nuclear magnetic resonance (NMR), Fourier transform infrared (FTIR) spectroscopy, UV-Vis spectroscopy, electron paramagnetic resonance (EPR) spectroscopy, powder X-ray diffraction, and a variety of the other techniques were used to support this model. Moreover, it has been proposed that PDAs are composed of mixtures of covalently linked indoles and physically bound trimers wherein two dopamines and one dihydroxyindole are coupled to each other by π- π interaction and hydrogen bonding (**Scheme 1.3c**).[28] New models and experimental evidence regarding the chemical structure of PDA and melanins are still emerging and have conflicted with others previously proposed.[29] Even given our knowledge of melanin's basic

subunits, their comprehensive organization remains unclear. It has been a subject of debate whether melanin and PDAs are crosslinked polymers or supramolecular aggregates.

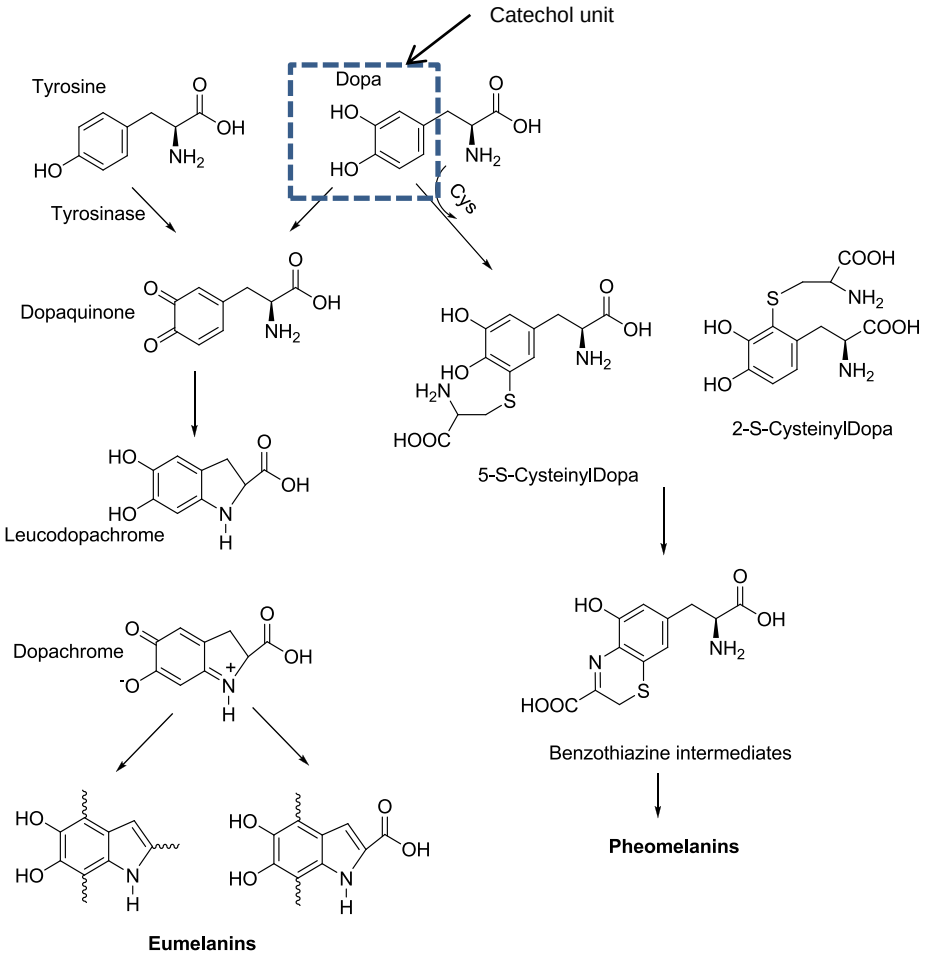

Scheme 1.2: Bio-synthetic pathways to eumelanins and pheomelanins. Reprinted with permission from Shanmuganathan, K. et al., Macromolecules 2011, 12, 625. Copyright 2011 American Chemical Society.

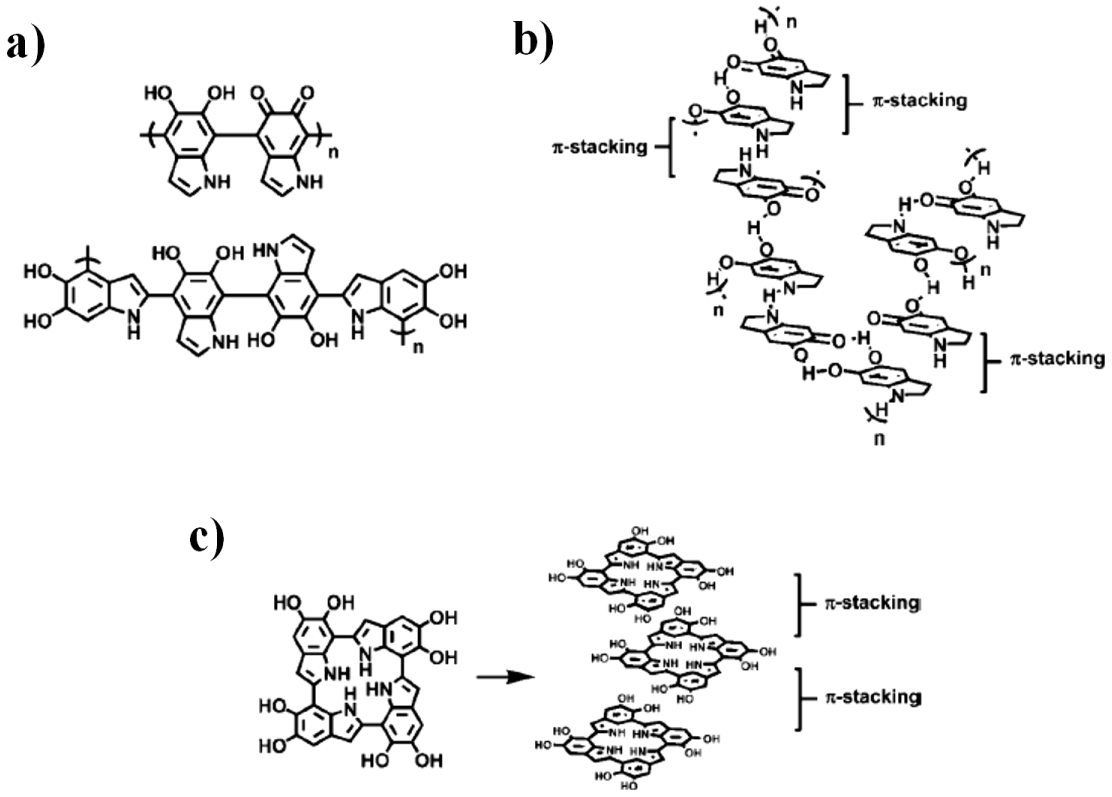

Scheme 1.3: Proposed chemical structures of polydopamine (PDA). a) Model based on covalent bonding between monomers, b) predominantly supramolecular bonding interactions, and c) a mixture of supramolecular and covalent bonding interactions. Reprinted with permission from Dreyer, D. R. et al., Chem. Sci. 2013, 4, 3796. Copyright 2013 American Chemical Society.

1.2.2 RADICAL SCAVENGING CAPABILITY

A key structural unit contributing to many different functions of melanins is assumed to be the catecholic unit. This unit's contribution has recently attracted significant amounts of attention in melanins and other analogues.[8] There is increasing evidence suggesting that cellular melanin functions similarly to an antioxidant in the body by (1) inhibiting free radicals, (2) deactivating electronically excited oxidizing species, (3) sequestering redox active metal ions such as iron and copper, and (4) scavenging intermediate radicals such as peroxyl and alkoxyl.[30] For example, researchers have studied

the interaction of synthetic melanins with specifically generated oxidizing and reducing free radicals. They have reported that synthetic melanins are powerful scavengers of carbon-centered radicals.[24, 31] Recently, Ju et al. polymerized melanin-like nanoparticles from dopamine hydrochloride and then demonstrated, using EPR spectroscopy, the nanoparticles' strong radical scavenging activity.[32] In addition, we reported that melanins displayed a significant thermal and thermooxidative stabilization effect in commercial polymers[33] and PDA also substantially delayed the peak decomposition of PMMA in copolymer architectures.[34]

1.2.3 Optical Behavior of Melanins and PDA

Melanin is responsible for the coloring of human eyes, skin, and hair, but it also protects us from harmful ultraviolet radiation and oxidative stress. Researchers would like to take advantage of these properties in engineered materials by using melanin as protective coatings for polymers and electronics, but natural melanin is tough to work with due to its poor solubility in common processing solvents. Researchers have developed synthetic melanin that mimics the behavior of the natural version and readily dissolves in basic aqueous solutions and organic solvents such as N,N-dimethylformamide (DMF) and dimethylsulfoxide (DMSO). It has been noted that natural and synthetic melanins have monotonic and broad band absorbance in the ultraviolet and visible range (**Figure 1.1**). In contrast to most organic materials, no distinct chromophoric bands are seen on the UV-Vis profile of melanins while the UV-Vis absorbance trace is not featureless and fits a single exponential form.[35] The photoabsorbance profile dramatically increases in the UV region, indicating a very useful property for human UV protection. Melanins are particularly known for their photoprotective functions in the body, largely absorbing ultraviolet and

visible light and dissipating it as heat.[33] However, our understanding of the molecular mechanism behind melanin dissipating the absorbed radiation is still unclear.

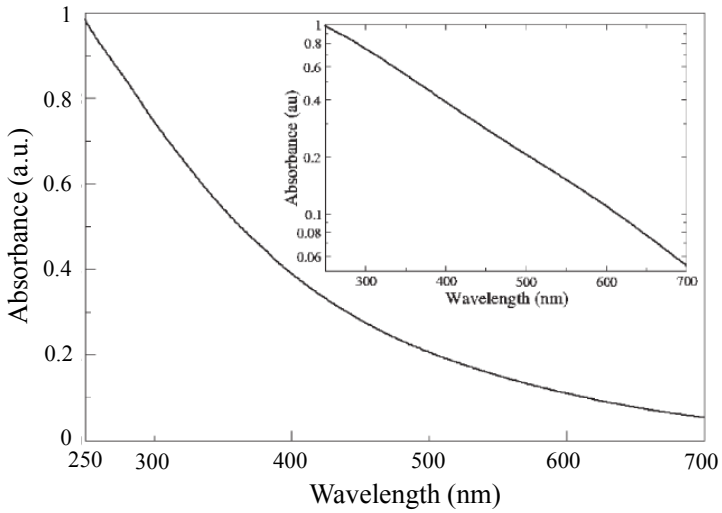

Figure 1.1: Photoabsorbance as a function of wavelength of a synthetic melanin aqueous solution (0.0025 wt%). The same data is shown on a log–linear plot in the inset demonstrating the excellent fit of the raw data to an exponential form. Reprinted with permission from Meredith, P. et al., Soft Matter 2006, 2, 37. Copyright 2006 Royal Society of Chemistry.

PDA nanoparticles were synthesized by oxidative polymerization of dopamine in alkaline aqueous solution and photoabsorbance was directly measured from the solution.[32] The PDA aqueous solution showed the same monotonic, broad band UV-Vis absorption spectrum over a wavelength range from 200 to 800 nm as natural and synthetic melanins. This suggests that it possessed a similar photoprotection function to that of natural melanin in human skin.

1.2.4 MUSSEL-INSPIRED SURFACE MODIFICATION

Scientists found another useful biomolecule from mussels, which shows strong attachment to virtually all types of organic and inorganic surfaces. Catechol and amine

groups are thought to be crucial for this adhesion function, although as of yet the adhesion mechanism is not fully understood (**Figure 1.2a**).[16] Scientists identified dopamine that contains both functionalities (**Figure 1.2b**). This simple structural mimic of the mussel protein is a building block for surface coatings with strong adhesion to virtually any bulk material surface. Simple immersion of substrates in a polymerizing dopamine solution results in spontaneous deposition, which imparts hydrophilicity of the surface and functionality for secondary reactions (**Figure 1.2c**).[16] The picture on the right of **Figure 1.2c** compares two cherry tomatoes. The tomato on the left is a raw cherry tomato with a fairly low energy surface. Water droplets are dewetted from its surface. The tomato on the right is a PDA-treated cherry tomato and its surface energy has been greatly enhanced, such that the water droplets are stuck stably at the nonplanar geometry.[36]

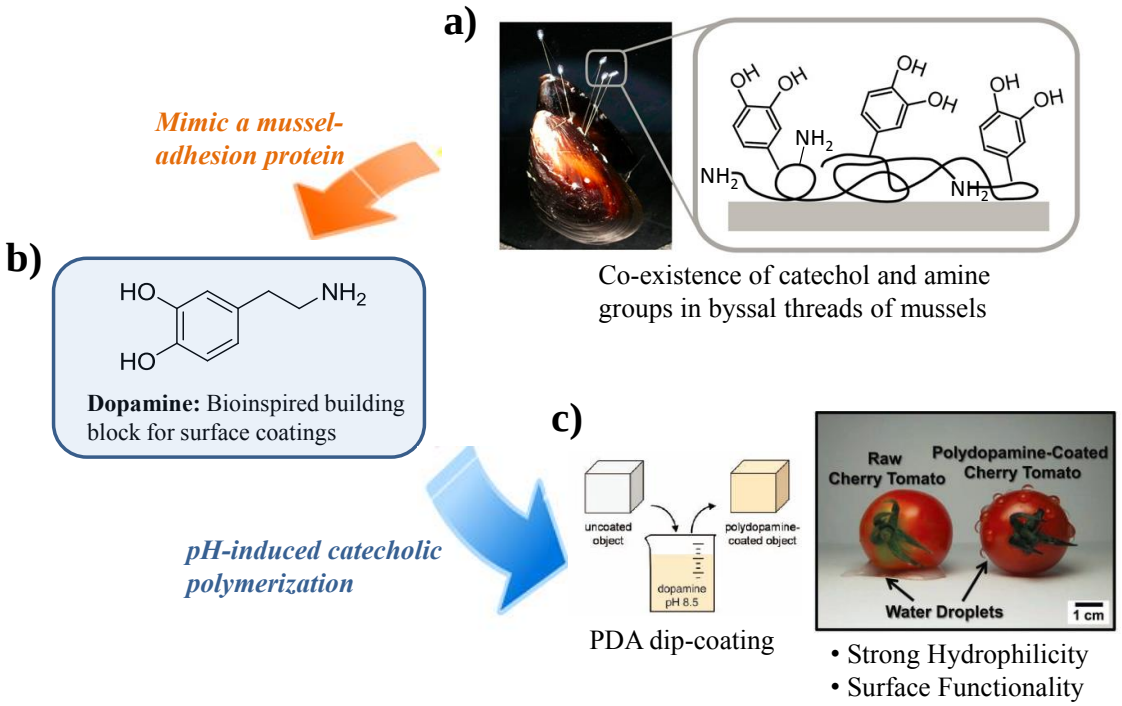

Figure 1.2: a) Chemistry of universal attachment of mussels. Reprinted with permission from Ku, S. H. et al., Biomaterials 2006, 2, 37. Copyright 2006 Elsevier. b) Chemical structure of dopamine contains both amine and catechol. c) Illustration of dopamine dip-coating process and a picture of comparison between raw cherry tomato and PDA-treated one. Reprinted with permission from Lee, H. et al., Science 2007, 318, 426. Copyright 2007 The American Association for the Advancement of Science. Reprinted with permission from Kim, B. H. et al., Adv. Mater. 2011, 23, 5618. Copyright 2011 John Wiley and Sons.

This mussel-inspired coating approach has been demonstrated with almost all kinds of inorganic and organic surfaces, regardless of chemical compositions and the geometry of substrates. The treatment provides the surface reaction sites for the formation of a secondary ad-layer.[16] Under mild basic conditions along with mild heating, catechols undergo oxidation and transform into a quinone form.[37] The oxidized quinone form of a catechol can react with various functional groups like thiol, amine, and even quinone itself via Michael addition (**Scheme 1.4a**) or Schiff base (**Scheme 1.4b**) reactions for grafting functional layers.[38] In addition, the hydroxyl groups of catechols can be coupled with other

hydroxyl groups or epoxide groups under mild heating in organic solvents.[36, 39] This versatile grafting chemistry associated with catechols has been extensively exploited to impart useful surface properties to a variety of substrates. Such chemistry has also been used in a wide spectrum of areas including anti-biofouling,[16] energy storage devices,[40] biomedical engineering,[41-44] nanopatterning,[36] membrane technology,[45-46] oil/water separation,[47] and so on.

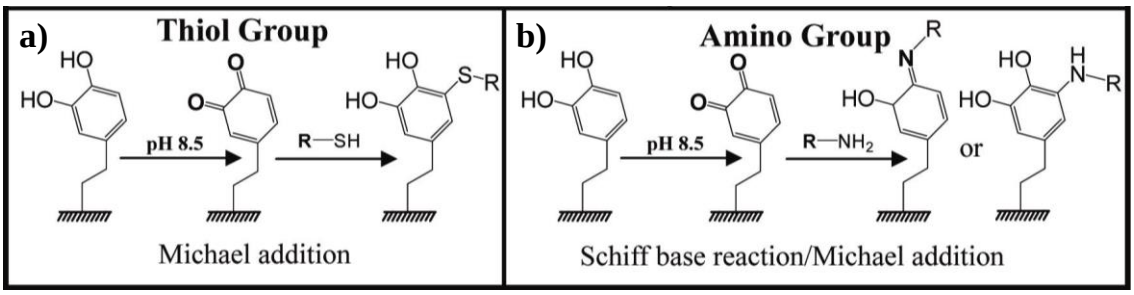

Scheme 1.4: Catechol oxidative chemistry for attachment of a) thiol and b) amine functionalized molecules to dopamine coatings. Reprinted with permission from Xu, L. Q. et al., Macromolecules 2010, 43, 8336. Copyright 2010 American Chemical Society.

PDA coatings support subsequent coupling reactions with many organic species to generate functional organic ad-layers. Messersmith and co-workers prepared fouling-resistant surfaces by covalently grafting amine- or thiol-terminated methoxy-poly(ethylene glycol) (mPEG) onto the PDA-coated substrates.[16] Specifically, an mPEG-modified substrate revealed a sharp reduction in protein adsorption as well as in fibroblast cell attachment relative to an uncoated control sample. Similar grafting chemistry has been applied onto membranes where the creation of polyethylene glycol (PEG) ad-layer on the membrane surface endowed significant fouling resistance and high water flux.[46] Zhang et al. recently developed water repellent magnetic naoparticles which should be useful in oil/water separation. PDA coatings were used to functionalize nanoparticles to

subsequently graft Ag and fluorine such that superhydrophobic surfaces formed under environmentally benign conditions without any intricate instrumentations.[47] In addition, PDA surface coatings show zwitterionic character that pH-switchable in water. In acidic conditions, a PDA layer is positively charged and allows good permeability of anions. On the other hand, the PDA layer obtains a negative charge under basic conditions so that cations can easily pass through the PDA thin film on an electrode. The PDA film exhibits fully reversible, pH-switchable permselectivity for both cationic and anionic redox-active probe molecules.[48] PDA deposition was also used for surface nanopatterning on low surface-energy substrate materials such as Teflon, graphene, and gold.[36] Catechol groups have played multiple roles, acting as further chemical modification sites for nanopatterning as well as a universal surface adhesive on low surface-energy substrates. Dopamine was also used for surface immobilization schemes and antifouling surfaces,[17, 32] where the substrates were dip-coated with dopamine-based initiators followed by surface-initiated polymerization and the grafting of a variety of polymer brushes like PEG and other peptidomimetic polymers.[17] Multifunctional ligands have been synthesized by simply combining PEG, polyethylenimine, and PDA, and then applied onto a variety of inorganic nanoparticles of Fe_3O_4, MnO, and Au.[19] This corona layer added biocompatibility and good stability in various harsh environments so that the functionalized inorganic nanoparticles could potentially be useful in biomedical applications. Moreover, a PDA-assisted surface-engineering technique has been used to improve the power and safety of Li-ion batteries.[40] PDA functionalized onto the surface of a polyethylene separator and the PDA coating was further developed by silicification to form a diatom-inspired silica coating. Consequently, the added silica coating achieved enhanced power, reduced thermal shrinkage, and enhanced the safety of Li-ion batteries. In sum, this bioinspired chemistry as well as the aforementioned catecholic polymers have been the source of numerous breakthroughs in

many areas over the last decade. Meanwhile, researchers have developed new routes to the modification of various substrates and the preparation of functional materials via simple processes.

1.3 OBJECTIVE

Bioinspired catecholic polymers such as PDA and melanins possess a number of interesting properties. These unique properties make such polymers potentially useful for a variety applications in a range of areas. Indeed, the polymers exhibit extraordinary features compared to many conventional polymers and organic materials. Not surprisingly, these materials have attracted, during the last decade, a great deal of interest from researchers who yearn to exploit those properties in engineered materials.

The overall objective of the next few chapters is to develop a melanin-based polymer architecture, so that the functional aspects of melanin chemistry can be realized in the form of mechanically robust films and multifunctional coatings. Bioinspired catecholic polymers like melanins and PDA display a suite of functions including high thermal stability, UV protection, antifouling behavior, universal surface attachment, and radical inhibition, among many other properties. Given this fact, new knowledge regarding the chemical synthesis and characterization of melanin-like polymers could enable their widespread use as thermal stabilizers, antifouling coatings, and flame-retardant foams, to name a few, and all this comes with an expected environmentally friendly aspect. The outcomes of this research have the potential to influence several different fields including polymer chemistry, polymer physics, biology, and material science.

1.4 REFERENCES

1. Faure, E.; Falentin-Daudre, C.; Jerome, C.; Lyskawa, J.; Fournier, D.; Woisel, P.; Detrembleur, C. *Prog. Polym. Sci.* **2013,** *38,* 236-270.

2. Sedo, J.; Saiz-Poseu, J.; Busque, F.; Ruiz-Molina, D. *Adv. Mater.* **2013,** *25*, 653-701.
3. Borman, S. *Chem. Eng. News* **1992,** *70*, 26-26.
4. http://www.rhodia.com/en/binaries/GPS_2011_09_v1_Catechol_gb.pdf. (04/14/2015)
5. http://monographs.iarc.fr/ENG/Monographs/vol71/mono71-18.pdf. (04/14/2015)
6. Schweigert, N.; Zehnder, A. J. B.; Eggen, R. I. L. *Environ. Microbiol.* **2001**, *3*, 81-91.
7. Heo, J.; Kang, T.; Jang, S. G.; Hwang, D. S.; Spruell, J. M.; Killops, K. L.; Waite, J. H.; Hawker, C. J. *J. Am. Chem. Soc.* **2012**, *134*, 20139-20145.
8. Ye, Q.; Zhou, F.; Liu, W. M. *Chem. Soc. Rev.* **2011**, *40*, 4244-4258.
9. d'Ischia, M.; Napolitano, A.; Pezzella, A.; Meredith, P.; Sarna, T. *Angew. Chem. Int. Ed.* **2009**, *48*, 3914-3921.
10. Watt, A. A. R.; Bothma, J. P.; Meredith, P. *Soft Matter* **2009**, *5*, 3754-3760.
11. Liu, Y.; Simon, J. D. *Pigm. Cell. Res.* **2003**, *16*, 72-80.
12. Zeise, L.; Murr, B. L.; Chedekel, M. R. *Pigm. Cell. Res.* **1992**, *5*, 132-142.
13. Chen, S.-R.; Jiang, B.; Zheng, J.-X.; Xu, G.-Y.; Li, J.-Y.; Yang, N. *Food Chem.* **2008**, *111*, 745-749.
14. Tu, Y. G.; Xie, M. Y.; Sun, Y. Z.; Tian, Y. G. *Pigm. Cell. Melanoma R.* **2009**, *22*, 134-136.
15. Cubo, M. T.; Buendia-Claveria, A. M.; Beringer, J. E.; Ruiz-Sainz, J. E. *Appl. Environ. Microbiol.* **1988**, *54*, 1812-1817.
16. Lee, H.; Dellatore, S. M.; Miller, W. M.; Messersmith, P. B. *Science* **2007**, *318*, 426-430.
18. Deziderio, S. N.; Brunello, C. A.; da Silva, M. I. N.; Cotta, M. A.; Graeff, C. F. O. *J. Non-Cryst. Solids* **2004**, *338*, 634-638.
19. Ling, D.; Park, W.; Park, Y. I.; Lee, N.; Li, F.; Song, C.; Yang, S.-G.; Choi, S. H.; Na, K.; Hyeon, T. *Angew. Chem. Int. Ed.* **2011**, *50*, 11360-11365.
20. Postma, A.; Yan, Y.; Wang, Y.; Zelikin, A. N.; Tjipto, E.; Caruso, F. *Chem. Mater.* **2009**, *21*, 3042-3044.
21. Zhang, X.; Wang, S.; Xu, L.; Feng, L.; Ji, Y.; Tao, L.; Li, S.; Wei, Y. *Nanoscale* **2012**, *4*, 5581-5584.
22. McGinnes.J; Corry, P.; Proctor, P. *Science* **1974,** *183*, 853-855.
23. Ito, S.; Wakamatsu, K. Chemistry of Melanin. In The Pimentary System; Nordlund, J.J; Boissy, R.E; Hearing, V.J.; King, R.A.; Oetting, W.S.; Ortonne, J. Eds.; Blackwell Publishing Ltd: Malden, 2006; Second ed, pp 282-310.
24. Rozanowska, M.; Sarna, T.; Land, E. J.; Truscott, T. G. Free Radic. Biol. Med. 1999, 26, 518.
25. Meredith, P.; Sarna, T. Pigm. Cell. Res. 2006, 19, 572.
26. Bernsmann, F.; Ponche, A.; Ringwald, C.; Hemmerle, J.; Raya, J.; Bechinger, B.; Voegel, J. C.; Schaaf, P.; Ball, V. *J. Phys. Chem. C* **2009,** *113*, 8234-8242.
27. Shalev, T.; Gopin, A.; Bauer, M.; Stark, R. W.; Rahimipour, S. *J. Mater. Chem.* **2012,** *22*, 2026-2032.
28. Hong, S.; Na, Y. S.; Choi, S.; Song, I. T.; Kim, W. Y.; Lee, H. *Adv. Funct. Mater.* **2012,** *22*, 4711-4717.

29. Liebscher, J.; Mrowczynski, R.; Scheidt, H. A.; Filip, C.; Hadade, N. D.; Turcu, R.; Bende, A.; Beck, S. *Langmuir* **2013,** *29*, 10539-10548.
30. Sarna Tadeusz, Swartz, H. A. The Physical Properties of Melanins. In *The Pimentary System;* Nordlund, J.J; Boissy, R.E; Hearing, V.J.; King, R.A.; Oetting, W.S.; Ortonne, J. Eds.; Blackwell Publishing Ltd: Malden, 2006; Second ed, pp 311-341.
31. Dunford, R.; Land, E. J.; Rozanowska, M.; Sarna, T.; Truscott, T. G. *Free Radical Biol. Med.* **1995,** *19*, 735-740.
32. Ju, K. Y.; Lee, Y.; Lee, S.; Park, S. B.; Lee, J. K. *Biomacromolecules* **2011**, *12*, 625-632..
33. Shanmuganathan, K.; Cho, J. H.; Iyer, P.; Baranowitz, S.; Ellison, C. J. *Macromolecules* **2011**, *44*, 9499-9507.
34. Cho, J. H.; Shanmuganathan, K.; Ellison, C. J. *ACS Appl. Mater. Interfaces* **2013**, *5*, 3794-3802.
35. Meredith, P.; Powell, B. J.; Riesz, J.; Nighswander-Rempel, S. P.; Pederson, M. R.; Moore, E. G. *Soft Matter* **2006,** *2*, 37-44.
36. Kim, B. H.; Lee, D. H.; Kim, J. Y.; Shin, D. O.; Jeong, H. Y.; Hong, S.; Yun, J. M.; Koo, C. M.; Lee, H.; Kim, S. O. *Adv. Mater.* **2011,** *23*, 5618-5622.
37. Xu, L. Q.; Yang, W. J.; Neoh, K.-G.; Kang, E.-T.; Fu, G. D. *Macromolecules* **2010,** *43*, 8336-8339.
38. Wu, J. J.; Zhang, L.; Wang, Y. X.; Long, Y. H.; Gao, H.; Zhang, X. L.; Zhao, N.; Cai, Y. L.; Xu, J. *Langmuir* **2011,** *27*, 13684-13691.
39. Janes, D. W.; Thode, C. J.; Willson, C. G.; Nealey, P. F.; Ellison, C. J. *Macromolecules* **2013,** *46*, 4510-4519.
40. Kang, S. M.; Ryou, M. H.; Choi, J. W.; Lee, H. *Chem. Mater.* **2012,** *24*, 3481-3485.
41. Shultz, M. D.; Reveles, J. U.; Khanna, S. N.; Carpenter, E. E. *J. Am. Chem. Soc.* **2007,** *129*, 2482-2487..
42. Lee, H.; Rho, J.; Messersmith, P. B. *Adv. Mater.* **2009,** *21*, 431-434.
43. Chien, H. W.; Kuo, W. H.; Wang, M. J.; Tsai, S. W.; Tsai, W. B. *Langmuir* **2012,** *28*, 5775-5782.
44. Ku, S. H.; Ryu, J.; Hong, S. K.; Lee, H.; Park, C. B., General functionalization route for cell adhesion on non-wetting surfaces. *Biomaterials* **2010,** *31* (9), 2535-2541.
45. McCloskey, B. D.; Park, H. B.; Ju, H.; Rowe, B. W.; Miller, D. J.; Freeman, B. D. *J. Membrane Sci.* **2012,** *413*, 82-90.
46. McCloskey, B. D.; Park, H. B.; Ju, H.; Rowe, B. W.; Miller, D. J.; Chun, B. J.; Kin, K.; Freeman, B. D. *Polymer* **2010**, *51*, 3472-3485.
47. Zhang, L.; Wu, J. J.; Wang, Y. X.; Long, Y. H.; Zhao, N.; Xu, J. *J. Am. Chem. Soc.* **2012,** *134*, 9879-9881.
48. Yu, B.; Liu, J. X.; Liu, S. J.; Zhou, F. *Chem. Commun.* **2010,** *46*, 5900-5902.

Chapter 2: Thermooxidative Stabilization of Polymers Using Natural and Synthetic Melanins

2.1 INTRODUCTION

In recent years, there has been tremendous interest in extracting and using biopolymers like cellulose,[1-3] chitin[4-5] and collagen[6] as reinforcements in composites, tissue engineering scaffolds, transparent gas barrier films, etc. Melanins constitute another fascinating class of biopolymers found in the hair, skin, inner ear, eye and brain of living animals[7]. They have been attributed to several different functions in the human body that include absorption of ultraviolet radiation (photoprotection) and dissipation into harmless heat, metal-ion chelation, thermoregulation, antibiotic activity and free-radical quenching.[8-9] Among the different types of melanins, the most widely studied forms are eumelanins and pheomelanins. Both of these pigments are derived from the common precursor dopaquinone formed via the oxidation of L-tyrosine by tyrosinase.[10] Eumelanins are brown and black pigments derived from oxidative polymerization of 5,6-dihydroxyindole (DHI) and 5,6-dihydroxyindole-2-carboxylic acid (DHICA), while pheomelanins are red and yellow pigments derived from cysteinyl dopa units[11-12] (see **Scheme 1.2**). Even given this knowledge of basic subunits, the comprehensive organization of the subunits in melanins is still not clear. It is under debate whether melanins are highly cross-linked heterogeneous polymers or oligomers condensed into nanoaggregates,[7, 13] while accumulating evidence suggests supramolecular organization of protomolecules into stacked sheets with a regular spacing of about 3.7Å.[14]

Natural melanins are amorphous pigments that are insoluble in almost all organic solvents and this has limited physical and chemical analysis of these materials. In recent years, researchers have circumvented this issue to some extent by developing synthetic pathways for melanin-like polymers that are soluble in organic solvents like N,N-

dimethylformamide and dimethyl sulfoxide.[8,15] Although exact structural differences between synthetic melanins and their natural counterparts are not completely clear, the fact that synthetic melanins exhibit similar physical and chemical properties to natural melanins has led to renewed interest in synthetic melanin-like polymers for their optical, electronic and other properties.[16-18] Notwithstanding the voluminous research on the physiological functions of melanin and its related structural aspects, there have been few attempts[17, 19-20] to create functional polymeric materials and composites which incorporate this biopolymer. In fact, exploiting the many desirable functional properties of melanins to augment the properties of other polymers still remains largely unexplored. Given that melanins can be extracted either from many natural sources such as cuttlefish (*Sepia officinalis*),[21-22] chicken feathers,[23-24] bacteria,[25] etc. or synthesized from various indole precursors, makes it even more attractive for this purpose.

Towards this end, it is demonstrated here that natural melanins and melanin-like synthetic biopolymers have potential as antioxidant additives for certain commercial polymers explored here as model systems due to their well-known degradation pathways. There is increasing evidence suggesting that cellular melanin functions similarly as an antioxidant in the body by (1) scavenging free radicals, (2) deactivating electronically excited oxidizing species, (3) sequestering redox active metal ions such as iron and copper and (4) scavenging intermediate radicals such as peroxyl and alkoxyl.[26] Dunford et al.[27] and Rozanowska et al.[11] studied the interaction of synthetic melanins with specifically generated oxidizing and reducing free radicals and found that synthetic melanins are good scavengers of carbon-centered radicals with corresponding rate constants in the range of 10^7-10^8 $(M\text{-}s)^{-1}$. The efficiency of scavenging depends on the redox potential, electric charge and the lifetime of the radicals. Very recently, Ju et al. synthesized melanin-like

nanoparticles from dopamine hydrochloride and studied their radical scavenging abilities by electron spin resonance spectroscopy.[28]

Since radical initiated chain scission is a common thermo-oxidative degradation pathway for most synthetic commercial polymers, it was of interest in the present study to determine if melanins could be used as an effective thermal stabilizer in polymers such as poly(methyl methacrylate) (PMMA), polypropylene (PP) and polystyrene (PS), that have well known thermo-oxidative degradation pathways. Most dramatically, synthetic melanins derived from oxidation of L-3-(3,4-dihydroxyphenyl) alanine (L-dopa) (**Scheme 1.2**), significantly enhance PMMA's onset of thermal and thermo-oxidative stability by 50-90 ^{o}C when incorporated in small amounts (0.5-5 wt%). Further, similar thermo-oxidative stabilization of PMMA and PP can be attained by incorporating natural melanin extracted from the ink sac of *Sepia Officinalis* at similar loadings.

2.2 PHOTOABSORBANCE AND SOLUBILITY OF SYNTHETIC AND NATURAL MELANIN

Melanins have been difficult to characterize owing to their heterogeneous structure, intractable chemical properties and solubility issues. One efficient way to evaluate synthetic melanins for melanin-like properties is to determine their photoabsorbance behavior. Melanins are particularly known for their photoprotective functions in the body, largely absorbing ultraviolet and visible light and dissipating it as heat. **Figure 2.1a** shows the UV-Vis absorbance of synthetic melanins. The broad band monotonic absorbance of these synthetic melanins derived from oxidation of L-dopa in the entire UV-Vis range is essentially identical to that of natural melanins extracted from *Sepia Officinalis*. Like natural melanins, solutions of synthetic L-dopa derived melanins appear dark brown to black depending on concentration (**Figure 2.1b, c**).

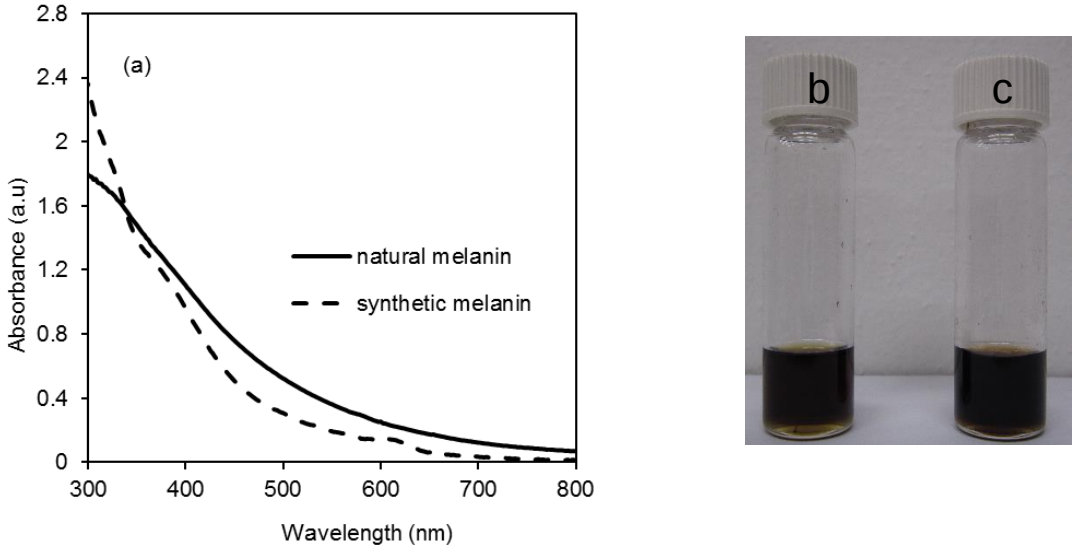

Figure 2.1: (a) UV-Vis absorbance spectra of natural and synthetic melanin in Soluene™ (both at 0.05 mg/mL). Solutions of synthetic melanin (b) and natural melanin (c) dispersed in Soluene™ at a concentration of 1 mg/mL. Reprinted with permission from Shanmuganathan, K. and Cho, J. H. et al., Macromolecules 2011, 12, 625. Copyright 2011 American Chemical Society.

2.3 THERMOGRAVIMETRIC ANALYSIS OF SYNTHETIC AND NATURAL MELANIN

Further the thermal degradation behavior of synthetic melanins are similar to that of natural melanins both in nitrogen and air atmosphere (**Figure 2.2**). Both of them display a multi-step weight loss arising from chemical heterogeneity of these pigments and the presence of different volatile species. The low temperature weight losses can be ascribed to loss of water since melanins are hygroscopic containing as much as 10-30% water.[29-31] Sepia melanins have been reported to have a protein fraction that is very tightly bound to a chromatophoric component. Not much is known about the nature and binding of this protein component.[22] These proteins and other organic components may be responsible for the slight differences observed in decomposition behavior of Sepia melanins as compared to synthetic melanins. Here, synthetic melanins appear to be slightly more thermally stable than natural Sepia melanins in contrast to a previous report; however, the preparation

protocols of natural and synthetic melanins were not the same as in the present study.[30] Sepia melanin has more thermally stable residue at high temperatures compared to synthetic melanins in both air (**Figure 2.2a**) and nitrogen (**Figure 2.2b**). Perhaps this difference could result from significant metal ion content in natural melanins.[32]

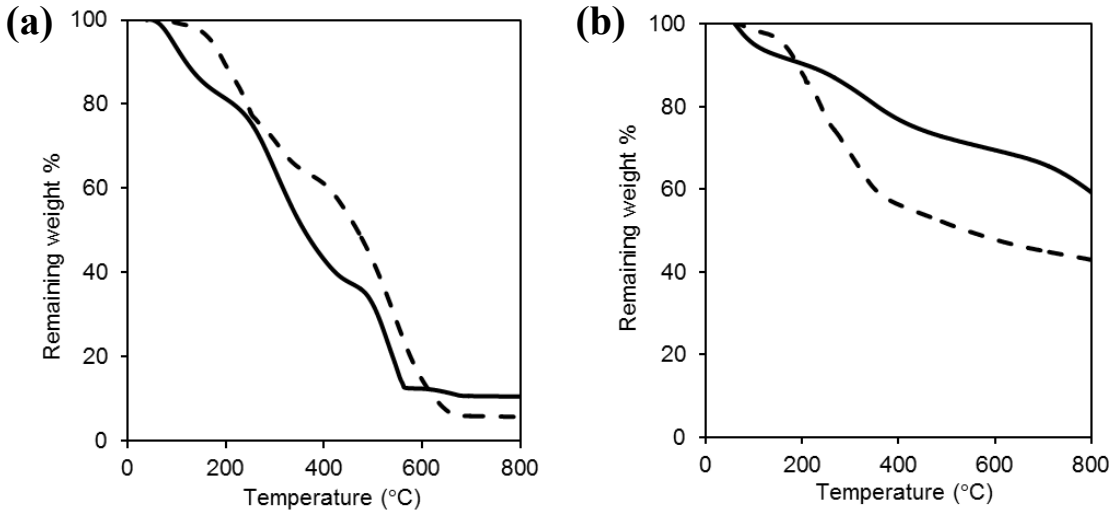

Figure 2.2: Thermogravimetric analysis plots of synthetic (dashed line) and natural melanin (solid line) (a) in air (b) in nitrogen at 20 °C/min. Reprinted with permission from Shanmuganathan, K. and Cho, J. H. et al., Macromolecules 2011, 12, 625. Copyright 2011 American Chemical Society.

2.4 THERMOGRAVIMETRIC ANALYSIS OF PMMA AND PMMA-SYNTHETIC MELANIN BLENDS IN NITROGEN

Figure 2.3 shows the thermal degradation behavior of PMMA with and without addition of synthetic L-dopa derived melanin. PMMA is known to degrade under elevated temperature by radical initiated chain scission followed by chain unzipping.[33-36] Hence it was of interest to determine if the radical scavenging abilities of melanin could be used to enhance the thermal stability of PMMA. As seen in **Figure 2.3**, synthetic L-dopa-derived melanin has a significant thermal stabilization effect on PMMA. While neat PMMA starts to degrade at ~ 230 °C (**Figure 2.3b**), the addition of as little as 0.5 wt% synthetic melanin

shifts the onset decomposition temperature to ~ 300 °C. As the concentration of synthetic melanin is increased to 1 and 5 wt%, there is a further increase in the onset decomposition temperature of PMMA to about 320 °C. It is important to mention that the addition of 0.5-1 wt% melanin into PMMA still results in 100 micron thick films with greater than 80% light transmission from 350-800 nm as measured by UV-vis absorbance spectroscopy. The films appear slightly brownish in color and no aggregates are visible to the eye indicating the dispersion is reasonably good.

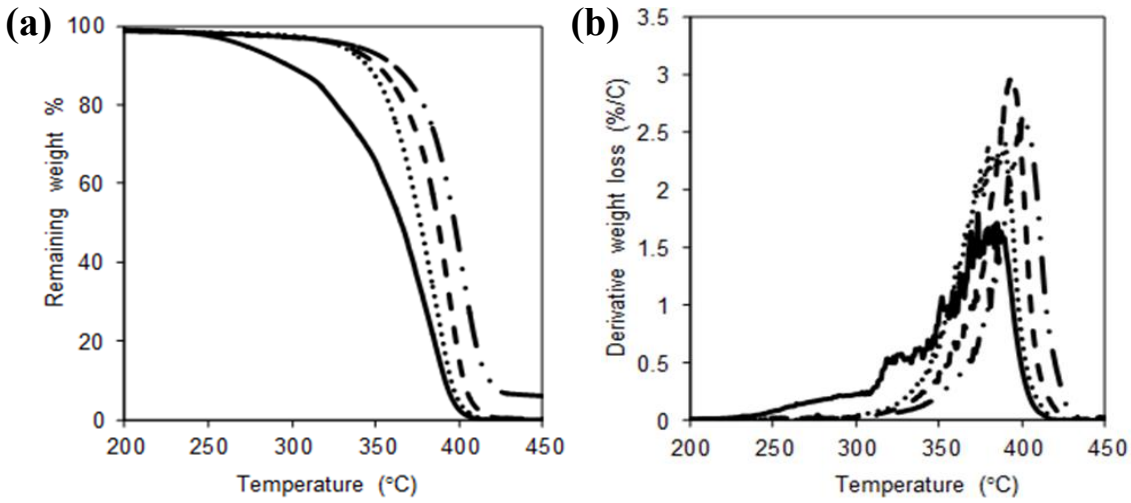

Figure 2.3: (a) Thermogravimetric analysis and (b) derivative thermogravimetric analysis plots of PMMA and PMMA-synthetic melanin blends in a nitrogen atmosphere: 0 wt% (solid line), 0.5 wt% (dotted line), 1 wt% (dashed line) and 5 wt% (dash dot line) synthetic melanin. All samples were heated in nitrogen at 2 ^{o}C/min. Similar results are observed for heating rates of 20 ^{o}C/min. Reprinted with permission from Shanmuganathan, K. and Cho, J. H. et al., Macromolecules 2011, 12, 625. Copyright 2011 American Chemical Society.

Thermal degradation of neat PMMA has been widely investigated.[33-37] Although it is well-accepted that the polymer degrades by chain-end unzipping and random chain scission events, structural differences arising from polymerization conditions lead to

significant variation in PMMA decomposition behavior and kinetics. For example, anionically polymerized PMMA is typically more thermally stable than free radically polymerized PMMA (commercial PMMA such as that used in this study is typically free radically polymerized) due to the absence of molecular features introduced during free radical termination.[35] Kashiwagi et al.[35] reported a three step weight loss for free radically polymerized PMMA. The low temperature weight losses (around 160 °C and 270 °C) have been attributed to head-to-head repeat unit linkages from termination by combination and from unsaturated chain ends from termination by disproportionation, respectively, while the high temperature weight loss step (> 300 °C) is attributed to random main-chain scission events. Other studies[33] show a two-step weight loss arising from unsaturated chain-end scission followed by random main-chain scission at higher temperature. The presence of unsaturated chain ends causes the polymer to start unzipping at about 220-230 °C producing smaller fragments resembling monomers. We also observed here (**Figure 2.3b**) a low temperature weight loss beginning at ~ 230 °C for neat PMMA. However, incorporation of melanin eliminated the low temperature weight losses in PMMA and the onset of decomposition was shifted to 300-320 °C.

It has been shown by other researchers that melanins can interact with a range of oxidizing and reducing free radicals where the radical scavenging properties depend on the lifetime of radicals, their redox potential and electric charge.[11] Melanins can react with radicals either by a simple one electron transfer process or by radical addition. The fact that the low temperature weight loss of PMMA is eliminated by incorporation of melanin suggests that melanin scavenges the radicals arising at the unsaturated chain end and exerts a blocking effect on the unzipping depolymerization mechanism. Therefore, degradation of PMMA containing melanin proceeds mostly via main-chain random scission at temperatures above 300 °C. Other research has shown that similar thermal stability, where

low temperature degradation at 230 °C is eliminated and degradation processes above 300 °C dominate,[34] has been imparted to PMMA synthesized with thiol end-groups instead of unsaturated chain ends.

To gain further insight into this mechanism, both PMMA and PMMA-melanin samples were heated in the thermogravimetric analyzer (TGA) to 320 °C at 20°C/min in nitrogen and immediately cooled, the temperature where 10% weight loss is observed in neat PMMA and where main-chain scission events have just started emerging. They were dissolved in N,N-dimethylformamide (DMF) (concentration of ~3 mg/ml) and injected into a gel permeation chromatography (GPC) with a DMF mobile phase and analyzed using both refractive index and diode-array absorbance detectors. While melanins absorb broadly in the UV and visible wavelengths (**Figure 2.1**), PMMA doesn't have a characteristic photoabsorbance in this regime.

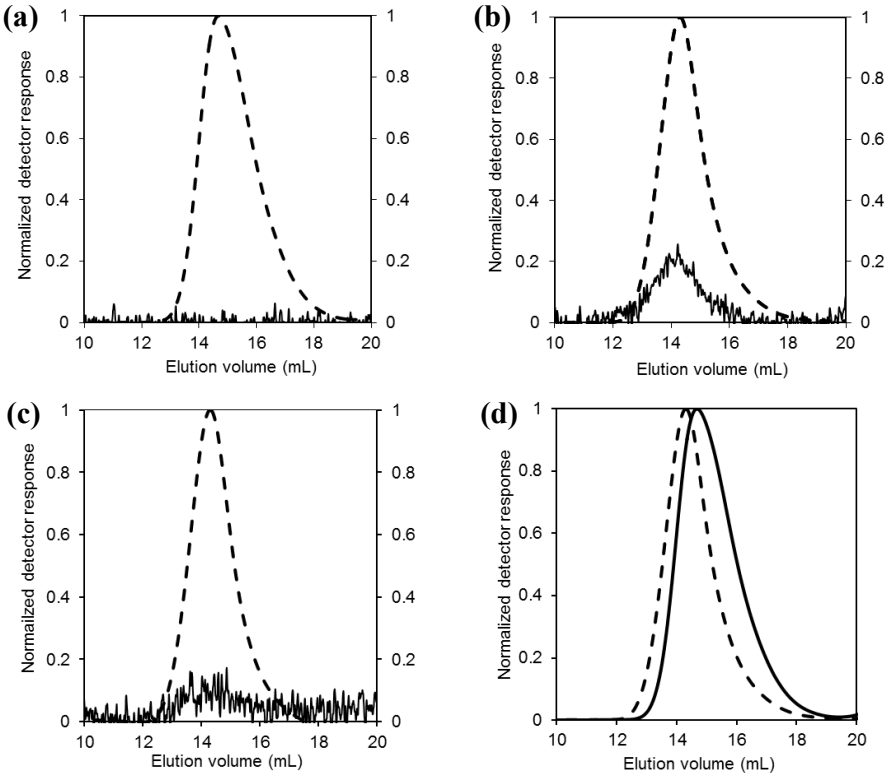

Figure 2.4: Gel permeation chromatograms of (a) PMMA (b) PMMA-5% synthetic melanin heated to 320 ^{o}C in TGA in nitrogen, and (c) melt compounded PMMA-5% synthetic melanin composite not run in the TGA. Refractive index signal (dashed line), photoabsorbance signal (solid line). (d) Comparison plot of chromatogram of PMMA (solid line) and PMMA-5% synthetic melanin composite (dashed line) indicating the higher molecular weight of the composite in comparison to neat PMMA after heating the samples to 320 ^{o}C in nitrogen. Reprinted with permission from Shanmuganathan, K. and Cho, J. H. et al., Macromolecules 2011, 12, 625. Copyright 2011 American Chemical Society.

As can be seen in **Figure 2.4a**, neat PMMA heated to 320 °C in the TGA displays only a refractive index signal with no characteristic absorbance at the visible wavelength of 650 nm. However, PMMA-5% synthetic melanin composite heated to 320 °C in the TGA shows both refractive index and photoabsorbance peaks at the same elution volume (**Figure 2.4b**) suggesting that melanin becomes covalently linked to PMMA chains during

the heating process. This is supporting evidence for the hypothesis that melanins covalently attach to the radical end of the PMMA chain and hinder chain unzipping following chain-end scission. It should be noted here that the PMMA used in this study is a commercial sample of high molecular weight (M_w ~ 350,000 g/mol). While the molecular weight characterization of melanins still remains a major challenge owing to its structural heterogeneities, the solvent soluble synthetic melanin in this study appears in our chromatograms at elution volumes greater than 20 mL. As a control experiment, the chromatogram of PMMA-5% synthetic melanin immediately following melt compounding shown in **Figure 2.4c** exhibits a small photoabsorbance peak that is barely distinguishable from the instrument baseline at the same elution volume of the refractive index peak. This is likely due to the same attachment mechanism of melanin onto the PMMA chain which occurs to a lesser extent during melt compounding of melanin with PMMA at 220 ^{o}C for 10 minutes. We also observe from **Figure 2.4d** that PMMA-5% synthetic melanin composite heated to 320 °C in the TGA elutes much earlier than neat PMMA heated to similar conditions, indicating melanin can prevent significant molecular weight loss. This suggests that melanin, by its radical scavenging action, can stabilize PMMA such that it retains its molecular weight during thermal processing at elevated temperatures. Since molecular weight is a structural parameter which has significant influence on the mechanical and flow properties of polymers, this could be particularly advantageous in polymer processing and demanding thermal applications.

2.5 ACTIVITY OF MELANIN ON THE THERMAL DEGRADATION OF PMMA

In order to quantitate the activity of melanin on the thermal degradation of PMMA, the activation energy for decomposition of PMMA and the melanin blends was determined using the Flynn-Wall-Ozawa method.[38-39] In this method, the kinetics of thermal

decomposition of polymers is evaluated based on an iso-conversion principle. When a sample is decomposed at different heating rates, the temperature (T) for a given conversion or percentage weight loss changes with heating rate (β) due to the interplay of heating rate with decomposition kinetics. By plotting log β against 1/T for a given conversion, the activation energy can be determined from the slope of the line fitting the data (**Figure 2.5**) using the equation (**Eq. 2.1**), where T is temperature (in Kelvin), β is the heating rate (K/min), E is activation energy (kJ/mol) and R is the universal gas constant (kJ/mol-K).

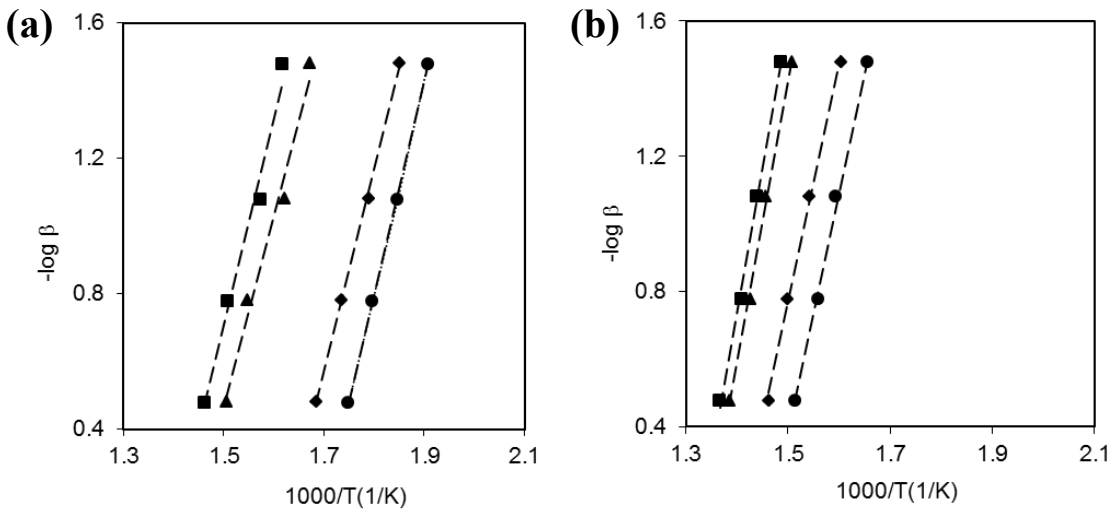

Figure 2.5: Iso-conversion plots used to determine the activation energy based on the thermal decomposition data of (a) PMMA and (b) PMMA-5% synthetic melanin blends run at different heating rates (β). Each symbol represents a particular weight loss condition: 5% weight loss (solid circles), 10% weight loss (solid diamond), 50% weight loss (solid triangles), 70% weight loss (solid squares) and the dashed line connecting a set of symbols represents the temperature at which a given degree of weight loss occurs at various heating rates (β). Activation energies determined from the slope of the dashed lines using **Eq. 2.1** are listed in **Table 2.1**. Reprinted with permission from Shanmuganathan, K. and Cho, J. H. et al., Macromolecules 2011, 12, 625. Copyright 2011 American Chemical Society.

Conversion	Activation energy (E), kJ/mol	
	PMMA	PMMA-5% synthetic melanin
5 %	114	129
10 %	109	128
50%	103	150
70 %	112	154

Table 2.1: Activation energies for thermal decomposition of PMMA and PMMA-5% synthetic melanin blends determined by Flynn-Wall-Ozawa method. The expected standard error in the determination of activation energies by this method has been reported to be +/- 10%.[37] Reprinted with permission from Shanmuganathan, K. and Cho, J. H. et al., Macromolecules 2011, 12, 625. Copyright 2011 American Chemical Society.

$$\frac{d(\log \beta)}{d\left(\frac{1}{T}\right)} = -0.4567\frac{E}{R} \qquad \textbf{Eq. 2.1}$$

The activation energy for the thermal decomposition of neat PMMA was between 103-114 kJ/mol falling within the broad range of values (60-320 kJ/mol) found in literature.[33] This wide variation can be attributed to structural differences in PMMA arising from different polymerization conditions and also the use of a wide variety of methods to determine this activation energy. While the activation energy of PMMA reported here remained closely similar across different degrees of conversion, the activation energy of PMMA-5% melanin increased slightly with higher degrees of conversion but was always higher than neat PMMA. This indicates the superior thermal resistance of PMMA-melanin blends originates from enlarged activation energy for decomposition, likely by diverting the primary degradation mechanism to main-chain scission events which only take place at higher sample temperatures.

2.6 THERMAL STABILITY OF PMMA-NATURAL MELANIN AND PMMA-SYNTHETIC MELANIN BLENDS IN AIR

More significantly, synthetic melanin also enhances the thermal stability of PMMA in air, a far more oxidative environment. As can be seen in **Figure 2.6**, incorporation of 5 wt % synthetic melanin in PMMA enhances the onset decomposition temperature from 230 ^{o}C to 300 ^{o}C when PMMA is heated in air. The 70-80 ^{o}C shift in decomposition temperature of PMMA in an air atmosphere represents a significant thermo-oxidative stabilization effect that could be potentially useful in extending the thermal processing and use temperature of this commercially relevant polymer. In comparison, montmorillonite, which is widely used to enhance mechanical and flame retardant properties of polymers, does not have a significant effect on the thermal stability of PMMA (**Figure 2.6**).

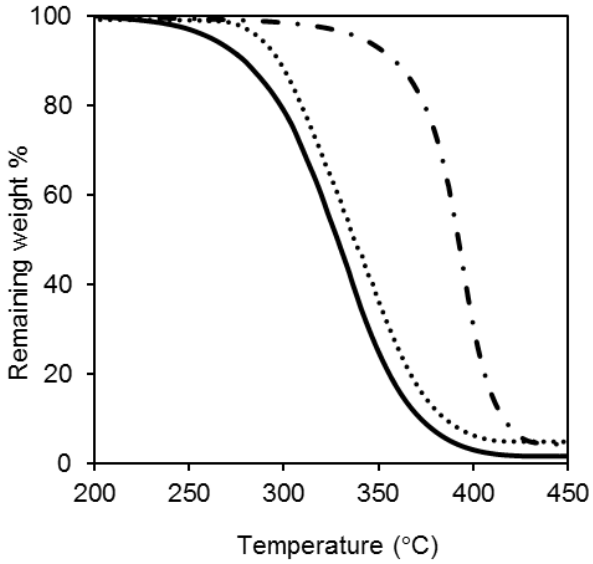

Figure 2.6: Thermogravimetric analysis plots of PMMA blends in air at a heating rate of 20 ºC/min: PMMA-5 wt% synthetic melanin composite (dash dot line) showing significant increase in the onset decomposition temperature as compared to neat PMMA (solid line) or PMMA-5 wt% montmorillonite composite (dotted line). Reprinted with permission from Shanmuganathan, K. and Cho, J. H. et al., Macromolecules 2011, 12, 625. Copyright 2011 American Chemical Society.

Figure 2.7 shows that the thermo-oxidative stabilization effect from adding synthetic melanin to PMMA can also be attained with melanins derived from natural sources. Melanins isolated from the ink sacs of *Sepia officinalis* (cuttlefish) are commonly accepted as a standard for natural eumelanins.[22] Mild and generally applicable protocols for isolating melanins from Sepia ink without altering their native composition have been established previously.[21-22] Using this procedure, we obtained a black powder of natural eumelanin and melt compounded them with the same PMMA. As shown in **Figure 2.7**, natural Sepia melanin also has a significant thermo-oxidative stabilization effect in PMMA but the amount of enhancement in the onset temperature of the degradation (~ 50 ºC) is

slightly less compared to synthetic melanin. This could be due to several reasons. Natural melanin has a significant amount of bound protein that is probably easy to degrade and which cannot be removed during extraction even after several washing cycles. Natural melanin is also not as dispersible in PMMA or simple organic solvents as compared to synthetic melanins due to its more particulate nature, possibly from metal ions which participate in inter- and intra-molecular ionic bonds. In fact, the natural melanin in **Figure 2.1c** was made into a suspension using Soluene™, a special solvent from Perkin Elmer which contains surfactants and other dispersing aids. Therefore, natural melanin added at similar loadings may be less effective in radical scavenging action due to its presence in larger aggregates rather than in a fully dispersable form as for synthetic melanins. It is also possible that synthetic melanin is not perfectly representative of natural Sepia melanin structure even though the same basic structural units are present. It has been very difficult to definitively establish these differences for reasons mentioned earlier and more research is ongoing in this area in a number of research groups.

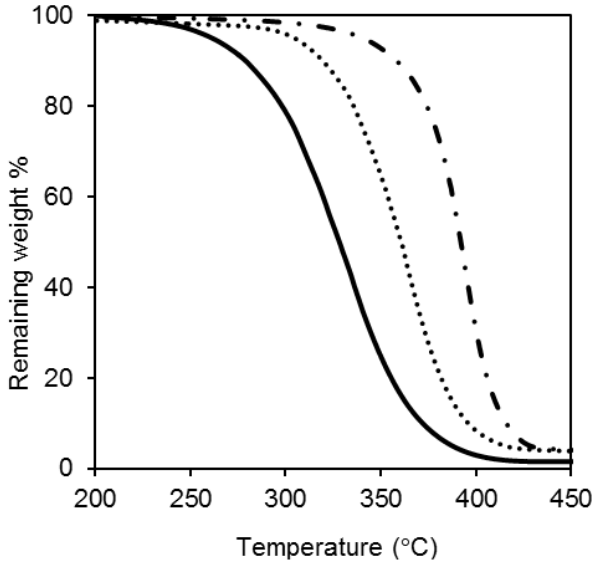

Figure 2.7: Thermogravimetric analysis plots of PMMA-natural melanin blends in air at a heating rate of 20 °C/min: Natural Sepia melanin also significantly enhances the thermo-oxidative stability of PMMA but the effect is less compared to synthetic melanin: PMMA (solid line), PMMA-5 wt% natural sepia melanin (dotted line), PMMA-5 wt% synthetic melanin (dash dot line). Reprinted with permission from Shanmuganathan, K. and Cho, J. H. et al., Macromolecules 2011, 12, 625. Copyright 2011 American Chemical Society.

2.7 THERMOOXIDATIVE STABILIZATION EFFECT OF NATURAL MELANIN ON PP AND PS

In order to establish generality of the thermal stabilization properties of melanins applied to other polymers as well, we incorporated 5 wt% natural Sepia melanin into PP and PS, two widely used polymers with very different chemistries and degradation pathways. PP is well known for thermal degradation by radical attack due to the presence of tertiary hydrogens with low dissociation energy.[40] PS on the other hand is reported to undergo degradation via random chain scission followed by intra- and inter-molecular radical transfer.

As seen in **Figure 2.8**, incorporation of melanin enhanced the onset decomposition temperature of PP by ~50 °C, while the effect on the thermo-oxidative stability of PS was much less. It should be noted here that many polymers degrade at lower temperature in air than in nitrogen. In the presence of oxygen, the radicals produced by chain scission form peroxy radical intermediates and hydroperoxides. This appears to shift the rate limiting step from random chain scission to decomposition of hydroperoxide radicals either during the early stages of degradation or throughout the process.[41] The effects of these on the radical scavenging role of melanin are not clear. The general radical scavenging action of melanin depends on several factors such as the reactivity and lifetime of radicals, steric hindrances, etc.[10] which can be translated to some extent to melanin's stabilization activity in polymers. The fact that we observe less thermal stabilization effect of melanin on PS could be due to the resonance stabilization of radicals by pendant aromatic groups or steric hindrance restricting the accessibility of melanin to these units. This is the subject of future investigations.

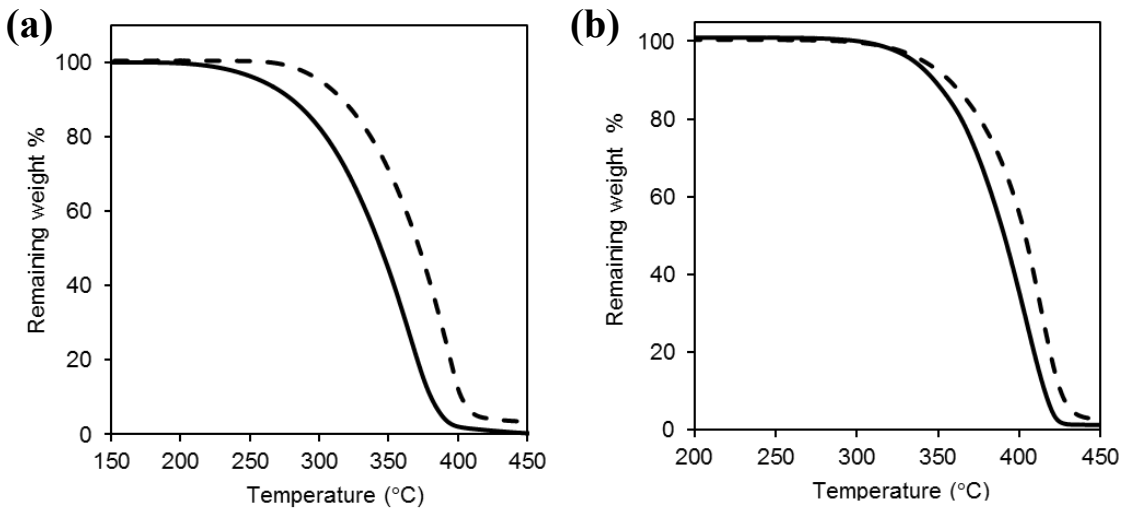

Figure 2.8: Thermogravimetric analysis plots of (a) PP (solid line) and PP-5 wt% natural sepia melanin composite (dashed line), (b) PS (solid line) and PS-5 wt% natural sepia melanin composite (dashed line) in air at a heating rate of 20 ^{o}C/min. Reprinted with permission from Shanmuganathan, K. and Cho, J. H. et al., Macromolecules 2011, 12, 625. Copyright 2011 American Chemical Society.

2.8 CONCLUSION

Melanin, a biomacromolecule well-known for its various functions in living systems, was investigated for its potential thermal stabilization capability in model synthetic polymers with well-known degradation pathways. Synthetic melanin derived from the oxidation of L-dopa significantly enhanced the thermal and thermo-oxidative stability of PMMA when incorporated even in very low amounts of 0.5 wt%. The low temperature weight losses below 300 ^{o}C associated with chain-end scission arising from weak unsaturated ends in free-radically polymerized PMMA were eliminated. The presence of melanin also delayed the onset of decomposition to above 300 ^{o}C. Combined thermal degradation and chromatography studies indicate that melanin scavenges the radical end of the chain and exerts a blocking effect on subsequent depolymerization.

Natural melanin derived from the ink sac of Sepia Officinalis also exerts significant thermal stabilization behavior in PMMA and other polymers like PP, and to a lesser extent in PS. Finally, this biopolymer can be harvested in large quantities from many natural sources like cuttlefish, chicken feathers, bacteria, etc. or synthesized from various indole precursors and could be used to enhance thermal and thermooxidative stability of commercial polymers, possibly without detrimental effects on the environment over traditional small molecule additives.

2.9 EXPERIMENTAL

2.9.1 MATERIALS

L-dopa, benzoyl peroxide, dimethyl sulfoxide (DMSO) and acetonitrile were all purchased from Sigma Aldrich (USA). All reagents were used as received without further purification. PMMA (Mw = 350,000 g/mol) and PS (Mw = 350,000 g/mol) were purchased from Sigma Aldrich (USA) and used as received. PP (grade 3746G) was kindly provided by Exxon Mobil and used as received.

2.9.2 SYNTHESIS OF MELANIN-LIKE POLYMERS FROM L-DOPA

Melanin-like polymers were synthesized by oxidation of L-dopa following the procedure outlined by Deziderio et al..[8] In a typical procedure, 3.0 g of L-dopa and 3.7 g of benzoyl peroxide were added to about 400 ml of anhydrous DMSO in a round bottom flask. The flask was quickly sealed with an air-tight stopper and the solution was stirred with a magnetic stir bar for 28 days at room temperature. The solution turned pink and then black within 2 hours and after 28 days a black solution was obtained. To collect the synthetic melanin product, excess DMSO was evaporated using a rotary evaporator with the water bath set to 100 ^{o}C leaving behind a viscous, concentrated black melanin solution.

Dropwise addition of this solution into about 600 ml of acetonitrile resulted in precipitation of melanin-like black aggregates. The precipitate was extracted by centrifugation at 3000 rpm for 10 minutes, re-dispersed in acetonitrile and centrifuged several times until the supernatant was clear. Then the material was dried in vacuum for 2 days to yield black powder of synthetic melanin. This melanin powder was readily redissolvable in DMF and DMSO.

2.9.3 Extraction of Sepia Eumelanin

Ink of Sepia Officinalis was provided by Epitek, Inc. (NJ, USA). Natural melanin was extracted from this ink using the procedure outlined by Liu and Simon.[21] Briefly, 24 ml of the ink was dispersed in 225 ml of de-ionized water in a polycarbonate centrifuge tube and stirred for 20 min. The solution was centrifuged in an Ultracentrifuge (Sorvall RC5B, Sorvall Instruments, Newton, CT, USA) at RCF 20000 g and 4 ^{o}C for 15 minutes. The top solution was decanted and the viscous mass at the bottom was re-dispersed in about 225 ml of de-ionized water by stirring for 15 minutes. This was centrifuged and the solid in the bottom was re-dispersed again. After 6 such cycles, the solid mass deposited at the bottom was dried in vacuum for 2 days to yield dry powder of natural eumelanin.

2.9.4 Preparation of Polymer-Melanin Blends

Specific weight fractions of synthetic or natural eumelanin were incorporated into various polymers by melt compounding in a twin screw DSM microcompounder at 100 rpm for 10 minutes at compounding temperatures typical for each commercial polymer with a dry nitrogen purge: PMMA (220 ^{o}C), PS (220 ^{o}C) and PP (180 ^{o}C). Neat polymers were also run through the microcompounder at similar conditions to have identical thermo-mechanical history and serve as appropriate controls.

2.9.5 THERMOGRAVIMETRIC AND CHROMATOGRAPHIC ANALYSIS

Thermal decomposition behavior of the various polymer-melanin blends was determined using a thermogravimetric analyzer (DSC/TGA 1, Mettler Toledo). Samples were heated in the TGA furnace from 30 ^{o}C at indicated heating rates in nitrogen or air atmosphere. To determine activation energies, PMMA and PMMA- 5wt % synthetic melanin blends were heated in nitrogen atmosphere in TGA at different heating rates: 2 ^{o}C/min, 5 ^{o}C/min, 10 ^{o}C/min and 20 ^{o}C/min. For molecular weight analysis by gel permeation chromatography (GPC), samples were heated in the TGA up to 320 ^{o}C, the residue was then completely dissolved in HPLC grade DMF and filtered with 0.2 μm pore size filters. These samples were analyzed using an Agilent 1100 series GPC (Agilent Technologies, USA) equipped with Viscotek I-series mixed bed high and medium molecular weight columns and refractive index and diode-array absorbance detectors.

2.9.6 UV-VIS SPECTROSCOPY

Photoabsorbance behavior of synthetic and natural eumelanins was obtained from a 0.05 mg/mL solution in Soluene™ (Perkin Elmer), a solvent that disperses both eumelanins, using a UV-Vis Spectrophotometer (Hewlett Packard 8452A Diode Array).

2.10 REFERENCES

1. Mendez, J.; Annamalai, P. K.; Eichhorn, S. J.; Rusli, R.; Rowan, S. J.; Foster, E. J.; Weder, C. *Macromolecules* **2011,** *44*, 6827.
2. Pei, A.; Malho, J.-M.; Ruokolainen, J.; Zhou, Q.; Berglund, L. A. *Macromolecules* **2011,** *44*, 4422.
3. Capadona, J. R.; Van Den Berg, O.; Capadona, L. A.; Schroeter, M.; Rowan, S. J.; Tyler, D. J.; Weder, C. *Nat. Nano* **2007,** *2*, 765.
4. Morin, A.; Dufresne, A. *Macromolecules* **2002,** *35*, 2190.
5. Madihally, S. V.; Matthew, H. W. T. *Biomaterials* **1999,** *20*, 1133.
6. Yeo, I.-S.; Oh, J.-E.; Jeong, L.; Lee, T. S.; Lee, S. J.; Park, W. H.; Min, B.-M. *Biomacromolecules* **2008,** *9*, 1106.
7. d'Ischia, M.; Napolitano, A.; Pezzella, A.; Meredith, P.; Sarna, T. *Angew. Chem.-Int. Edit.* **2009,** *48*, 3914.

8. Deziderio, S. N.; Brunello, C. A.; da Silva, M. I. N.; Cotta, M. A.; Graeff, C. F. O. *J. Non-Cryst. Solids* **2004,** *338*, 634.
9. Brenner, M.; Hearing, V. J. *Photochem. Photobiol.* **2008,** *84*, 539.
10. Ito, S.; Wakamatsu, K. Chemistry of Melanin. In *The Pimentary System;* Nordlund, J.J; Boissy, R.E; Hearing, V.J.; King, R.A.; Oetting, W.S.; Ortonne, J. Eds.; Blackwell Publishing Ltd: Malden, 2006; Second ed, pp 282-310.
11. Rozanowska, M.; Sarna, T.; Land, E. J.; Truscott, T. G. *Free Radic. Biol. Med.* **1999,** *26*, 518.
12. Meredith, P.; Sarna, T. *Pigm. Cell. Res.* **2006,** *19*, 572.
13. Clancy, C. M. R.; Simon, J. D. *Biochemistry* **2001,** *40*, 13353.
14. Watt, A. A. R.; Bothma, J. P.; Meredith, P. *Soft Matter* **2009,** *5*, 3754.
15. Lawrie, K. J.; Meredith, P.; McGeary, R. P. *Photochem. Photobiol.* **2008,** *84*, 632.
16. Abbas, M.; D'Amico, F.; Morresi, L.; Pinto, N.; Ficcadenti, M.; Natali, R.; Ottaviano, L.; Passacantando, M.; Cuccioloni, M.; Angeletti, M.; Gunnella, R. *Eur. Phys. J. E* **2009,** *28*, 285.
17. Bothma, J. P.; de Boor, J.; Divakar, U.; Schwenn, P. E.; Meredith, P. *Adv. Mater.* **2008,** *20*, 3539.
18. Bettinger, C. J.; Bruggeman, P. P.; Misra, A.; Borenstein, J. T.; Langer, R. *Biomaterials* **2009,** *30*, 3050.
19. Kim, E.; Liu, Y.; Baker, C. J.; Owens, R.; Xiao, S.; Bentley, W. E.; Payne, G. F. *Biomacromolecules* **2011,** *12*, 880.
20. Lee, H.; Dellatore, S. M.; Miller, W. M.; Messersmith, P. B. *Science* **2007,** *318*, 426.
21. Liu, Y.; Simon, J. D. *Pigm. Cell. Res.* **2003,** *16*, 72.
22. Zeise, L.; Murr, B. L.; Chedekel, M. R. *Pigm. Cell. Res.* **1992,** *5*, 132.
23. Chen, S.-R.; Jiang, B.; Zheng, J.-X.; Xu, G.-Y.; Li, J.-Y.; Yang, N. *Food Chemistry* **2008,** *111*, 745.
24. Tu, Y. G.; Xie, M. Y.; Sun, Y. Z.; Tian, Y. G. *Pigment Cell Melanoma Res.* **2009,** *22*, 134.
25. Cubo, M. T.; Buendia-Claveria, A. M.; Beringer, J. E.; Ruiz-Sainz, J. E. *Appl. Environ. Microbiol.* **1988,** *54*, 1812.
26. Sarna Tadeusz, Swartz, H. A. The Physical Properties of Melanins. In *The Pimentary System;* Nordlund, J.J; Boissy, R.E; Hearing, V.J.; King, R.A.; Oetting, W.S.; Ortonne, J. Eds.; Blackwell Publishing Ltd: Malden, 2006; Second ed, pp 311-341.
27. Dunford, R.; Land, E. J.; Rozanowska, M.; Sarna, T.; Truscott, T. G. *Free Radic. Biol. Med.* **1995,** *19*, 735.
28. Ju, K.-Y.; Lee, Y.; Lee, S.; Park, S. B.; Lee, J.-K. *Biomacromolecules* **2011,** *12*, 625.
29. Goncalves, P. J.; Baffa, O.; Graeff, C. F. O. *J. Appl. Phys.* **2006,** *99*, 104701.
30. Simonovic, B.; Vucelic, V.; Hadzi-Pavlovic, A.; Stepien, K.; Wilczok, T.; Vucelic, D. *J. Therm. Anal. Calorim.* **1990,** *36*, 2475.
31. Gómez-Marín, A. M.; Sánchez, C. I. *J. Non-Cryst. Solids* **2010,** *356*, 1576.
32. Hong, L.; Simon, J. D. *J. Phys. Chem. B* **2007,** *111*, 7938.
33. Holland, B. J.; Hay, J. N. *Polym. Degrad. Stabil.* **2002,** *77*, 435.
34. Hu, Y.-H.; Chen, C.-Y. *Polym. Degrad. Stabil.* **2003,** *82*, 81.

35. Kashiwagi, T.; Inaba, A.; Brown, J. E.; Hatada, K.; Kitayama, T.; Masuda, E. *Macromolecules* **1986,** *19*, 2160.
36. Manring, L. E.; Sogah, D. Y.; Cohen, G. M. *Macromolecules* **1989,** *22*, 4652.
37. Hirata, T.; Kashiwagi, T.; Brown, J. E. *Macromolecules* **1985,** *18*, 1410.
38. Ozawa, T. *J. Therm. Anal. Calorim.* **1970,** *2*, 301.
39. Flynn, J. H.; Wall, L. A. *J. Polym. Sci. Part B: Polym. Lett.* **1966,** *4*, 323.
40. Waldman, W. R.; De Paoli, M. A. *Polym. Degrad. Stabil.* **1998,** *60*, 301.
41. Peterson, J. D.; Vyazovkin, S.; Wight, C. A. *Macromol. Chem. Phys.* **2001,** *202*, 775.

Chapter 3: Melanin Multilayer Films with Broadband UV Protection Behavior

3.1 INTRODUCTION

Melanin shows promise as a widely available biocompatible polymer with a myriad of useful properties, such as semiconduction,[1] broadband UV absorption,[2-4] anti-oxidant behavior,[5] photoelectric behavior,[3] and free-radical scavenging.[5] In nature, melanin is responsible for the brown-black coloring in human pigmentation[3] and it protects the skin, hair and eyes from the harmful effects of UV radiation.[4, 6] Historically, melanin has been very difficult to adapt for broad use in materials applications as it is nearly completely insoluble in all common solvents and usually exists as granular aggregates.[3, 5] However, recent research has focused on producing synthetic melanin, which is soluble in organic solvents[5] enabling processability into pure melanin thin films by spin coating or drop casting.[7] A particularly attractive recent development is that synthetic melanin has been produced which is dispersible in mildly basic water,[5] which allows for melanin to be effectively processed without organic solvents.

Layer-by-layer (LbL) assembly is a powerful and versatile technique to deposit polymers, nanoparticles, or colloids from aqueous solutions into functional thin films which are typically no thicker than 1 μm.[8-9] These nanocoatings are deposited by alternately exposing a substrate to positively and negatively charged polyelectrolytes that are adsorbed as nanolayers, a pair of which is known as a "bilayer," (BL) most often through electrostatic attractions.[8] This technique has been used to produce thin films which can be anti-flammable,[10] impermeable to gasses,[11] capable of separating hydrogen,[12] antimicrobial,[13] super-hydrophilic,[14] anti-reflective,[15] among many other useful properties.

In this work, thin films of synthetic melanin and poly(allylamine hydrochloride) (PAH) were fabricated via layer-by-layer assembly in ambient conditions from dilute

aqueous solutions to produce extremely thin, well-adhered films with broad UV-protection capabilities (**Figure 3.1a**). As far as we are aware, this is the first time melanin has been deposited as a durable thin film from water. These coatings absorb over 63% of the UV light that is most damaging to human eyes (265 nm < λ < 275 nm)[16] with only a 108 nm coating added (**Figure 3.1b**). In addition, these films can be used to reduce UV damage to a thin conductive organic film of poly(3,4-ethylenedioxythiophene):poly(styrene sulfonate) (PEDOT:PSS). This novel method of producing melanin thin films will hopefully allow for a wide variety of uses for melanin to be realized.

3.2 PAH/MELANIN LAYER-BY-LAYER ASSEMBLY

Melanin-containing multilayer films were initially grown on silicon wafers and thickness was measured using ellipsometry and profilometry, as shown in **Figure 3.2a**. There was excellent agreement between the two methods. The melanin-PAH multilayer films grew in a linear manner, depositing 1.7 nm per bilayer. The mass of the films was determined after each deposition step using quartz crystal microbalance (QCM), shown in **Figure 3.2b**, and the concentration of each component was calculated as in previous work.[10-11] The films contained 37 wt% melanin and the melanin concentration was independent of the number of bilayers. This is a significant enhancement over previous work where only 5 wt% melanin was melt blended with common thermoplastic polymers that also exhibited some visible melanin aggregation.[5]

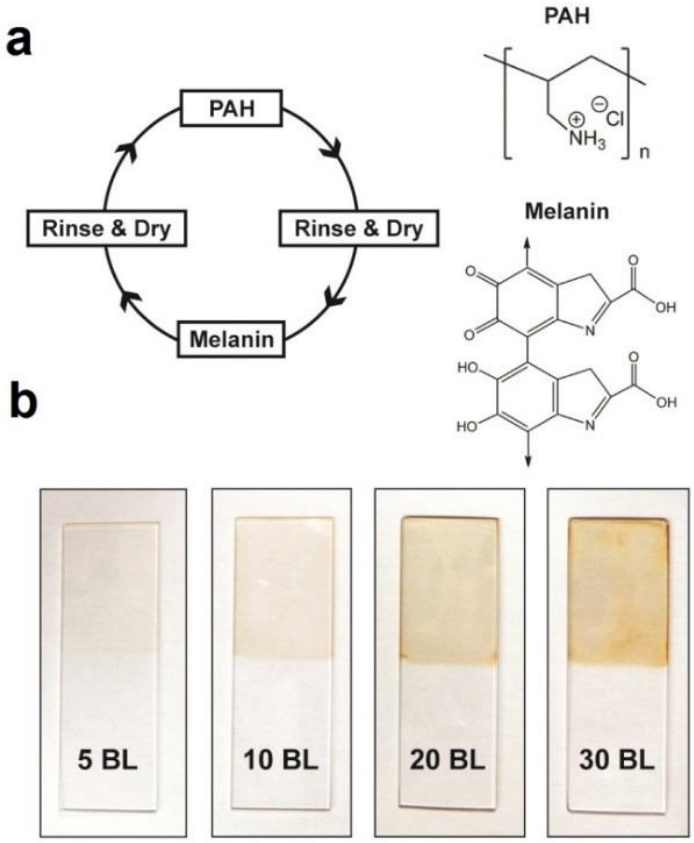

Figure 3.1: (a) Schematic of the layer-by-layer (LbL) deposition process with associated chemical structures of deposited polyelectrolytes, and (b) photographs of different numbers of bilayers (BL) in the multilayer film deposited on quartz. Reprinted with permission from Guin, T. and Cho, J. H. et al., ACS Macro Lett. 2015, 4, 335. Copyright 2015 American Chemical Society.

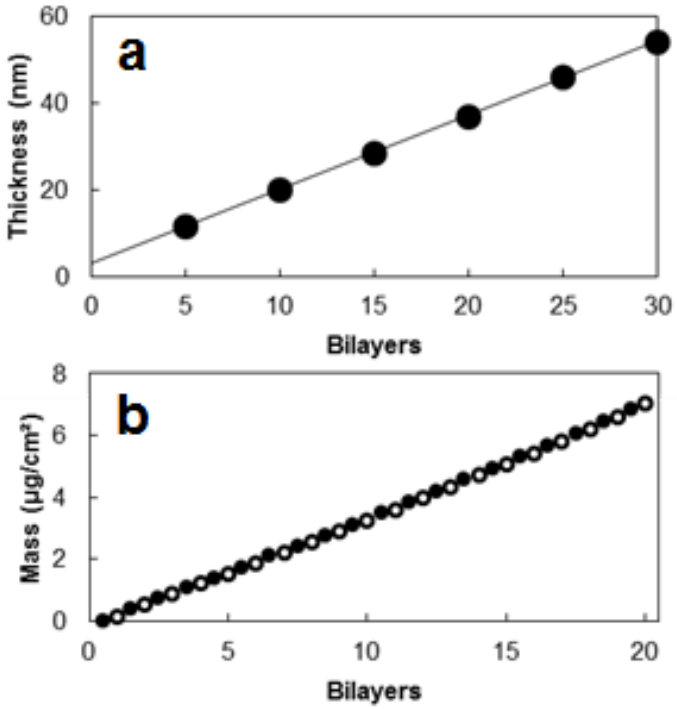

Figure 3.2: (a) Thickness of melanin-PAH multilayer films measured by profilometry and ellipsometry as a function of the number of bilayers, and (b) mass deposited measured by QCM as a function of the number of bilayers (filled points: PAH, open points: melanin). Reprinted with permission from Guin, T. and Cho, J. H. et al., ACS Macro Lett. 2015, 4, 335. Copyright 2015 American Chemical Society.

3.3 SURFACE TOPOGRAPHY OF MULTILAYER FILMS

To determine surface topography of the films, atomic force microscopy (AFM) images were obtained for multilayer films on quartz substrates (**Figure 3.3**). A five bilayer film is composed of small islets on top of a thinner film, which is indicative of a pattern of "island-growth" in the beginning stages of deposition.[17] The islets become larger with additional bilayers, eventually coalescing into large islands (**Figure 3.3b**). As the film preferentially grows outward from the initial islets, the film roughness increases with each deposition (R_a (5 BL) = 3.4 nm, R_a (30 BL) = 9.3 nm).[17] Previous work with melanin thin films spin coated from dimethylsulfoxide (DMSO) reported a surface roughness less than

0.4 nm at a film thickness of 30 nm.[18] The authors theorize that the low surface roughness of the spin coated melanin film is due to self-arrangement of the melanin during solvent evaporation.[18] The relatively higher roughness of the layer-by-layer deposited films is possibly due to hindrance effects of the PAH layers, which the melanin is adsorbed to. The electrostatic forces between the PAH and the melanin likely prevent the melanin from rearranging into a smoother film, and instead the film maintains the island topography of the initial bilayers.

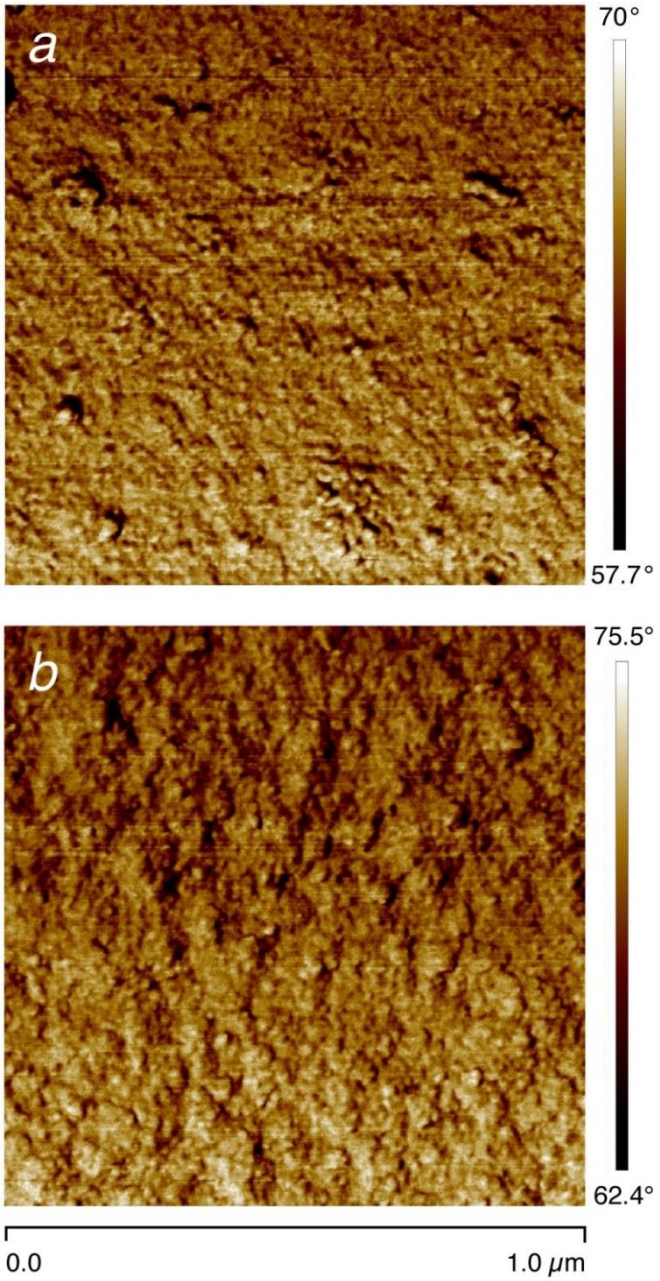

Figure 3.3: AFM phase images of (a) 5 bilayer and (b) 30 bilayer melanin-PAH multilayer films deposited on quartz substrates. Reprinted with permission from Guin, T. and Cho, J. H. et al., ACS Macro Lett. 2015, 4, 335. Copyright 2015 American Chemical Society.

3.4 OPTICAL PROPERTIES

The melanin multilayer films on quartz substrates display broadband UV light absorption from 200 - 700 nm, shown in **Figure 3.4a**. Vertebrates use melanin to prevent eye damage from short wavelength UV light, particularly from 265–275 nm,[6, 16, 19] and a 30 bilayer melanin-containing multilayer film absorbed 63% of the harmful light in this range. As a comparison, neat melanin and PAH were spin coated onto quartz from water (**Figure 3.4**). The multilayer films have optical properties very similar to natural melanin, displaying a broad absorbance of UV and visible light which decreases slightly at higher wavelengths (**Figure 3.4a**).[2-3] Spin coated melanin films displayed an additional peak at 280 nm, which is most likely due to the quinone in the melanin backbone (**Figure 3.1a**) reverting to a catechol in ambient conditions.[20] It is interesting to note that the backbone quinone melanin in the multilayer film did not revert back to a catechol in dry conditions, which may be due to interactions between the amine of the PAH and the quinone. The absorbance spectrum of the melanin multilayer films is atypical of an organic chromophore and would typically be associated with scattering effects due to aggregated particles in the film.[3] However, melanin is known to display this broadband absorption curve even when well-solvated and, combined with the nature of the deposition method, is consistent with well-dispersed melanin in the multilayer film.[2] **Figure 3.4b** shows that the absorbance of the films at various wavelengths of UV light is directly proportional to the thickness of the deposited films. This is additional evidence that the melanin concentration of the film remains constant with increasing bilayers. Interestingly, though the multilayer film is only 37 wt% melanin as determined by QCM, the total absorbance of the film is remarkably similar to a spin coated film composed entirely of melanin of similar thickness (**Figure 3.4b**). As the UV absorbance of the film is primarily derived from the melanin content, we theorize that the total melanin content of the films is similar between the spin coated

and LbL films, despite the additional PAH in the LbL films. It is well established that the conformation of the polyelectrolytes in LbL-assembled films allows for very dense films, with densities exceeding the densities of the individual components. [8, 11-12]

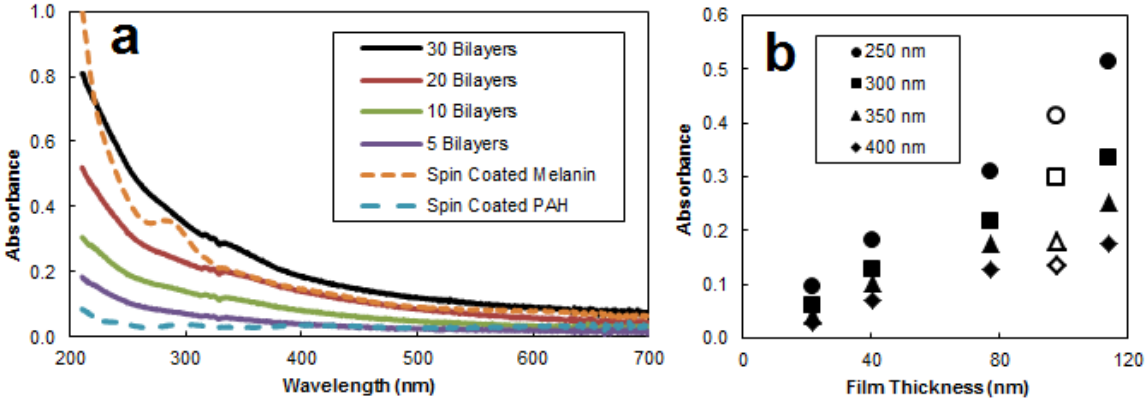

Figure 3.4: (a) Absorbance spectrum of various bilayers of melanin-PAH multilayer films and spin coatings of the constituent polyelectrolytes on fused quartz, and (b) the absorbance of the multilayer films (filled points) and spin coated pure melanin films (open points) as a function of film thickness. Reprinted with permission from Guin, T. and Cho, J. H. et al., ACS Macro Lett. 2015, 4, 335. Copyright 2015 American Chemical Society.

3.5 UV Protection to Electrically Conductive Polymer Films

UV absorbance and anti-oxidant properties of melanin are well-established,[3] so melanin-PAH multilayer thin films were deposited on spin coated PEDOT:PSS films to impart UV protection. PEDOT:PSS films were exposed to a 400 W mercury arc lamp which degraded the film over time, and the degradation was continuously monitored by electrical resistance, as shown in **Figure 3.5**. Uncoated PEDOT:PSS quickly degrades in UV light,[21-22] becoming 80% more resistive after 1 hour of exposure (**Figure 3.5a**). The degradation of the film initially increased rapidly, but approached a steady state after 10 min in which the resistance increased linearly with time. This increase in resistance of the PEDOT:PSS is due to over-oxidation, which causes chain scission and reduced π

transitions of the PEDOT and desulfonation of the PSS.[21] When the melanin multilayer film was added on top of the PEDOT:PSS, the UV damage to the PEDOT:PSS was significantly reduced. With 30 bilayers added, the film increased the longevity of the PEDOT:PSS by 550% (**Figure 3.5**). The decrease in UV damage was directly proportional to the thickness of the multilayer film (**Figure 3.5b**). It should be noted that the melanin multilayer film was not itself conductive, and only marginally decreased the conductivity of the underlying PEDOT:PSS. Synthetic melanin has previously been shown to have powerful anti-oxidant properties which can be used for a myriad of purposes, such as enhancing the thermal stability of polymers.[5] Similarly, we have shown that the anti-oxidant and UV-absorbing properties of synthetic melanin can be used to improve the UV stability of conducting polymers.

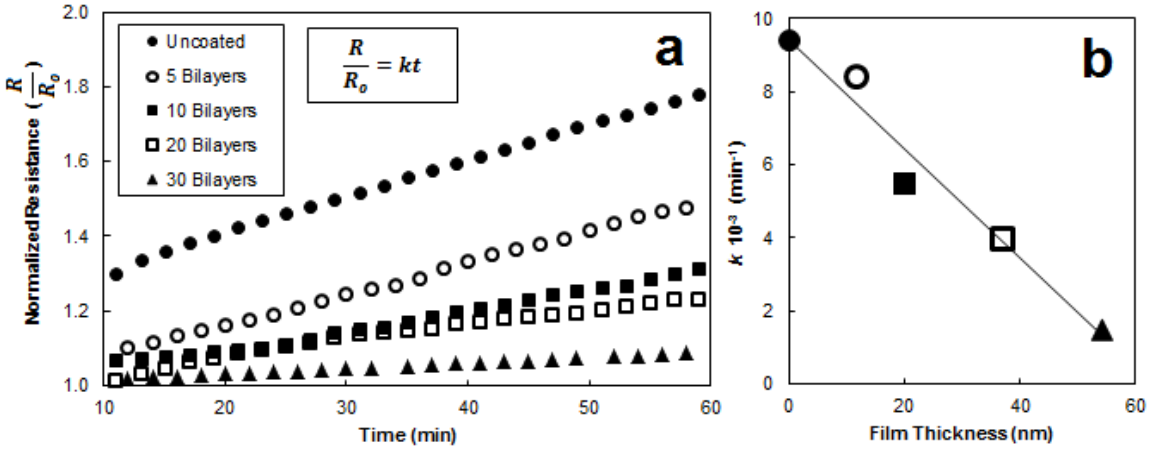

Figure 3.5: (a) Resistance of spin coated PEDOT:PSS films coated with melanin-PAH multilayer films as a function of time exposed to UV light, and (b) the associated slope of the resistance as a function of melanin-PAH multilayer film thickness. Reprinted with permission from Guin, T. and Cho, J. H. et al., ACS Macro Lett. 2015, 4, 335. Copyright 2015 American Chemical Society.

3.6 CONCLUSIONS

Thin films composed of synthetic melanin and PAH were successfully fabricated via layer-by-layer assembly. A 108 nm thick film contained over 37 wt% melanin and was capable of absorbing 63% of short wavelength UV light from 265-275 nm. These films were also highly protective of organic conductive polymer films, increasing the usable time of PEDOT:PSS under UV light exposure by 550%. It is possible that layer by layer assembly will allow melanin thin films to be produced conformally on a variety of devices/substrates to be used as environmentally-friendly organic semiconductors, free radical scavengers, or anti-fouling agents.

3.7 EXPERIMENTAL

3.7.1 SYNTHESIS OF WATER-SOLUBLE MELANIN

Water-soluble melanin was produced by oxidative polymerization of L-3-(3,4-dihydroxyphenyl) alanine (L-dopa) according to a reported procedure.[5, 7] 33.8 g of L-dopa and 41.6 g of benzoyl peroxide were mixed together in 4.5 L of anhydrous DMSO, which was purified using activated alumina. The solution was quickly sealed and stirred at room temperature. Once the reaction was started, the solution gradually turned pink and then black in 2 hours. The reaction was stopped after 28 days and the solution was concentrated by evaporating excess DMSO at 100 ^{o}C using a rotary evaporator. Subsequently, melanin was precipitated by drop-wise addition of the concentrated melanin solution into a large quantity of acetonitrile under vigorous stirring and the resulting precipitates were retrieved by centrifugation (3600 rpm, 10 min). Finally, the material was dried under vacuum at room temperature for 2 days and then at 70 ^{o}C for 1 day until a constant weight was reached and a black powder of synthetic melanin was obtained with 85% yield.

3.7.2 LAYER-BY-LAYER DEPOSITION

Melanin solution for LbL assembly was prepared by adding 0.1 wt% synthetic melanin to 0.001 M NaOH (Sigma Aldrich, Milwaukee, WI), and sonicating in a 10 L Branson 5510 ultrasonic cleaner for 30 min. The melanin solution for spin coating was prepared by adding 10 wt% melanin to 1 M NaOH and sonicating for 30 min. After solvation, the pH of the melanin solution was adjusted to pH 10 with 1 M NaOH and the solution was used immediately, as it was found that it was not storage stable over long periods of time. PAH solution was prepared by adding either 0.1 wt% PAH (120-200 kDa, Polysciences, inc. Warrington, PA) for LbL assembly or 10 wt% for spin coating into 18 MΩ deionized (DI) water, and adjusting the pH to 10 using 1 M NaOH. LbL assembled films were constructed by alternately dipping a prepared substrate into PAH and melanin solutions, beginning with the PAH solution. The first depositions were both 5 min, while subsequent depositions were 1 min each. In between deposition, films were rinsed thoroughly with DI water and dried with a stream of filtered air. After the desired number of bilayers were deposited, the films were dried for 30 min at 70˚C to remove excess moisture.

3.7.3 PREPARATION OF PEDOT/PSS FILMS COATED WITH PAH/MELANIN MULTILAYER FILMS

UV protection of the LbL films was measured on poly(3,4-ethylenedioxythiophene):poly(styrene sulfonate) (PEDOT:PSS) (Clevious PH 1000, Heraeus, West Conshohocken, PA) which had been spin coated on glass slides. The glass slides were spin coated with a 1.3 wt% PEDOT:PSS solution for 60 sec at 3000 RPM using a WS-650 spin coater (Laurell Technologies, North Wales, PA) and then annealed with the methanol “drop then drip” method outlined by Alemu et. al. LbL assembled films were then deposited on top of the PEDOT:PSS and two leads, 16 mm apart, were connected to

the coated slide using clamps and silver adhesive (Electron Microscopy Sciences, Hatfield, PA). The slides were exposed to a 400 W mercury lamp and the resistance was measured using a Keithley 2000 Multimeter (Cleveland, OH). The temperature of the slide was kept at 65°C using a 12 W fan.

3.7.4 Characterization of Film Growth, Structure, and Properties

Thickness of the film was measured on (1 0 0) silicon wafers, cleaned with a 10 min plasma treatment using a PDC-32G plasma cleaner (Harrick Plasma, Ithaca, NY) with both a P-6 profilometer (KLA-Tencor, Milpitas, CA) and an alpha-SE elliposometer (J.A. Woollam Co., Inc., Lincoln, NE). Mass of the films was measured on Ti/Au crystals using a Maxtek Research QCM from Infinicon (East Syracuse, NY), with a frequency range of 3.8-6 MHz. The UV absorption and roughness of the films and was measured on fused quartz slides (Structure Probe, Inc., West Chester, PA) which had been cleaned using 30 min 4:1 piranha treatment (caution! Piranha solution reacts violently with organic materials.) AFM images were taken using a Bruker Dimension Icon AFM (Billerica, MA) in intermittent tapping mode. The UV absorption of the films was measured using a USB2000 UV-Vis spectrometer (Ocean Optics, Dunedin, FL) from 200 to 900 nm.

3.8 References

1. McGinness, J.; Corry, P. *Science* **1974,** *183*, 853-855.
2. Stark, K. B.; Gallas, J. M.; Zajac, G. W.; Eisner, M.; Golab, J. T. *J. Phys. Chem. B 2* **2003,** *107*, 11558-11562.
3. Meredith, P.; Sarna, T. *Pigment cell res.* **2006,** *19*, 572-94.
4. Kim, B. G.; Kim, S.; Lee, H.; Choi, J. W. *Chem. Mater.* **2014,** *26*, 4757-4764.
5. Shanmuganathan, K.; Cho, J. H.; Iyer, P.; Baranowitz, S.; Ellison, C. J. *Macromolecules* **2011,** *44*, 9499-9507.
6. Hill, H. Z.; Li, W.; Xin, P.; Mitchell, D. L. *Pigment cell res.* **1997,** *10*, 158-161.
7. Deziderio, S. N.; Brunello, C. A.; da Silva, M. I. N.; Cotta, M. A.; Graeff, C. F. O. J. Non-Cryst. Solids 2004, 338, 634.

8. Bertrand, P.; Jonas, A.; Laschewsky, A.; Legras, R. *Macromol. Rapid Comm.* **2000,** *21*, 319-348.
9. Lvov, Y.; Decher, G.; Mohwald, H., Assembly. *Langmuir* **1993,** *9*, 481-486.
10. Cain, A. A.; Nolen, C. R.; Li, Y.-C.; Davis, R.; Grunlan, J. C. *Polym. Degrad. Stab.* **2013,** *98*, 2645-2652.
11. Priolo, M. A.; Gamboa, D.; Holder, K. M.; Grunlan, J. C. *Nano Lett.* **2010,** *10*, 4970-4.
12. Yang, Y. H.; Bolling, L.; Priolo, M. A.; Grunlan, J. C. *Adv. Mater.* **2013,** *25*, 503-8.
13. Joshi, M.; Khanna, R.; Shekhar, R.; Jha, K. *J. Appl. Polym. Sci.* **2011,** *119*, 2793-2799.
14. Nuraje, N.; Asmatulu, R.; Cohen, R. E.; Rubner, M. F. *Langmuir* **2011,** *27*, 782-91.
15. Shimomura, H.; Gemici, Z.; Cohen, R. E.; Rubner, M. F. *ACS Appl. Mater. Interfaces* **2010,** *2*, 813-20.
16. Pitts, D. G.; Cullen, A. P.; Hacker, P. D. *Invest. Ophthalmol. Vis. Sci.* **2003,** *16*, 932-939.
17. Picart, C.; Lavalle, P.; Hubert, P.; Cuisinier, F. J. G.; Decher, G.; Schaaf, P.; Voegel, J.-C. *Langmuir* **2001,** *17*, 7414-7424.
18. Wünsche, J.; Cicoira, F.; Graeff, C. F. O.; Santato, C. *J. Mater. Chem. B* **2013,** *1*, 3836.
19. Gandini, S.; Autier, P.; Boniol, M. *Prog. Biophys. Mol. Biol.* **2011,** *107*, 362-6.
20. Wu, J.; Zhang, L.; Wang, Y.; Long, Y.; Gao, H.; Zhang, X.; Zhao, N.; Cai, Y.; Xu, J. *Langmuir* **2011,** *27*, 13684-91.
21. Alemu, D.; Wei, H.-Y.; Ho, K.-C.; Chu, C.-W. *Energy Environ. Sci.* **2012,** *5*, 9662.
22. Dawidczyk, T. J.; Walton, M. D.; Jang, W.-S.; Grunlan, J. C. *Langmuir* **2008,** *24*, 8314-8318.

Chapter 4: Bioinspired Catecholic Copolymers for Antifouling Surface Coatings

4.1 INTRODUCTION

Mussel-inspired catechol chemistry has attracted tremendous attention in recent years[1] for promoting adhesion of coatings on organic and inorganic surfaces,[2] modifying low surface energy substrates,[3] making free radical scavenging nanoparticles,[4] etc. It is interesting to note that the ortho-dihydroxyphenyl group, referred to as a 'catechol' group, is also a common structural feature in natural melanins derived from oxidative polymerization of 5,6-dihydroxyindole (DHI) and 5,6-dihydroxyindole-2-carboxylic acid (DHICA),[5-6] or synthetic melanin-like polymers[7] derived from different monomers like L-3-(3,4-dihydroxyphenyl)-alanine (L-dopa), dopamine, etc. (**Scheme 4.1a**). The catecholic unit is assumed to be a key structural unit responsible for many different functions of melanins and this has led to renewed interest in catechols and catechol derivatives.[1] (It is likely that quinones and catechols are present simultaneously in these molecules in a reversible manner depending on conditions.) Recent reports on mussel adhesive proteins postulate a significant role of catechol bearing L-dopa, that is present in significant quantity at the foot of *Mytilus edulis,* in the strong tethering ability of mussels to various surfaces.[2] This stimulated great interest in using catecholic molecules like dopamine for surface immobilization schemes and antifouling surfaces,[8] where the substrates were dip-coated with dopamine based initiators followed by surface initiated polymerization and grafting of a variety of polymer brushes like polyethylene glycol (PEG), and other peptidomimetic polymers.[8-9]. Recently, Jiang et al. developed a zwitterionic poly(carboxybetaine) with biomimetic adhesive catechol groups that can be applied to surfaces via the convenient "graft to" approach.[10] While these approaches used dopamine units merely for anchoring antifouling polymers like PEG to the substrate, a more recent report demonstrated that

polydopamine (PDA) coatings by themselves enhance the fouling resistance on water purification membranes.[11]

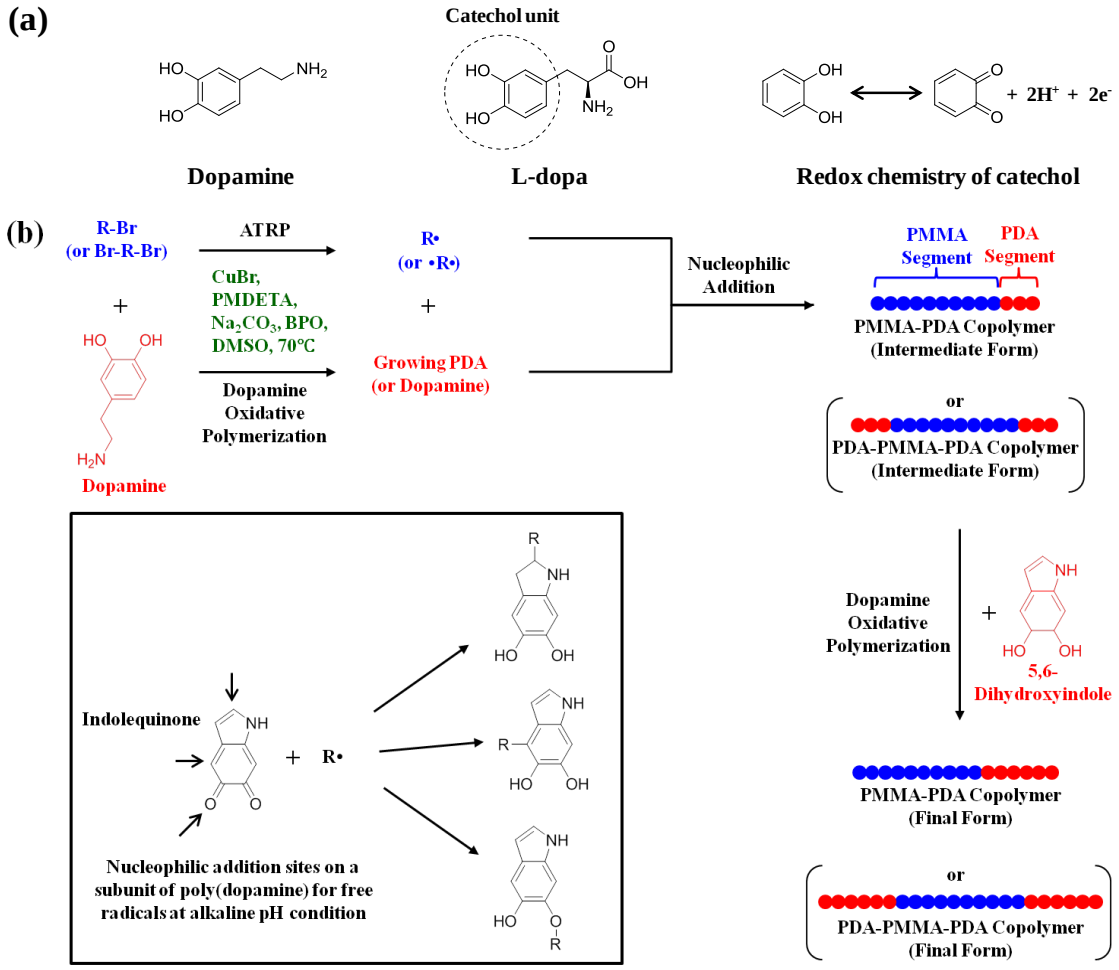

Scheme 4.1: (a) Chemical formula of dopamine and L-dopa, and redox chemistry of catechol. (b) Copper catalyzed and pH-induced nucleophilic addition of PMMA radicals to polydopamine, combined with dopamine oxidative polymerization. R-Br or Br-R-Br, prepared by ARGET ATRP, was used as a macroinitiator for generating a carbon nucleophile. R represents the PMMA chain. The boxed inset shows the nucleophilic addition sites on a subunit of PDA. Reprinted with permission from Cho, J. H. et al., ACS Appl. Mater. Interfaces 2013, 5, 3794. Copyright 2013 American Chemical Society.

Gradual growth and accumulation of biomass, commonly referred as 'biofouling' is a major problem affecting surfaces that are in contact with fluids containing proteins,

cells and microorganisms. Biofouling is also a serious problem in marine environments where the increased drag due to biofouling can result in a 40% fuel consumption increase in large commercial vessels[12] with hull corrosion and crevice formation as other costly detrimental effects. Furthermore, leaching of active ingredients such as copper and organic biocides from traditional antifouling coatings on marine vessels has led to increasingly stringent regulation of these biocidal coatings.[13] This has stimulated tremendous interest in the development of non-biocidal technologies to control fouling. Though the above-mentioned approaches which involve dip-coating substrates with dopamine or dopamine initiators (followed by growth of antifouling polymers in some cases) can be a convenient antifouling approach for smaller surfaces like filtration membranes and medical implants, they are less applicable to larger surfaces like ships, buoys, and wave energy converters. We believe that grafting PDA onto other commonly used coating polymers such as poly(methyl methacrylate) (PMMA) could enable facile spray coating of large objects such as ship hulls with polydopamine (PDA) containing polymers in the same way paints are applied, rendering them fouling resistant. To this end, we developed a synthetic approach to prepare poly(methyl methacrylate)-polydopamine diblock (PMMA-PDA) diblock and PDA-PMMA-PDA triblock copolymers only from commercially available monomers. The resulting block copolymers show enhanced chemical processability, mechanical stability and good fouling resistance. These structured polymers, derived from modern controlled polymerization methods, differ from previous approaches[14-15] where specialized dopa/dopamine containing monomers were synthesized and incorporated into random copolymers.

4.2 PMMA-PDA COPOLYMERIZATION

Our synthetic approach to make these block copolymers involved two steps. First, PMMA with a bromine end group at one or both ends of the PMMA chain was synthesized using established activators regenerated by electron transfer atom transfer radical polymerization (ARGET ATRP) procedures.[16-20] PMMA with the Br end group, obtained by precipitation and purification, was then transferred into a polymerizing dopamine solution. Copper (I) bromide was used to remove the Br end-group from PMMA macroinitiators (dormant form) and to generate a carbon nucleophile as a PMMA macro-radical (active form), which then coupled with dopamine monomers or growing PDAs in solution. Since fully grown PDAs have very limited solubility in organic solvents, one can expect poor reaction conversion when coupling already synthesized PDA with PMMA macroinitiators. In fact, direct coupling of pure PDA and PMMA-Br in dimethylsulfoxide (DMSO) was attempted and it was observed that PDA was attached to PMMA but at very low PDA content, as confirmed by UV-Vis photoabsorbance of the purified product. Radical scavenging properties of quinones and the nucleophilic addition of carbon-centered radicals to quinones are well-known.[21-22] Recent studies have described Michael addition chemistries between *o*-quinone and nucleophilic groups such as thiols and amines for mussel-inspired layer-by-layer assembly of multilayer films,[2, 23-25] and the same catechol chemistry with carbon nucleophiles as an electron donor instead of a heteroatom nucleophile was employed in this study. The dopamine or growing PDA segments linked to PMMA chains (intermediate form) were further polymerized with dopamine monomers in the solution. Eventually, PMMA-Br and Br-PMMA-Br macroinitiators resulted in PMMA-PDA diblock and PDA-PMMA-PDA triblock copolymers (final form), respectively (**Scheme 4.1b**), which were then thoroughly purified. Typically, dopamine polymerization is conducted in aqueous conditions.[2, 4] However, in this work, dopamine

oxidative polymerization was carried out in DMSO, using published procedures for the synthesis of melanin-like polymers but with slight modifications.[7, 26] Sodium carbonate was added for neutralization of dopamine-HCl to develop a basic solution.[4] The oxidized quinone form of catechol is favorable for dopamine self-polymerization and the Michael addition reaction.[2, 23-25] The oxidized form is postulated to drive the transformation of dopamine monomer toward 5,6-dihydroxyindole, which upon further oxidation and intermolecular crosslinking yields a heterogeneous polymer.[2] Wei et al. also reported that dopamine polymerization is promoted and activated at high pH in the presence of oxidants such as ammonium persulfate.[27] We also found that dopamine solutions in DMSO quickly turn black in the presence of Na_2CO_3, suggesting that an alkaline pH is essential for spontaneous dopamine polymerization (**Figure 4.1**).

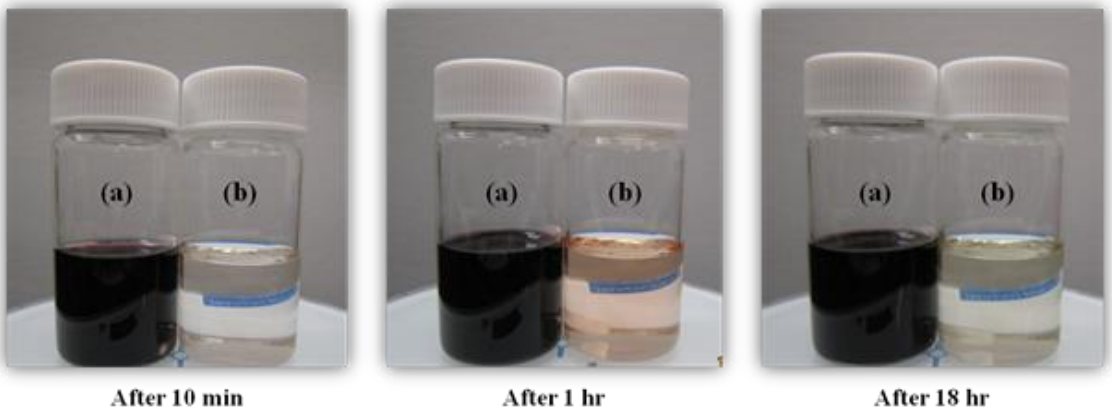

Figure 4.1: Photographs illustrating the effect of sodium carbonate on dopamine oxidative polymerization reaction: (a) with or (b) without sodium carbonate (53 mg, 0.05 M). Dopamine-HCl (75 mg, 0.40 mmol), benzoyl peroxide (BPO) (97 mg, 0.40 mmol), and DMSO (10 ml) added in all cases. Reprinted with permission from Cho, J. H. et al., ACS Appl. Mater. Interfaces 2013, 5, 3794. Copyright 2013 American Chemical Society.

SEC equipped with RI and photoabsorbance detectors was used to confirm the formation of copolymer. A homogeneous shift of the SEC RI traces towards higher molecular weight suggests PDA attachment to the PMMA macroinitiator (**Figure 4.2a, b**). While PMMA macroinitiators show no photoabsorbance (**Figure 4.2c, d**), PDA exhibits a broad band photoabsorbance in the UV and visible wavelengths. Both RI and photoabsorbance peaks appearing at the same elution volume confirms that polydopamine is covalently linked to PMMA (**Figure 4.2c, d**). (The ~0.2 min offset in peak location of the photoabsorbance trace compared to the RI trace is due to intermediate tubing between the two detectors). The absolute number average molecular weights (M_n) of PMMA-Br and Br-PMMA-Br macroinitiators were 9,600 and 14,300 g/mol, respectively, with corresponding polydispersity indices (PDI) of 1.46 and 1.49. After PDA attachment, the M_n of PMMA-PDA and PDA-PMMA-PDA were 12,900 g/mol (PDI=1.31) and 17,100 (PDI=1.48) (based on PMMA standard calibration), respectively. PDA content of PMMA-PDA and PDA-PMMA-PDA by nitrogen combustion analysis was 7.8 wt% and 9.3 wt%, respectively.

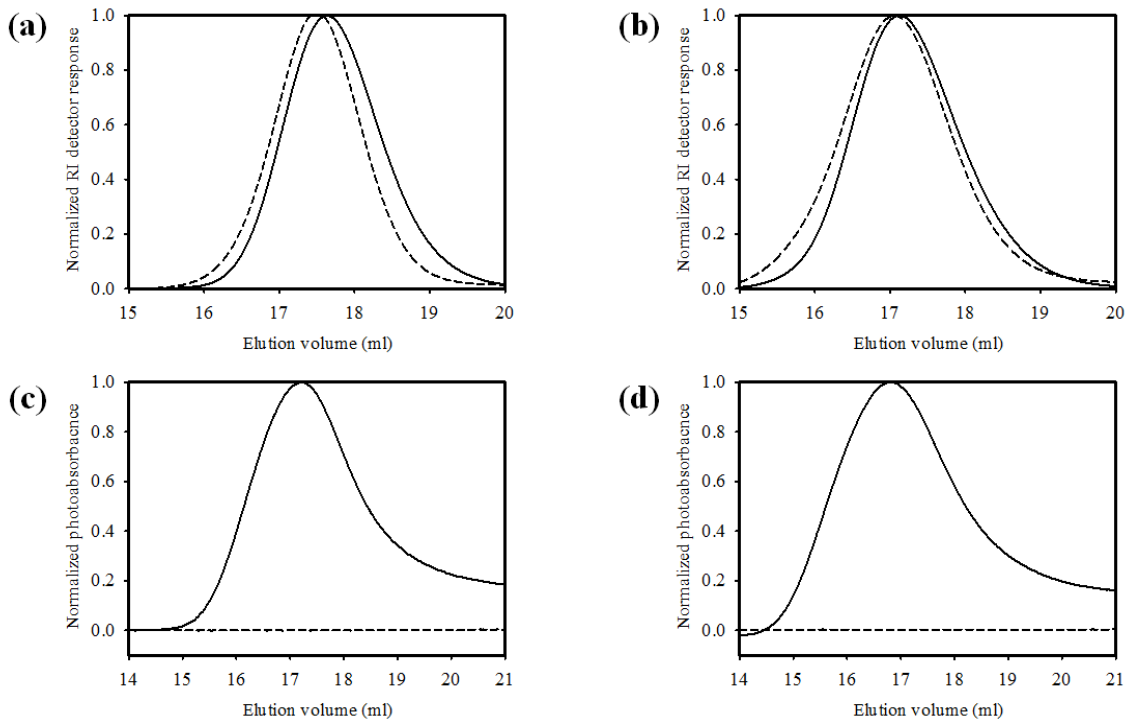

Figure 4.2: Size exclusion chromatograms (RI signal) of (a) PMMA-Br and (b) Br-PMMA-Br macroinitiators before (solid line) and after (dashed line) chain extension with PDA. SEC traces from light absorbance (λ: 450 nm) for (c) PDA-PMMA (solid line), PMMA-Br (dashed line), (d) PDA-PMMA-PDA (solid line), , and Br-PMMA-Br (dashed line). Reprinted with permission from Cho, J. H. et al., ACS Appl. Mater. Interfaces 2013, 5, 3794. Copyright 2013 American Chemical Society.

As further evidence for the successful coupling of PDA to the PMMA macroinitiator, we observed a broad band monotonic photoabsorbance for the copolymers, which is characteristic of PDA and other natural and synthetic melanins (**Figure 4.3**).[5,28] The absorbance intensities were found to increase with PDA content in the copolymer and, as expected, the PDA-PMMA-PDA triblock copolymer solutions in N,N-dimethylformamide (DMF) were much darker than PMMA-PDA at identical concentrations (inset in **Figure 4.3**). It is simply deduced that PDA-PMMA-PDA triblock copolymers could contain roughly twice the amount of PDA in each molecule compared

to PMMA-PDA diblock copolymer when Br-PMMA-Br and PMMA-Br have roughly similar molecular weights.

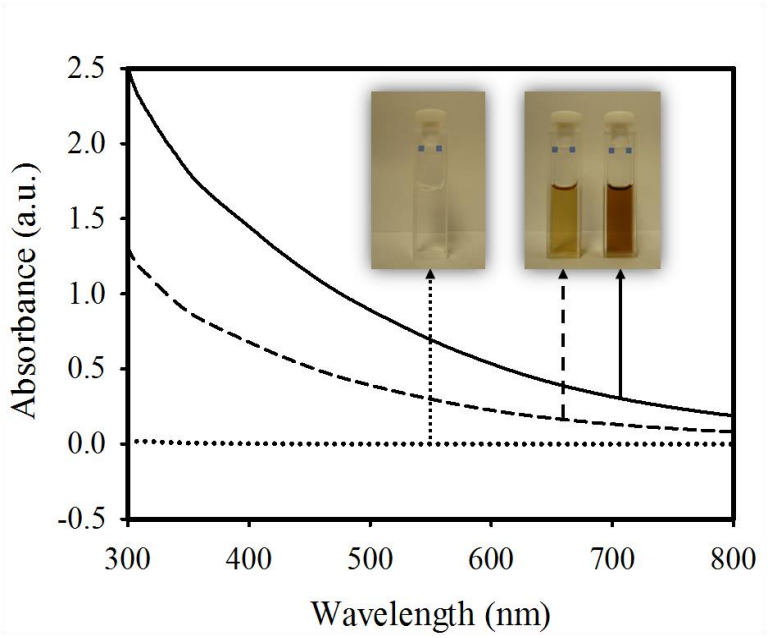

Figure 4.3: UV-vis absorbance spectra of PMMA-Br (dotted line), PMMA-PDA (dashed line), and PDA-PMMA-PDA (solid line) in DMF at 1 mg/ml. Reprinted with permission from Cho, J. H. et al., ACS Appl. Mater. Interfaces 2013, 5, 3794. Copyright 2013 American Chemical Society.

4.3 THERMAL ANALYSIS

The copolymers also displayed interesting thermal behavior (**Figures 4.4** and **Figure 4.5**). The peak decomposition of PMMA-PDA and PDA-PMMA-PDA was 16 °C and 43 °C higher, respectively, than that of neat PMMA (**Figure 4.4c, d**). PMMA is known to degrade under elevated temperature by radical initiated chain scission followed by chain unzipping.[29-32] The free radical scavenging behavior of melanin is well-known and it was recently demonstrated how this feature could be exploited in thermo-oxidative stabilization of PMMA and other thermoplastic polymers by simply blending 0.5-5 wt% natural or

synthetic melanins into the polymers.[28] It is interesting to note that coupling PDA, which has a similar catecholic group as melanin, onto the ends of PMMA also results in enhanced thermal stability. The thermal degradation mechanism of PMMA has been extensively studied, and Kashiwagi et al. suggested three steps of mass loss of free radically polymerized PMMA.[31] Initial thermal degradation at low temperature is ascribed to weak links and unsaturated end groups generated during termination of free radical polymerization, followed by random chain scission at high temperature.[28] **Figure 4.4c** and d show a substantial increase in the peak decomposition temperature after chain extension of PMMA macroinitiators by PDA, but there was little or no enhancement in the onset decomposition temperature. PMMA macroinitiators prepared by ARGET ATRP and their respective copolymers do not have unsaturated chain ends and head-to-head linkages from a chain termination step which are most susceptible to depolymerization.[30] Most of the PMMA chain ends are saturated and occupied by bromides, initiator fragments, or PDA. Therefore, the major thermal degradation mechanism of the macroinitiators and copolymers involves only random chain scission, and hence the thermal stabilization effect was observed mainly in the peak decomposition temperature, not in the onset (**Figure 4c, d**).

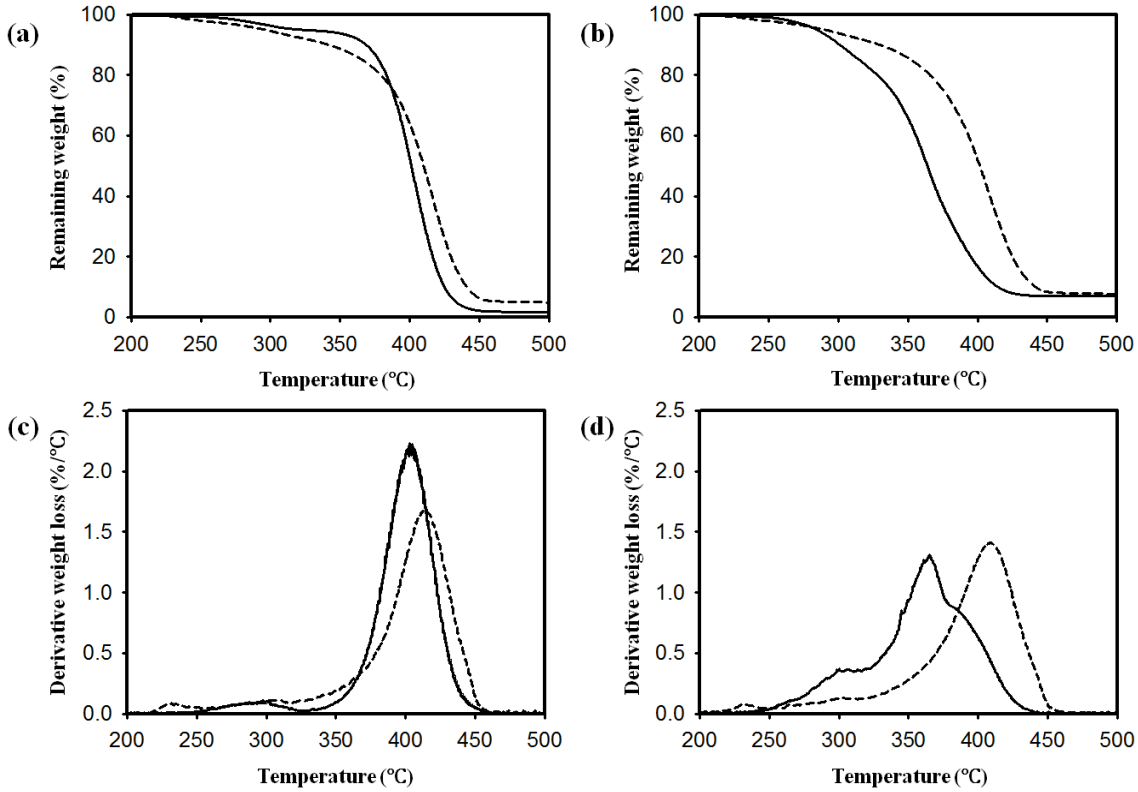

Figure 4.4: Thermogravimetric analysis of (a) PMMA-Br (solid line) and PMMA-PDA (dashed line), and (b) Br-PMMA-Br (solid line) and PDA-PMMA-PDA (dashed line). Derivative thermogravimetric analysis of (c) PMMA-Br (solid line) and PMMA-PDA (dashed line), and (d) Br-PMMA-Br (solid line) and PDA-PMMA-PDA (dashed line). All samples were heated in a nitrogen atmosphere at 20 °C/min. Reprinted with permission from Cho, J. H. et al., ACS Appl. Mater. Interfaces 2013, 5, 3794. Copyright 2013 American Chemical Society.

PMMA-PDA and PDA-PMMA-PDA copolymers also displayed two distinct glass transition temperatures (T_gs), which is a typical characteristic of a block copolymer. While PMMA macroinitiators and pure PDA have a T_g of about 110-115 °C and 100 °C respectively, the copolymers had two separate T_gs, one around 100 °C and another around 117 °C (**Figure 4.5** and **Table 4.1**) corresponding to PDA blocks (red arrows) and PMMA blocks (blue arrows), respectively. Pure PDA exhibits multistep T_g behavior whose origin is unknown but which is clearly reproduced in the block copolymers.

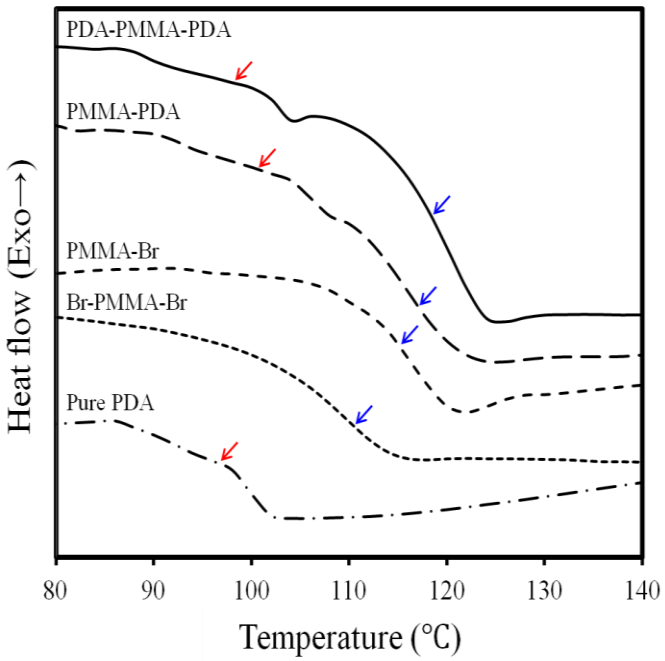

Figure 4.5: Differential scanning calorimetry (DSC) thermograms of PMMA-Br, Br-PMMA-Br, PMMA-PDA, PDA-PMMA-PDA, and pure PDA. T_g for each sample, taken as a midpoint of specific heat increment from the second heating run, was indicated by an arrow. Reprinted with permission from Cho, J. H. et al., ACS Appl. Mater. Interfaces 2013, 5, 3794. Copyright 2013 American Chemical Society.

Polymer	T_g (°C)
PMMA-Br	115
Br-PMMA-Br	111
PMMA-PDA	101 / 117
PDA-PMMA-PDA	98 / 118
Pure PDA	97

Table 4.1: Glass transition temperatures of PMMA macroinitiators and their respective copolymers. Reprinted with permission from Cho, J. H. et al., ACS Appl. Mater. Interfaces 2013, 5, 3794. Copyright 2013 American Chemical Society.

4.4 SOLVENT SOLUBILITY

One significant advantage of coupling polydopamine to a common coating polymer like PMMA is the enhanced solvent solubility of the copolymer. While PDA doesn't dissolve in many organic solvents except for moderate solubility in DMF and DMSO, which has been ascribed to strong hydrogen bonding and π-stacking among the subunits,[33] the copolymers dissolve in a variety of good solvents for PMMA (THF, DMF, cyclopentanone, toluene, acetone, methylene chloride, etc.) (**Table 4.2** and **Figure 4.6**). The enhanced solubility of these copolymers in organic solvents as compared to that of PDA has significant processing advantages. Smooth thin films could be made by spin coating the copolymer solutions from cyclopentanone or toluene on silicon wafers and glass slides, comparable to neat PMMA films, while spin-coated pure PDA films and PDA films deposited during oxidative polymerization exhibited macroscopic and microscopic surface roughness, respectively (**Figure 4.7**). These films were then used for water stability, surface characterization, and protein adsorption tests.

Solvent	Solubility		
	PMMA-PDA	PDA-PMMA-PDA	Pure PDA
Acetone	○	○	X
Acetonitrile	○	○	X
Anisole	○	○	X
Benzene	○	○	X
2-Butanone	○	○	X
Chlorobenzene	○	○	X
Chloroform	○	○	X
Cyclopentanone	○	○	X
DMF	○	○	△
DMSO	○	○	△
Methylene Chloride	○	○	X
Toluene	○	○	X
THF	○	○	X

(○: Good, △: Limited, X: Poor)

Table 4.2: Solubility chart of PMMA-PDA, PDA-PMMA-PDA, and pure PDA in various organic solvents. Good solubility was determined by a clear solution (no insoluble particles visible to the eye) at the concentration of 4 mg/ml (Experimental). Reprinted with permission from Cho, J. H. et al., ACS Appl. Mater. Interfaces 2013, 5, 3794. Copyright 2013 American Chemical Society.

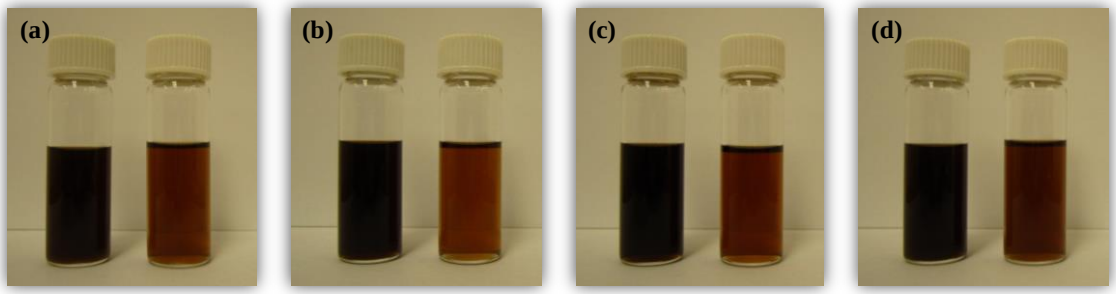

Figure 4.6: Photographs of solutions of PDA-PMMA-PDA (left) and PMMA-PDA (right) copolymers in (a) acetone, (b) cyclopentanone, (c) DMF, and (d) THF at a concentration of 4 mg/ml. Reprinted with permission from Cho, J. H. et al., ACS Appl. Mater. Interfaces 2013, 5, 3794. Copyright 2013 American Chemical Society.

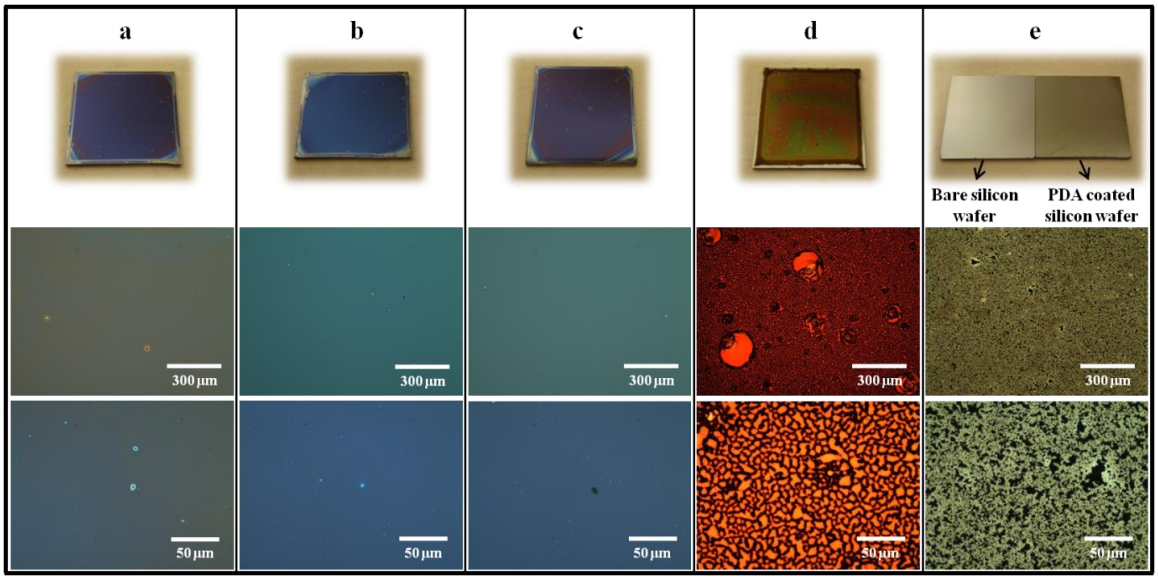

Figure 4.7: Photographs (top row) and optical microscopy images (bottom two rows) of spin-coated thin films of (a) PMMA-Br, (b) PMMA-PDA, (c) PDA-PMMA-PDA, (d) pure PDA, and (e) PDA films deposited during oxidative polymerization on silicon wafers at low (10x, middle row) and high (50x, bottom row) magnification. Each column includes three images of the same film at different imaging conditions. Reprinted with permission from Cho, J. H. et al., ACS Appl. Mater. Interfaces 2013, 5, 3794. Copyright 2013 American Chemical Society.

4.5 THIN FILM SURFACE CHARACTERIZATION

Water contact angle measurements were conducted to examine the surface wetting properties of the copolymer films. As shown in **Figure 4.8**, the static contact angles of PMMA-PDA (68.3°) and PDA-PMMA-PDA (64.7°) copolymers decreased by 6-10° compared to neat PMMA (74.6°), which indicates clearly that PDA incorporation made the surface of the copolymer coating more hydrophilic. X-ray photoelectron spectroscopy (XPS) spectra of the thin films also confirmed that the surface composition changes with incorporation of PDA (**Figure 4.9**). The N 1s peak was present in thin films of PMMA-PDA and PDA-PMMA-PDA copolymers but not PMMA-Br precursor. These two experiments serve to confirm the presence of PDA directly on the surface and suggest that strategies to attach additional antifouling polymers such as PEG to the PDA at the surface by Michael addition could be successful.

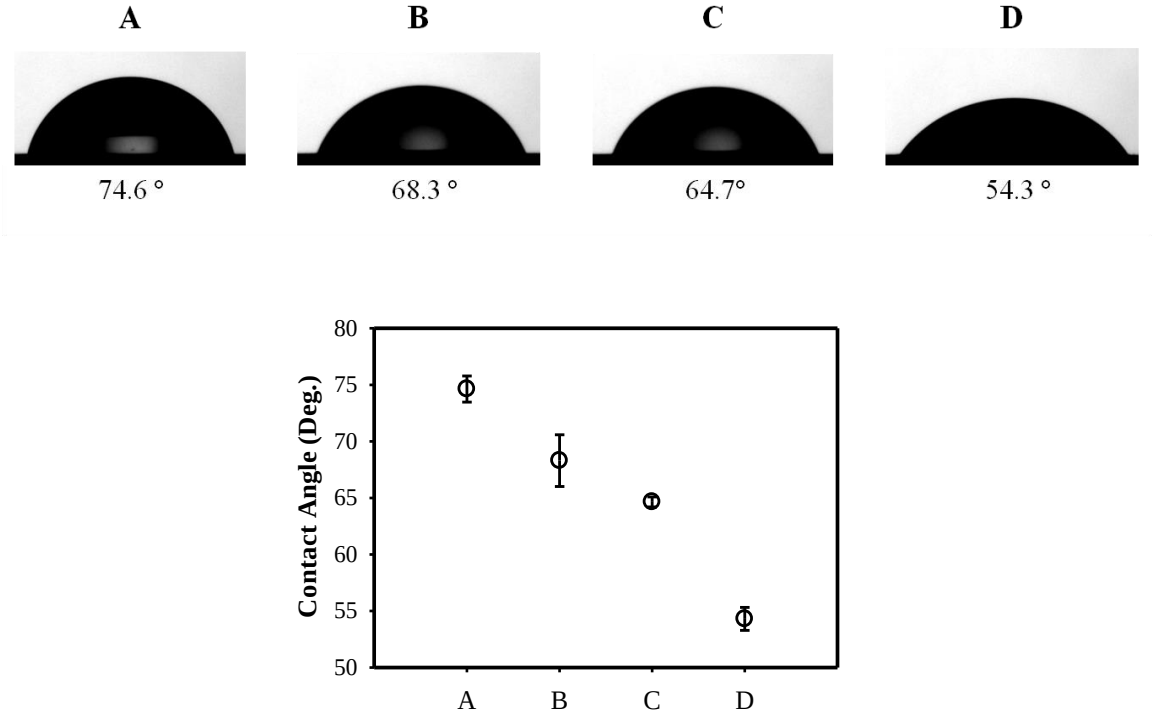

Figure 4.8: Water contact angle analysis of (A) PMMA (Mw = 350 kg/mol), (B) PMMA-PDA, (C) PDA-PMMA-PDA, and (D) PDA deposited by oxidative polymerization on silicon wafers. Error bars indicate standard deviation from ten measurements. Reprinted with permission from Cho, J. H. et al., ACS Appl. Mater. Interfaces 2013, 5, 3794. Copyright 2013 American Chemical Society.

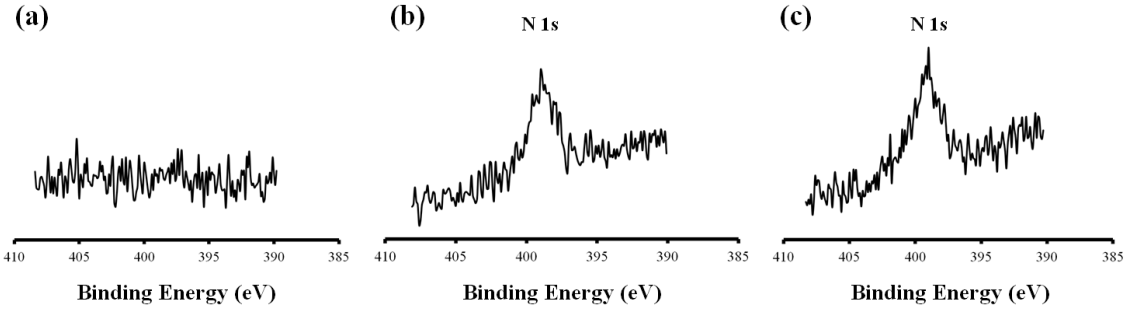

Figure 4.9: XPS spectra of (a) PMMA-Br, (b) PMMA-PDA and (c) PDA-PMMA-PDA thin films. Reprinted with permission from Cho, J. H. et al., ACS Appl. Mater. Interfaces 2013, 5, 3794. Copyright 2013 American Chemical Society.

4.6 THIN FILM PROTEIN ADSORPTION STUDIES

The copolymer films also showed strong antifouling behavior (**Figure 4.10**). Thin films of commercial PMMA and two copolymers were spin-coated, while PDA films were dip-coated on glass slides during dopamine polymerization. We used a commercial PMMA with high molecular weight as control instead of PMMA macroinitiators for this protein adsorption test due to its better stability in water. Protein adsorption behavior was determined using a previously reported procedure[34] by incubating the films in fluorescein conjugated bovine serum albumin (BSA-FL) (0.5 mg/ml in pH 7.4 phosphate buffered saline (PBS)) at 4 °C for 7 days. PMMA films showed the strongest fluorescence intensity from BSA-FL adsorption, but significantly lower intensities were measured from the copolymer films indicating less protein adsorption. Normalizing the data with the fluorescence intensity of pure PMMA films, we observed a ~40-50% reduction in protein adsorption for the copolymer films. For reference, the protein adsorption of pure PDA was also determined and we found that PDA-PMMA-PDA copolymer performs reasonably close in antifouling behavior to pure PDA deposited by dip-coating (**Figure 4.10**). Protein adsorption tests conducted for 60 mins before or after aging the films in ultrapure water for 24 h showed similar antifouling behavior (**Figure 4.11**). It is important to note here that the copolymers have much better chemical processability than PDA and can be easily spray coated onto large objects or objects with complicated geometries using common organic solvents. Another significant advantage of this block copolymer architecture is the superior stability of the PMMA-PDA and PDA-PMMA-PDA films both in pure water (pH 6.8-6.9) and slightly alkaline conditions (pH 8.5) (**Figure 4.12** and **Figure 4.13**). While films of PMMA macroinitiator precursors, having similar molecular weight to the copolymers, fractured and dewetted from the substrates upon immersion in water, the copolymer films

had superior stability in ultrapure or slightly alkaline water. Though PDA deposited on a silicon wafer by oxidative polymerization was stable in water, preformed PDA dissolved in Soluene^{TM} (Perkin-Elmer), a special solvent mixture that dissolves melanins, and then spin-coated on a silicon wafer also fractured and delaminated in water (**Figure 4.12** and **Figure 4.13**). This highlights the fact that PDA and PMMA complement each other in this copolymer architecture to result in a stable and easily processable antifouling coating. While PMMA adds mechanical stability and chemical processability, PDA provides wet substrate adhesion capabilities and antifouling behavior.[2, 35]

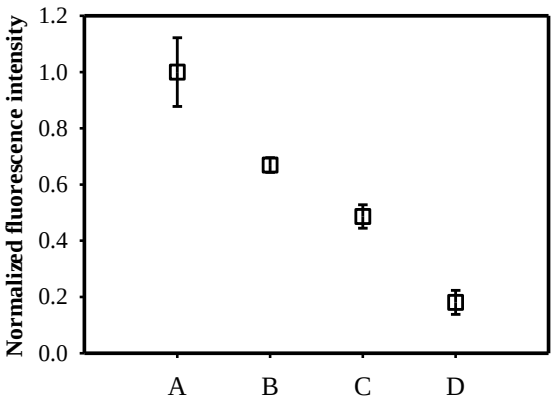

Figure 4.10: Normalized fluorescence intensity of thin films annealed at 140 °C for 10 hr under vacuum and then incubated in a 0.5mg/mL BSA-FL solution for one week at 4 ºC. (A) PMMA (M_w = 350 kg/mol), (B) PMMA-PDA, (C) PDA-PMMA-PDA, and (D) PDA deposited by oxidative polymerization after incubating with BSA-FL for a week. Reprinted with permission from Cho, J. H. et al., ACS Appl. Mater. Interfaces 2013, 5, 3794. Copyright 2013 American Chemical Society

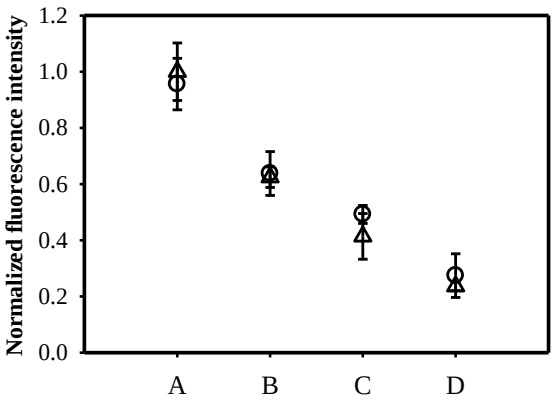

Figure 4.11: Normalized fluorescence intensity of thin films annealed at 140 °C for 10 hr under vacuum and then incubated in 1 mg/mL BSA-FL for 60 minutes (triangles), and thin films annealed at 140 °C for 10 hr under vacuum then water aged for 24 hours prior to incubation in 1 mg/mL BSA-FL (circles). Films of (A) PMMA (Mw = 350 kg/mol), (B) PMMA-PDA, (C) PDA-PMMA-PDA, and (D) PDA deposited by oxidative polymerization. Reprinted with permission from Cho, J. H. et al., ACS Appl. Mater. Interfaces 2013, 5, 3794. Copyright 2013 American Chemical Society

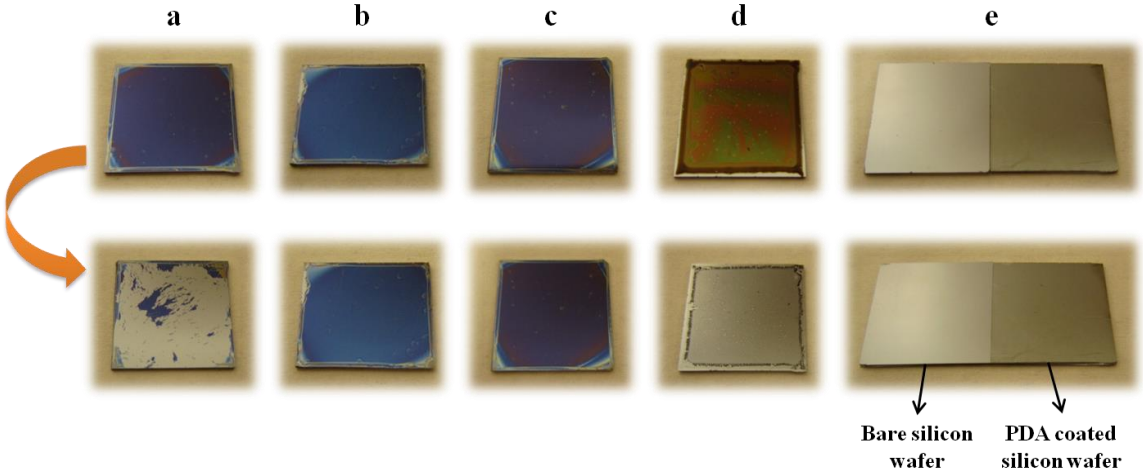

Figure 4.12: Photographs of spin-coated thin films of (a) PMMA-Br, (b) PMMA-PDA, (c) PDA-PMMA-PDA, (d) pure PDA , and (e) PDA deposited by oxidative polymerization on silicon wafer before (top) and after (bottom) immersion in water (pH 6.8-6.9) for 2 days. Reprinted with permission from Cho, J. H. et al., ACS Appl. Mater. Interfaces 2013, 5, 3794. Copyright 2013 American Chemical Society

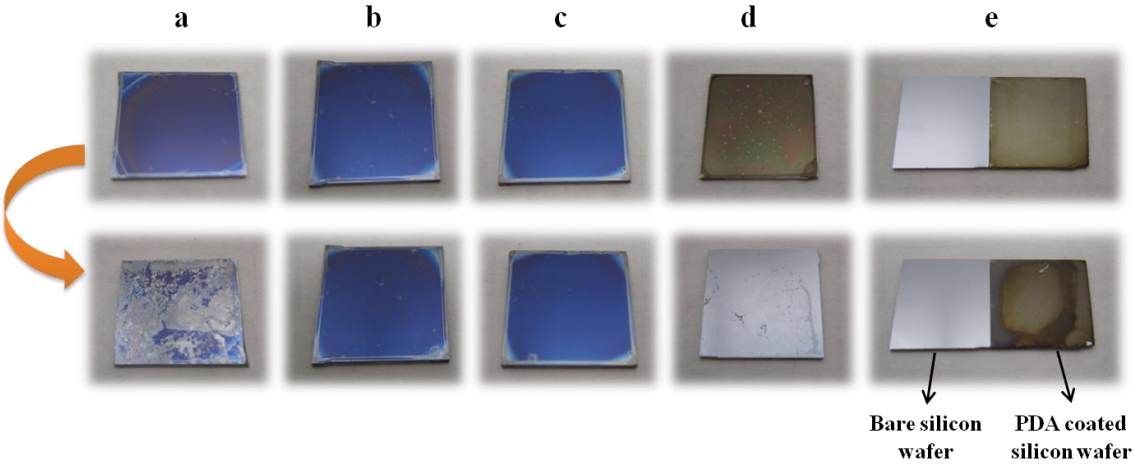

Figure 4.13: Photographs of spin-coated thin films of (a) PMMA-Br, (b) PMMA-PDA, (c) PDA-PMMA-PDA, (d) pure PDA, and (e) PDA deposited by oxidative polymerization on silicon wafer before (top) and after (bottom) immersion in 10mM Tris-HCl (pH 8.5) for a week. Reprinted with permission from Cho, J. H. et al., ACS Appl. Mater. Interfaces 2013, 5, 3794. Copyright 2013 American Chemical Society

4.7 CONCLUSIONS

A synthetic approach to prepare catecholic block copolymer architectures containing PMMA and PDA has been established. Chromatography, photoabsorbance and thermal analysis studies confirm successful coupling of PDA to PMMA ends to make block copolymers. While the solubility of PDA in organic solvents is very limited, the copolymers show very good solubility in a variety of organic solvents which could provide significant processing advantages and facilitate development of PDA containing functional materials. The copolymers can be easily spin coated into thin films and they have excellent stability in ultrapure water and slightly alkaline conditions as compared to spin coated PDA. Protein adsorption on the copolymers was 40-50% less as compared to neat PMMA and appeared to be a function of PDA content.

4.8 EXPERIMENTAL

4.8.1 MATERIALS

Anisole, methyl methacrylate (MMA), copper (II) bromide, cyclopentanone, ethyl 2-bromoisobutyrate (EBIB), and calcium hydride were purchased from Acros Organics. DMSO, tetrahydrofuran (THF), hexanes, DMF, sodium carbonate, and glass slides were obtained from Fisher Scientific. Benzene, dimethyl 2,6-dibromoheptanedioate (DMDBHD), copper (I) bromide, tin(II) 2-ethylhexanoate ($Sn(EH)_2$), dopamine-HCl, N,N,N',N'',N''-pentamethyldiethylenetriamine (PMDETA), BPO, PMMA(M_w = 350,000 g/mol), phosphate buffered saline (PBS, pH 7.4), and basic alumina were purchased from Sigma-Aldrich. Tris[2-(dimethylamino)ethyl]amine (Me_6TREN) was synthesized following a published procedure.[36] BSA-FL was purchased from Life Technologies. Ultrapure water (18.2 MΩ-cm) was obtained from a Thermo Scientific Barnstead E-pure water purification system. 10 mM Tris-HCl (pH 8.5) was prepared as needed. Anisole, MMA, and DMSO were purified by stirring with basic alumina and calcium hydride for 2 h and then filtered before use. Soluene™ was purchased from Perkin-Elmer and used as received.

4.8.2 SYNTHESIS OF PMMA MACROINITIATORS

MMA was initiated in anisole using either EBIB or DMDBHD, to synthesize a mono-functional macroinitiator (PMMA-Br) and a bi-functional macroinitiator (Br-PMMA-Br), respectively. For the synthesis of PMMA-Br, MMA (41.3 ml, 383 mmol), EBIB(625 µl, 4.3 mmol), copper (II) bromide (9.5 mg, 0.043 mmol), Me_6TREN (109 µl, 0.43 mmol), and anisol (39.7 ml) were placed in a schlenk flask and degassed by argon bubbling for 40 min. Polymerization was triggered by adding $Sn(EH)_2$ (138 µl, 0.43 mmol) to the flask. The sealed flask was placed in an oil bath maintained at 70 °C. After 10 h, the

polymerization was quenched with liquid nitrogen and the flask was opened to air. The mixture was diluted with THF and then passed through a basic alumina column three times to remove the copper complex. The polymer was precipitated by adding a large amount of hexane. Dissolution and precipitation were repeated three times and then the polymer was lyophilized using benzene. The purified polymer was analyzed using an Agilent 1100 series chromatography setup (Agilent Technologies, USA). Size exclusion chromatography (SEC) calibration curves were obtained with PMMA standards from Polymer Laboratories. In addition, Br-PMMA-Br was synthesized using a similar procedure with shorter reaction time (5 hr) and different molar ratios of MMA/DMDBHD/$CuBr_2$/Me6TREN/$Sn(EH)_2$ = 55/1/0.01/0.1/0.1 in anisole (50 wt% in the solution).

4.8.3 SYNTHESIS OF PMMA-PDA AND PDA-PMMA-PDA COPOLYMERS

For the synthesis of PMMA-PDA copolymer, two schlenk flasks were prepared simultaneously. PMMA-Br (2.5 g, 0.26 mmol) was fully dissolved in DMSO (20 ml) by stirring for 4 hr. Dopamine-HCl (1.2 g, 6.4 mmol), PMDETA (81 μl, 0.39 mmol), sodium carbonate (341.2 mg, 0.05 M), BPO (1.55 g, 6.4 mmol), and DMSO (44.4ml) were added to another schlenk flask, and also stirred for 4 hr. The solution color immediately turned black due to the pH-induced oxidative dopamine polymerization. Subsequently, oxygen was removed from both flasks by three freeze-pump-thaw cycles, and then copper (I) bromide was added to the flask containing dopamine in a glove box. PMMA-Br solution was transferred to the other flask containing copper (I) bromide catalyst to trigger the coupling reaction between Br ended PMMA and PDA, and the reaction was conducted at 70 °C for 2 days under vigorous stirring. The reaction was stopped by removing heat, quenching with liquid nitrogen, and opening the flask to air. The mixture was diluted with DMF and then run through a basic alumina column to remove the copper and ligand.

Subsequently, the resultant solution was concentrated by evaporating solvents at 100 °C under vacuum using a rotary evaporator. The polymer was precipitated by addition to a large amount of methanol and washed several times by ultrapure water and methanol to remove residual Na_2CO_3, BPO, dopamine monomer, and pure PDA unattached to PMMA. The purified copolymer was finally dried under vacuum at room temperature until a constant weight was reached. For synthesis of PDA-PMMA-PDA copolymer, two times molar ratio of dopamine-HCl and CuBr/PMDETA was used to grow PDA on both ends of PMMA. PDA-PMMA-PDA synthesis used a similar procedure with dopamine-HCl/ Br-PMMA-Br/CuBr/PMDETA = 50/1/3/3 with BPO content = 1 molar equivalent based on dopamine-HCl in DMSO solution (10 ml per 1 mmol of dopamine-HCl). Dark brown powder was obtained with 48-57% yield for both copolymers. All polymers were analyzed using an Agilent 1100 series SEC equipped with refractive index (RI) and photoabsorbance detectors.

4.8.4 CHARACTERIZATION

4.8.4.1 UV-VIS SPECTROSCOPY

Photoabsorbance of PMMA-Br, PMMA-PDA, PDA-PMMA-PDA was obtained from a 1 mg/mL solution in DMF using a UV-visible spectrophotometer (Evolution 220, Thermo Scientific).

4.8.4.2 SOLUBILITY TEST

A variety of good solvents for PMMA were chosen for this test. PMMA-PDA, PDA-PMMA-PDA and pure PDA (4 mg/mL) were separately placed in glass vials containing test solvent, and stirred for 12-24 h. Good solubility was confirmed by observing clear solution (no insoluble particles visible to the eye) at a concentration of 4 mg/mL. PDA-PMMA-PDA required a longer time to dissolve in the solvents than PMMA-

PDA since the content of PDA in PDA-PMMA-PDA is much higher than that of PMMA-PDA.

4.8.4.3 THERMOGRAVIMETRIC ANALYSIS

Thermal decomposition behavior of the copolymers was investigated using a thermogravimetric analyzer (DSC/TGA 1, Mettler Toledo). Samples were heated from 30 °C to 1000 °C at 20 °C/min under nitrogen atmosphere.

4.8.4.4 DIFFERENTIAL SCANNING CALORIMETRY

Samples were heated and scanned under a continuous nitrogen purge (50 ml/min) at 10 °C/min within the temperature range of 25-200 °C using a Mettler Toledo DSC 1. The T_g for each sample was taken as the midpoint step increment in the specific heat of the second heating cycle.

4.8.4.5 PROTEIN ADSORPTION

Solutions of PMMA (Sigma-Aldrich, M_w = 350,000 g/mol), PMMA-PDA, and PDA-PMMA-PDA in cyclopentanone were prepared at a concentration of 4 wt%. Films were spin-coated onto glass slides (25x25 mm) at 2000 rpm for 60 sec and annealed at 140 °C for 10 h under vacuum to remove residual solvents. Pure PDA thin films were formed on glass slides by dip-coating the substrate during oxidative polymerization.[2] Glass slides were placed in isopropyl alcohol and cleaned by ultrasonication, and then thoroughly rinsed with acetone and methanol. Dopamine solution (2 mg/mL) in 10mM Tris-HCl (pH 8.5) was prepared, and glass slides were immersed in the solution. The solution was continuously stirred for 3 days. The solution color turned black by alkaline pH-induced oxidative polymerization of dopamine. PDA-coated glass slides were rinsed with ultrapure water and dried with air. Film thickness measurements were carried out at multiple locations on each sample using a profilometer (Dektak 6M Stylus Profiler, Veeco

Instruments Inc.) (PMMA: 186 nm, PMMA-PDA: 105 nm, PDA-PMMA-PDA: 107 nm, PDA dip-coating: 57 nm). For short terms tests, films on glass slides were incubated in the 1 mg/ml BSA-FL solution at 4 °C for 60 min, and rinsed several times with ultrapure water.[34] For long-term protein adsorption tests, thin films were incubated with BSA-FL (0.5 mg/ml) in 7.4 pH PBS at 4°C for one week, and then gently washed several times with ultrapure water. All films were air-dried over night before fluorescence testing. All these procedures were carried out in the darkness to avoid photo-bleaching. Fluorescence spectroscopy was performed on polymer films on a Photon Technologies QuantaMaster 40 with a photomultiplier tube detection system with 2 nm excitation slits and 4 nm emission slits. The excitation and emission wavelengths used were 450 nm and 560 nm, respectively. The fluorescence intensity of each film of PMMA, PDA-PMMA, PDA-PMMA-PDA, and PDA was measured before and after immersion, and the intensity before incubation was subtracted from the intensity after immersion so as to take background fluorescence into account.[37] Finally, the intensities were normalized with the average fluorescence intensity of a protein adsorbed PMMA film (non-water aged), which had been annealed and then immediately incubated in BSA-FL solution similarly.

4.8.4.6 WATER STABILITY AND STRUCTURAL CHARACTERIZATION OF THIN FILMS

Thin films of PMMA-Br, PMMA-PDA and PDA-PMMA-PDA were spin-coated (2000rpm, 60 sec) on silicon wafers (15x15 mm) from cyclopentanone solutions (4 wt%), and annealed at 140 °C for 10 h under vacuum. In addition, free and pure PDA was synthesized according to a reported procedure,[4] and dissolved in Soluene™ (Perkin-Elmer) at a concentration of 4 wt%. The pure PDA film was then spin-coated onto a silicon wafer at 2000 rpm for 60 sec, and dried in the hood. PDA was also deposited by oxidative polymerization on a silicon wafer by simple immersion of the substrates into the

polymerizing dopamine solution (2mg/ml) in 10 mM Tris-HCl (pH 8.5) for 3 days.[2, 38] The thickness of the films was measured using a spectroscopic ellipsometer (VB-400 VASE Ellipsometer, J. A. Woollam Co., Inc.) using wavelengths from 382 to 984nm with a 65° angle of incidence (PMMA-Br: 103nm, PMMA-PDA: 114nm, PDA-PMMA-PDA: 94nm, PDA dip-coating: 52nm). The thickness of the spin-coated PDA film was difficult to measure due to macroscopic surface roughness. An optical microscope (Olympus BX60) with a camera was used to collect micrographs of the thin films at low (10x) and high (50x) magnifications. The water stability of the films was investigated by immersing them in ultrapure water for two days or in slightly alkaline 10 mM Tris-HCl (pH 8.5) for one week.

4.8.4.7 SURFACE PROPERTIES OF THIN FILMS

Water contact angles were measured with a Ramé-Hart, inc. NRL C.A. goniometer (Model #100-00). The volume of the water drop used for the measurement was 6 µl. An X-ray photoelectron spectroscopy (XPS, KRATOS Axis Ultra) instrument using a monochromatic Al Kα X-ray source (hν = 1486.5 eV) was used to analyze the surface composition of the films. The photoelectron take-off angle was normal to the surface of the sample and 45° with respect to the X-ray beam. High resolution spectra were collected and the pressure in the analysis chamber was typically 2x10-9 Torr during data acquisition.

4.9 REFERENCES

1. Ye, Q.; Zhou, F.; Liu, W. *Chem. Soc. Rev.* **2011**, *40*, 4244-4258.
2. Lee, H.; Dellatore, S. M.; Miller, W. M.; Messersmith, P. B. *Science* **2007**, *318*, 426-430.
3. Kim, B. H.; Lee, D. H.; Kim, J. Y.; Shin, D. O.; Jeong, H. Y.; Hong, S.; Yun, J. M.; Koo, C. M.; Lee, H.; Kim, S. O. *Adv. Mater.* **2011**, *23*, 5618-5622.
4. Ju, K. Y.; Lee, Y.; Lee, S.; Park, S. B.; Lee, J. K. *Biomacromolecules* **2011**, *12*, 625-632.
5. d'Ischia, M.; Napolitano, A.; Pezzella, A.; Meredith, P.; Sarna, T. *Angew. Chem., Int. Ed.* **2009**, *48*, 3914-3921.

6. Watt, A. A. R.; Bothma, J. P.; Meredith, P. *Soft Matter* **2009**, *5*, 3754-3760.
7. Deziderio, S. N.; Brunello, C. A.; da Silva, M. I. N.; Cotta, M. A.; Graeff, C. F. O. *J. Non-Cryst. Solids* **2004**, *338*, 634-638.
8. Dalsin, J. L.; Messersmith, P. B. *Mater. Today* **2005**, *8*, 38-46.
9. Statz, A. R.; Meagher, R. J.; Barron, A. E.; Messersmith, P. B. *J. Am. Chem. Soc.* **2005**, *127*, 7972-7973.
10. Gao, C. L.; Li, G. Z.; Xue, H.; Yang, W.; Zhang, F. B.; Jiang, S. Y. *Biomaterials* **2010**, *31*, 1486-1492.
11. McCloskey, B. D.; Park, H. B.; Ju, H.; Rowe, B. W.; Miller, D. J.; Chun, B. J.; Kin, K.; Freeman, B. D. *Polymer* **2010**, *51*, 3472-3485.
12. Chambers, L. D.; Stokes, K. R.; Walsh, F. C.; Wood, R. J. K. *Surf. Coat. Technol.* **2006**, *201*, 3642-3652.
13. Yebra, D. M.; Kiil, S.; Dam-Johansen, K. *Prog. Org. Coat.* **2004**, *50*, 75-104.
14. Lee, H.; Lee, B. P.; Messersmith, P. B. *Nature* **2007**, *448*, 338-U334.
15. Yu, M. E.; Deming, T. J. *Macromolecules* **1998**, *31*, 4739-4745.
16. Huang, Z. X.; Zhang, Y. M.; Li, H.; Luan, Y. H.; Liu, Y. G. *J. Polym. Sci., Part A: Polym. Chem.* **2008**, *46*, 1416-1426.
17. Kwak, Y.; Matyjaszewski, K. *Polym. Int.* **2009**, *58*, 242-247.
18. Min, K.; Gao, H. F.; Matyjaszewski, K. *Macromolecules* **2007**, *40*, 1789-1791.
19. Jakubowski, W.; Matyjaszewski, K. *Angew. Chem., Int. Ed.* **2006**, *45*, 4482-4486.
20. Jakubowski, W.; Min, K.; Matyjaszewski, K. *Macromolecules* **2006**, *39*, 39-45.
21. Hiemenz, P. C.; Lodge,T. P. *Polymer Chemistry*, 2nd ed.; CPC Press: Boca Raton, FL, 2007.
22. Moad, G.; Solomon, D. H. *The Chemistry of Free Radical Polymerization*, 1st ed.; Pergamon: Tarrytown, NY, 1995.
23. Pop-Georgievski, O.; Popelka, S.; Houska, M.; Chvostova, D.; Proks, V.; Rypacek, F. *Biomacromolecules* **2011**, *12*, 3232-3242.
24. Wu, J. J.; Zhang, L.; Wang, Y. X.; Long, Y. H.; Gao, H.; Zhang, X. L.; Zhao, N.; Cai, Y. L.; Xu, J. *Langmuir* **2011**, *27*, 13684-13691.
25. Xu, L. Q.; Yang, W. J.; Neoh, K. G.; Kang, E. T.; Fu, G. D. *Macromolecules* **2010**, *43*, 8336-8339.
26. da Silva, M. I. N.; Deziderio, S. N.; Gonzalez, J. C.; Graeff, C. F. O.; Cotta, M. A. *J. Appl. Phys.* **2004**, *96*, 5803-5807.
27. Wei, Q.; Zhang, F. L.; Li, J.; Li, B. J.; Zhao, C. S. *Polym. Chem.* **2010**, *1*, 1430-1433.
28. Shanmuganathan, K.; Cho, J. H.; Iyer, P.; Baranowitz, S.; Ellison, C. J. *Macromolecules* **2011**, *44*, 9499-9507.
29. Holland, B. J.; Hay, J. N. *Polym. Degrad. Stab.* **2002**, *77*, 435-439.
30. Hu, Y. H.; Chen, C. Y. *Polym. Degrad. Stab.* **2003**, *82*, 81-88.
31. Kashiwagi, T.; Inaba, A.; Brown, J. E.; Hatada, K.; Kitayama, T.; Masuda, E. *Macromolecules* **1986**, *19*, 2160-2168.
32. Manring, L. E.; Sogah, D. Y.; Cohen, G. M. *Macromolecules* **1989**, *22*, 4652-4654.
33. Dreyer, D. R.; Miller, D. J.; Freeman, B. D.; Paul, D. R.; Bielawski, C. W. *Langmuir* **2012**, *28*, 6428-6435.

34. Wang, H.; Li, L. L.; Tong, Q.; Yan, M. D. *ACS Appl. Mater. Interfaces* **2011**, *3*, 3463-3471.
35. Lee, H.; Scherer, N. F.; Messersmith, P. B. *Proc. Natl. Acd. Sci. U. S. A.* **2006**, *103*, 12999-13003.
36. Fu, G. D.; Xu, L. Q.; Yao, F.; Zhang, K.; Wang, X. F.; Zhu, M. F.; Nie, S. Z. *ACS Appl. Mater. Interfaces* **2009**, *1*, 239-243.
37. Taylor, M.; Urquhart, A. J.; Anderson, D. G.; Williams, P. M.; Langer, R.; Alexander, M. R.; Davies, M. C. *Macromol. Rapid Commun.* **2008**, *29*, 1298-1302.
38. Zhu, B. C.; Edmondson, S. *Polymer* **2011**, *52*, 2141-2149.

Chapter 5: Polydopamine-Assisted BCP Lithography on Soft Material Surfaces

5.1 INTRODUCTION

Block copolymers (BCPs) have gained considerable attention over the past several decades due to their ability to self-assemble into well-ordered morphologies on the 1-100 nm size scale. BCPs have been incorporated with metal nanocomposites to create mesoporous metallic materials,[1] used for stimuli-responsive drug delivery,[2-3] and are being considered as a "bottom-up" lithography supplement in nanolithography applications,[4] among many others.

The use of BCPs to supplement existing lithographic technology has been highlighted often in the microelectronics industry as a potential method to pattern ever-smaller features that are parts of circuits. Other potential applications in magnetic storage media, require isolated small, regularly spaced features. Although BCPs can self-assemble into small features, achieving desirable patterns still require the use of traditional lithographic techniques to guide the ordering into device relevant structures. However, with intense industrial and academic interest in this technology, methods for spin-coating, orienting, and aligning BCPs on silicon substrates have been widely studied and refined, though room for improvement and innovation still exists.

In contrast, BCP lithography has not been as aggressively pursued on soft plastic platforms in spite of its enormous potential for soft lithography.[5-6] The biggest challenge in adapting BCP lithography methods for soft plastic platforms is the increased difficulty of rendering the soft substrate non-preferential for contacting any block of the BCP (i.e., a neutral surface), a condition crucial for perpendicular orientation of BCP domains. BCPs require neutral substrates, or substrates for which both blocks of the BCP have equal affinity, to spontaneously orient domains perpendicularly to the substrate surface to serve

as etch masks in later processing. Silicon substrates with native oxide have silanol groups that provide a convenient and robust surface onto which random copolymer brushes can be grafted as a neutral interfacial layer. Other substrates, such as plastics, ceramics, or carbon, among others, do not have hydroxyl surface groups. This renders these other substrates chemically inert to most if not all grafting chemistries, making surface modification and neutralization a challenging process.

A possible solution to this challenge involves mussel-inspired surface engineering strategies that have attracted much attention in recent years not only due to the diverse practical properties of catecholic polymers, such as melanins and polydopamine (PDA), but also due to their universal adhesive nature.[7-10] A critical advantage of mussel-inspired surface modification procedures is that one-step simple immersion of a substrate in a dopamine solution quickly forms a conformal and uniform functional ad-layer on virtually all types of surfaces regardless of surface topography or chemical composition.[7] This spontaneous deposition provides a multifunctional ad-layer of PDA with many surface reaction sites available for secondary reactions.[7] Through subsequent attachment chemistries,[10] this functional layer affords the creation of new interfacial environments with tailored composition, structure, and thermophysical properties, which are applicable to a variety of fields including anti-biofouling,[7] energy storage devices,[11] biomedical engineering,[12-15] nanopatterning,[16] membrane technology,[17-18] oil/water separation,[19] and many more. PDA is a mechanically robust and thermally stable material with good chemical stability; as such, it is able to withstand a variety of post processing steps.[20-21] Additionally, it is an environmentally friendly and biocompatible material, so it has an environmental advantage over other toxic, substrate dependent chemical modifiers.[22]

PDA deposition produces a smooth planar sublayer formed by a three-dimensional island growth mechanism along with heterogeneous secondary grains with sizes ranging

up to several hundred nm.[23-24] These clusters of large particles attach to the planar PDA sublayer formed during the initial stage of coating. Because of the strong wet adhesive nature of mussel-foot-protein-derived PDA, these granules are very difficult to remove from the planar surface.[23-27] These protruding surface-bound granules can cause many defects when a secondary material is layered on top of them. Therefore, a continuous and smooth functional PDA layer is highly desirable and a critical consideration for merging PDA surface engineering with BCP nanopatterning.

In this study, we report BCP self-assembly on various substrates using PDA as a "universal adhesive layer." First, a smooth and continuous PDA layer is covalently attached to the substrates by optimizing deposition conditions. Second, a cross-linked surface treatment (XST) layer is prepared and grafted to the PDA-coated substrate. Finally, polystyrene-*block*-poly(methyl methacrylate) (PS-*b*-PMMA) is spin-coated on top of the XST and oriented by thermal annealing. It is generally challenging to attach XSTs onto substrates that lack surface functional groups such as hydroxyl groups; however, PDA coatings are capable of attaching to virtually any substrate and act as a universal adhesive layer between the substrate and the XST layer. The methodology that we developed in this study could contribute to more robust and unconventional forms of soft lithography for flexible electronics.[28-31] For example, BCP nanopatterned flexible substrates could be used as a rolling stamp for large-area nanoprinting on a planar surface or as a flexible stamp for nanoprinting on nonplanar and curved surfaces similar to elastomeric polydimethylsiloxane (PDMS) stamps for micron-to-submicron pattern transfer.[6, 32-33] Using this technology, long-range ordered nanopatterns with extremely small feature sizes could be transferred through a remarkably simple procedure with potential for high-throughput.

5.2 PDA FILM GROWTH AND SURFACE TOPOGRAPHY

Catecholic molecules such as PDA have displayed remarkable properties including long-lasting and powerful adhesion to virtually all types of organic and inorganic surfaces in a wet environment, similar to the adhesive proteins secreted by marine mussels, although the adhesion mechanism still remains elusive.[25] Hence, PDA was used to establish a universal adhesive coating with functional moieties present in its surface bound ad-layer.[7] After attachment of a neutral XST onto the PDA adhesive layer, the surface was chemically neutral to each component of the BCP so as to promote the perpendicular orientation of BCP lamellae.[34] This mussel-inspired interfacial engineering approach for BCP lithography could be applicable to virtually all kinds of surfaces.[7] However, an extremely smooth PDA layer is required to ensure the integrity of the subsequent nano-patterning over a large area. We studied the growth of PDA during deposition and its resultant surface topography so that we might produce a conformal and smooth functional nano-layer on a variety of soft material surfaces. Dopamine was spontaneously polymerized in basic water (pH 8.5), followed by immersion of a piece of Si wafer to facilitate the study of deposition of PDA (**Figure 5.1a**). Once immersed, the PDA deposition quickly evolved on the Si surface while, at the same time, the PDA spherical nanograins increased in number and size within the polymerizing solution (**Figure 5.1b and c**).[35] From the initial stage of the oxidative polymerization of dopamine, a number of PDA particles ranging in size up to several hundred nanometers were grown in solution and eventually strongly attached to the Si surface (**Figure 5.1**). Recently, Klosterman et al. showed that PDA deposited on surfaces revealed distinct spherical particles on a planar PDA sublayer which consisted of mound-like structured small islands with nearly uniform size and shape by high resolution AFM.[23] This planar PDA sublayer resulted in a smooth surface with average surface roughness less than 1 nm while the dramatic morphological discordance between the smooth bottom layer

and the spherical granules suggests that the spherical granules were nucleated and grown in the solution and later deposited onto the PDA surface sublayer during spontaneous dopamine polymerization. Occurrence of these particles on the surface only after 0.5 h of PDA coating strongly supported the above hypothesis as well.[24, 27] Such large PDA grains will cause many defects in a subsequently applied BCP thin film. Efforts were necessary to minimize the surface roughness while functionality was introduced to the surface. It was determined that Si wafers PDA-coated for less than 1 h and subsequently sonicated in mild basic water (pH 8.5) for 100 min resulted in a smooth PDA thin film and a vertically oriented BCP self-assembled nanopattern over a large area. Many conditions were examined including sonication for up to 200 min and replacing alkaline water with methanol or isopropanol, which also sparsely dissolves PDA, but many PDA particles still remained on the surface. Thus, mild basic buffer at pH 8.5 was selected for sonication in order to facilitate the detachment of weakly bound particles without any damage on the conformal sublayer. It has been supposed that the solubilization of PDA in basic aqueous conditions is due to deprotonation of its phenolic groups.[36]

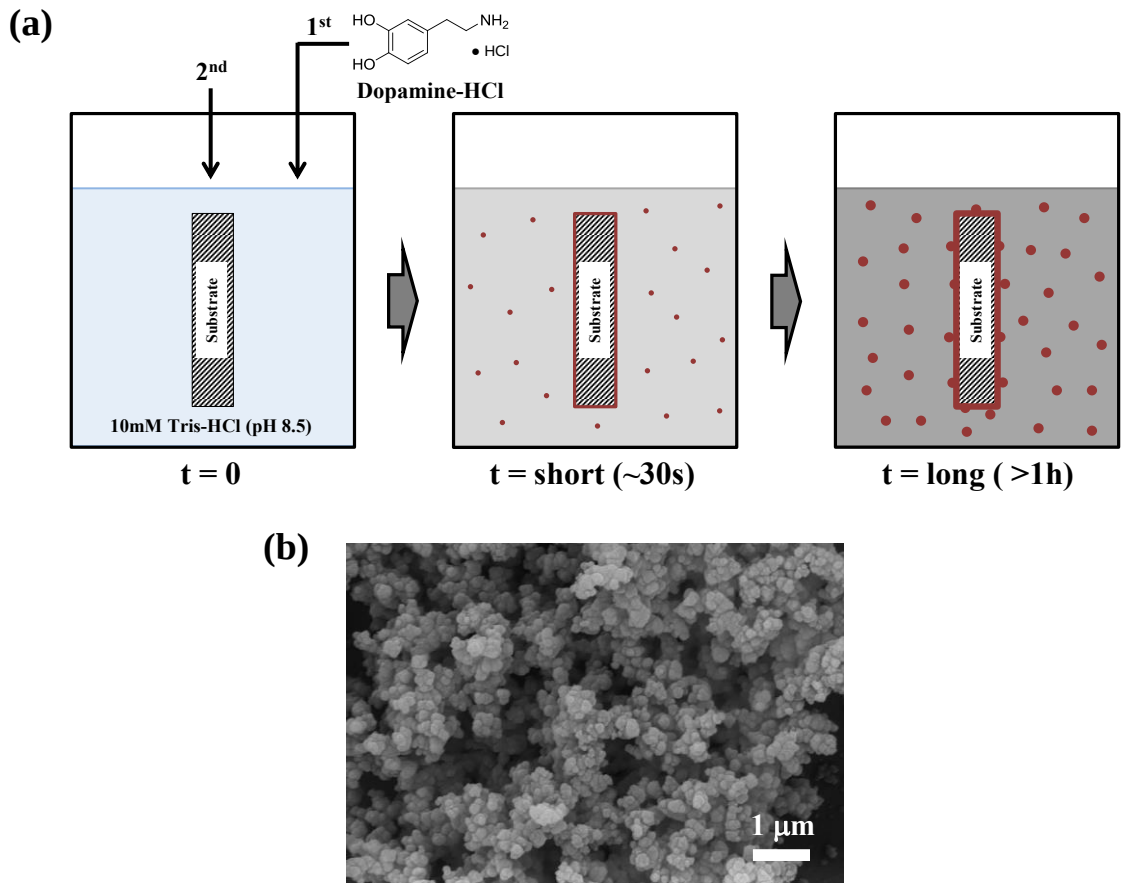

Figure 5.1: (a) Cartoon of dopamine oxidative polymerization process. (b) SEM of particles formed in solution after 3 days of dopamine polymerization.

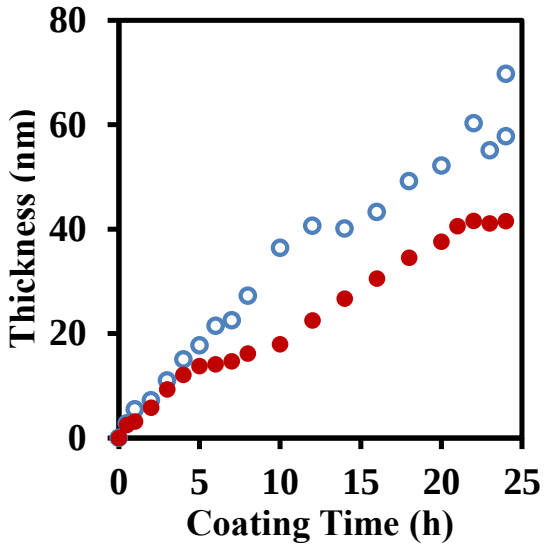

Figure 5.2: Thickness of PDA coating as a function of coating time (0-24 h) before (light blue open circles) and after (red solid circles) sonication.

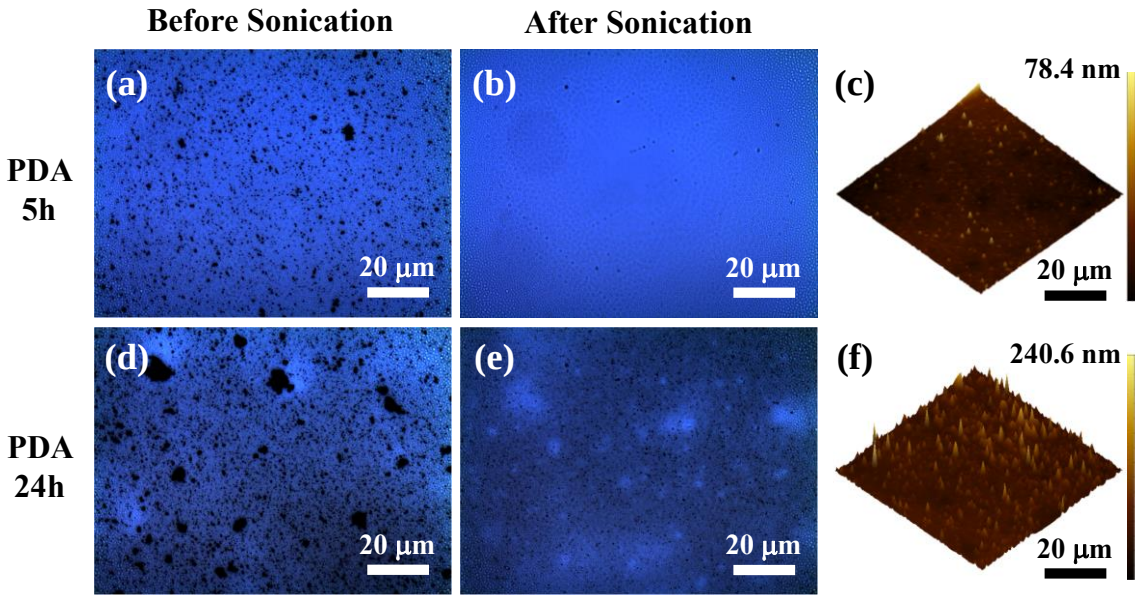

Figure 5.3: Optical microscopy images of PDA coating for 5 h (first row; a, b) and for 24 h (second row; d, e) on a Si wafer before (first column; a, d) and after (second column; b, e) sonication. AFM images (third column, 50µm × 50µm) of Si wafers that were PDA-coated for (c) 5 h and (f) 24 h after sonication.

As shown in **Figure 5.2**, the thickness of the PDA layer on a Si wafer was measured using ellipsometry as a function of the coating time. The PDA thickness measured by ellipsometry well matched that determined by atomic force microscopy (AFM).[24] The thickness of the PDA deposition gradually increased, reaching a value ranging from 58-70 nm after 24 h. Sonication in alkaline water (pH 8.5) reduced the apparent thickness of the PDA layer. This substantial reduction was largest for the thickest films (> 20 nm), indicating a large quantity of weakly bound PDA aggregates on the surface, that increased with the coating time. After sonication, a Si wafer PDA-coated for 5 h was smoother with few particles on its surface (**Figure 5.3a** and **Figure 5.3b**). The surface roughness of the 24h-PDA-coated Si wafer was even more rough with a good deal of aggregates on its surface even after sonication (**Figure 5.3d** and **Figure 5.3e**). In **Figure 5.3c** and **Figure 5.3f**, the samples shown as optical micrographs in **Figures 5.3b** and **Figure 5.3e** were visualized using AFM to quantitate the surface roughness. The images clearly showed a dramatic difference in the roughness of the two surfaces. Values of root-mean-square (RMS) roughness (50μm×50μm) were 3.3 ± 1.2 nm and 10.7 ± 1.9 nm for **Figure 5.3c** and **Figure 5.3f**, respectively. However, **Figure 5.3c** reveals the surface contains many particles with heights reaching up to 78 nm. This indicates this coating time may not be conducive to BCP lithography and motivates a closer examination of thinner PDA coats grown for shorter times (< 5 h). It is reasonable to suppose that the surface of the initially grown PDA thin films would reveal fewer particles of smaller size; at worst case, these might be more weakly bound to the PDA substrate attached layer and readily removed by sonication.

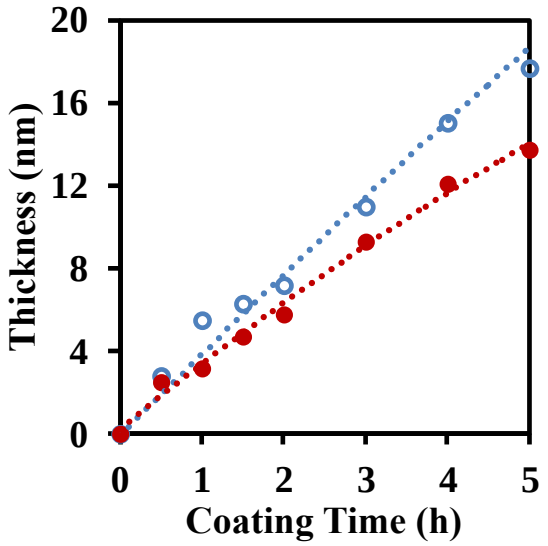

Figure 5.4: Thickness of PDA coating as a function of coating time (0-5 h) before (light blue open circles) and after (red solid circles) sonication.

Figure 5.4 shows the initial stage of PDA film growth on a Si surface. Once the dip-coating started in dopamine solution, the catecholic functional layer quickly (in 5 h) grew to 18 nm. Subsequent sonication cleaned the surface by removing the PDA nanoparticles and their aggregates from the surface, causing a considerable reduction in the overall thickness as measured by ellipsometry. Scanning electron microscopy (SEM) was used to observe the surface topography of PDA coatings on Si wafers before (**Figure 5.5**) and after (**Figure 5.6**) sonication. For a PDA surface coating applied for less than 1 h, nanoparticles were successfully removed from the surface by sonication in basic water without damaging the PDA conformal surface layer; the resulting cleaned 2-4 nm-thick PDA layer look more promising for defect-free BCP nanopatterning over a large area. On the other hand, for a PDA surface coating applied for longer than 1 h, numerous nanoparticles remained on the surface even after sonication (**Figure 5.6**). **Figure 5.7** represents the variation of static water contact angles on Si during the PDA coating time.

Once the spontaneous oxidative dopamine polymerization commenced with the immersion of the Si substrates, the contact angle was dramatically increased as a function of time and quickly reached a plateau, ranging from 52°-62°, in 1 h regardless of sonication. This implied the PDA coating for 1 h readily covered the surface while subsequent sonication in mild alkaline water endowed a smooth surface with no damage to the surface.

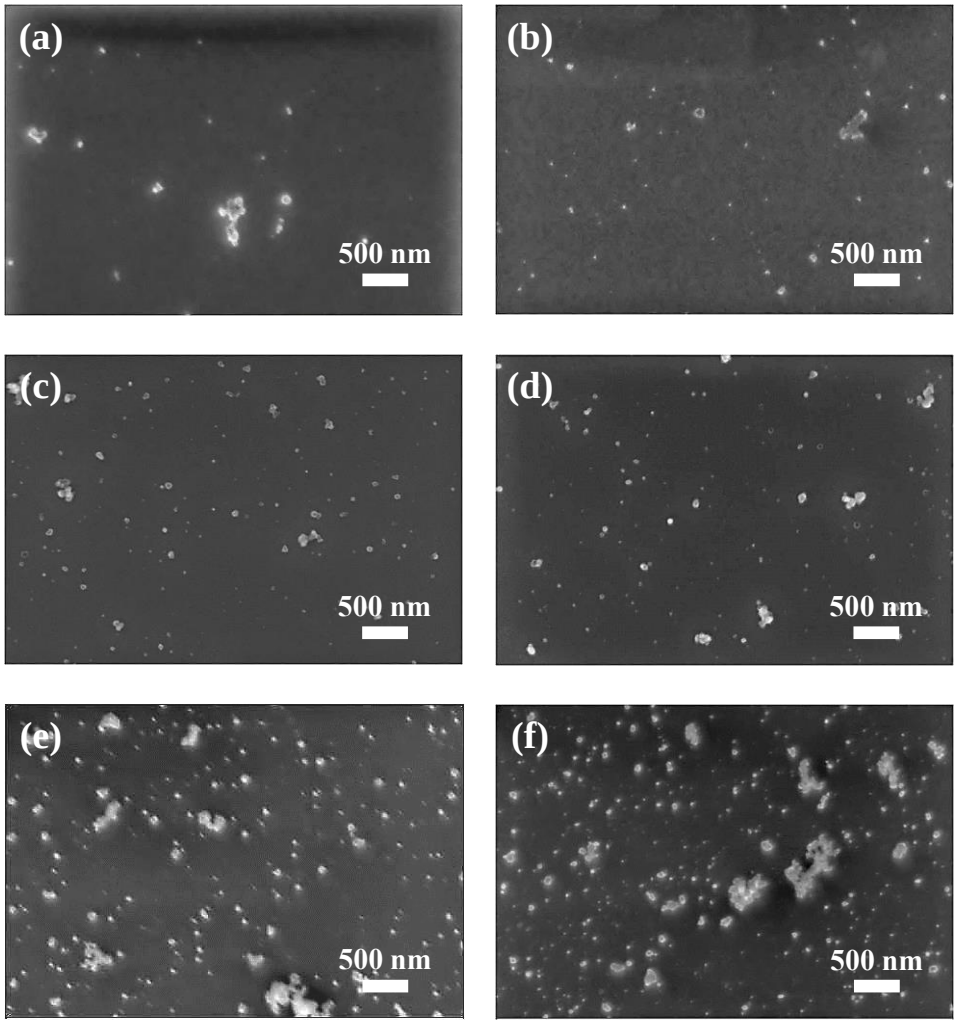

Figure 5.5: SEM images of Si wafers PDA-coated for (a) 0.5 h, (b) 1 h, (c) 2 h, (d) 3 h, (e) 4 h, and (f) 5 h.

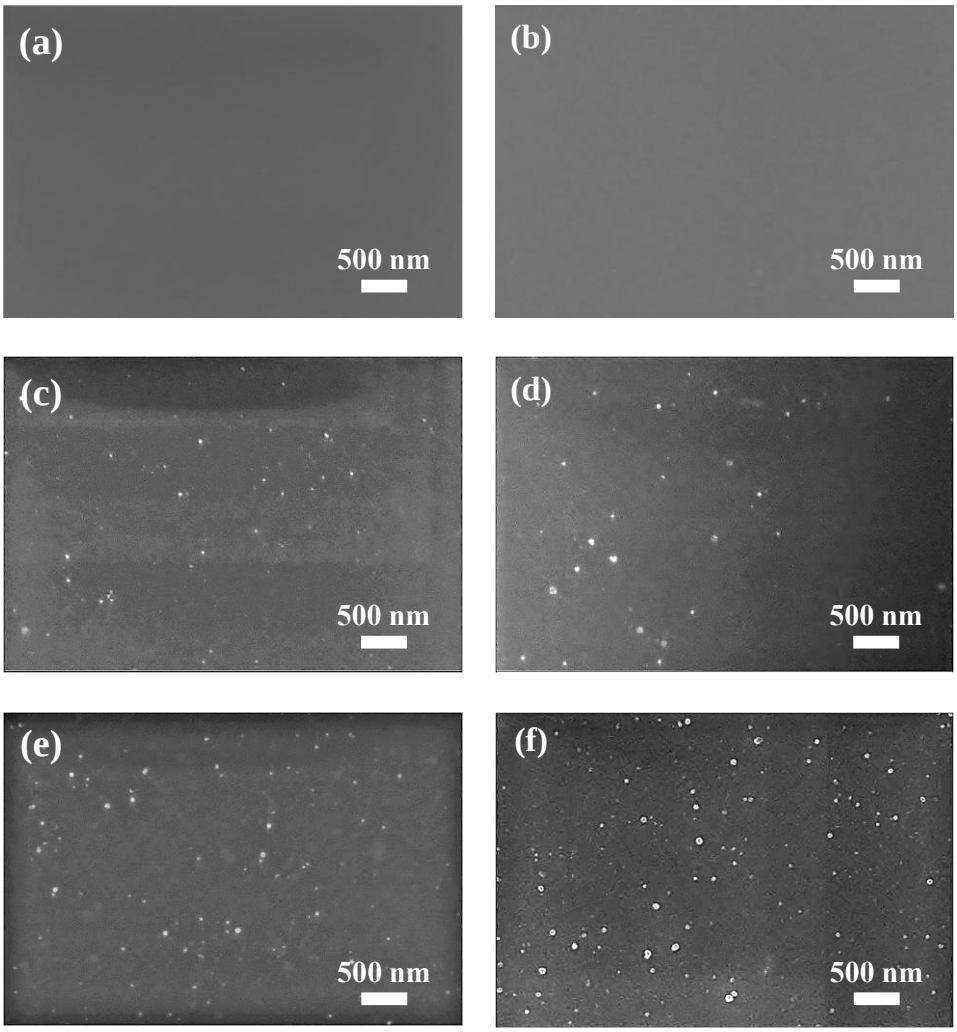

Figure 5.6: SEM images of Si wafers PDA-coated for (a) 0.5 h, (b) 1 h, (c) 2 h, (d) 3 h, (e) 4 h, and (f) 5 h after sonication.

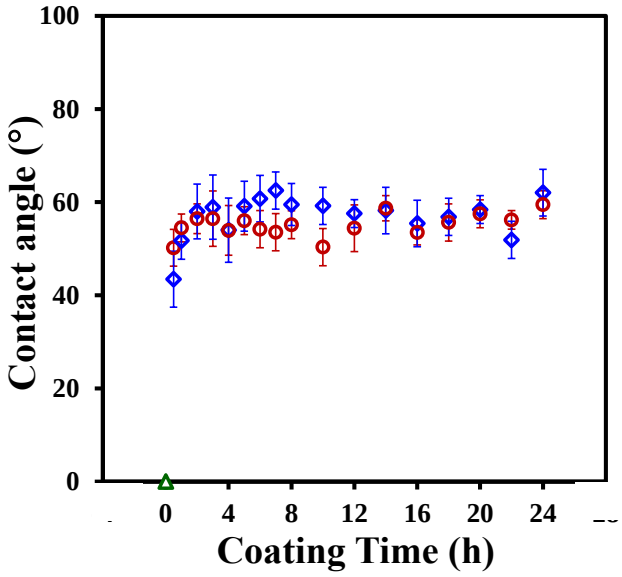

Figure 5.7: Static contact angles of bare Si wafer (green open triangle) and PDA coating on Si wafer before (red open circle) and after (blue open diamond) sonication as a function of coating time.

5.3 PDA-ASSISTED SURFACE ENGINEERING PROCESS

Figure 5.8a shows a potential procedure for PDA-assisted BCP lithography. Substrates were immersed for 1 h in a dopamine solution (2 mg/mL) in 10 mM Tris-HCl ((tris(hydroxymethyl)aminomethane)-hydrochloride) (pH 8.5), followed by sonication in basic water (pH 8.5). Subsequently, a neutral mat of poly(styrene-*co*-methyl methacrylate-*co*-glycidyl methacrylate) (P(S-*r*-MMA-*r*-G)) was grafted onto the PDA sublayer to promote perpendicular nanodomain orientation of the PS-*b*-PMMA lamellae. This facile and simple PDA universally adhesive surface treatment enabled the formation of a smooth, conformal, and mechanically robust thin functional template for secondary reactions with the mat. Hence, this PDA-assisted surface engineering technique should be widely applicable for lithography with a variety of BCPs on a broad range of surfaces.

A solution of P(S-*r*-MMA-*r*-G) was spin-coated onto PDA-coated substrates and then thermally annealed to facilitate the coupling of glycidyl groups of the random

copolymer with catechols on the PDA-coated surface, followed by rinsing with tetrahydrofuran (THF) to remove any unbound random copolymer (**Figure 5.8b**). This surface-anchored mat (~8 nm thick) was not preferentially wetted by either block of PS-*b*-PMMA and neutralized the surface to promote perpendicular orientation of lamellae on the substrates. As shown in **Figure 5.8c** and **Table 5.1**, the PDA treatment made water contact angles on a wide spectrum of substrates (native surfaces with contact angles of 0°-113°) converge within a range of 52°-68°, demonstrating a PDA-like chemical environment. Subsequent incorporation of a neutral polymer mat onto the PDA sublayer and following self-assembly of PS-*b*-PMMA finally resulted in consistent contact angles falling within the range of 81°-88°, the expected contact angle of a PS-*b*-PMMA surface. A continuous contact angle evolution eventually converged to the specific value expected of pure PDA and PS-*b*-PMMA for each step, regardless of the kind of underlying substrate material, thus demonstrating an efficient and substrate-independent surface modification technique.

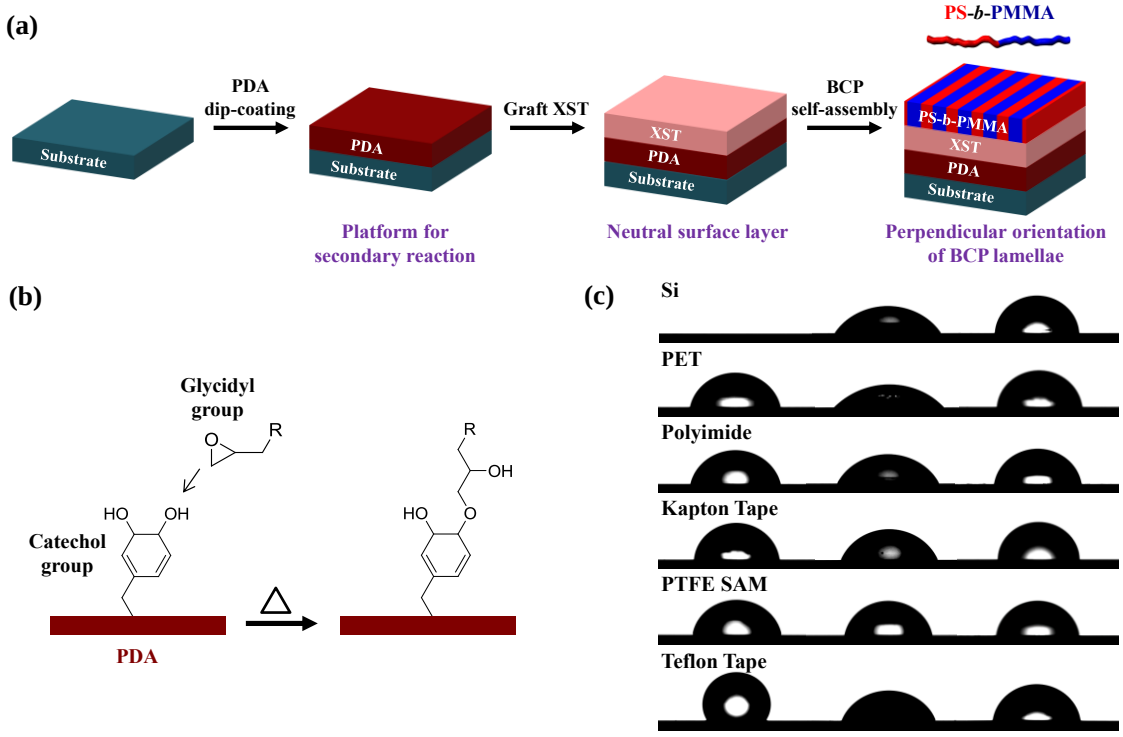

Figure 5.8: (a) A schematic of PDA-assisted PS-b-PMMA BCP lithography for soft material surfaces. (b) Formation of a cross-linked surface treatment (XST) layer. R represents P(S-*r*-MMA-*r*-G). (c) Pictures of water droplets on bare (left), polydopamine-treated (middle), and BCP self-assembled (right) substrates.

Substrate	Bare (°)	1 h PDA Coating (°)	BCP Treatment (°)
Si	< 5	52 ± 4	86 ± 1
Polyimide	76 ± 2	64 ± 3	81 ± 1
Kapton tape	88 ± 1	68 ± 3	88 ± 2
PTFE SAM	85 ± 4	60 ± 2	82 ± 2
Teflon tape	113 ± 3	68 ± 2	83 ± 2
PET	66 ± 3	56 ± 2	85 ± 2

Table 5.1: Evolution of static contact angles on various substrates during surface modification.

5.4 BCP NANOPATTERNING ON SOFT MATERIALS

As shown in **Figure 5.9a**, a smooth 1-h PDA coating on a Si wafer was obtained after sonication in mild basic water (pH 8.5) for 100 min. This 2-4 nm-thick PDA film exhibited a smooth surface with the maximum height of 8 nm and its root-mean-square roughness (3μm × 3μm) was 0.6 ± 0.1 nm such that this PDA layer was completely buried beneath the BCP and did not compromise the integrity of the BCP pattern (**Figure 5.9b** and **Figure 5.9c**). On the other hand, the surface of a 5-h PDA coating after sonication reveals many particles with heights ranging up to 77 nm (**Figure 5.9d** and **Figure 5.9f**). These are larger than the total thickness of the polymer ad-layers consisting of an XST layer (8 nm) and of BCP film (44 nm). The large particles penetrated the BCP thin film while creating many holes on the BCP nanopatterning layer (**Figure 5.9e**).

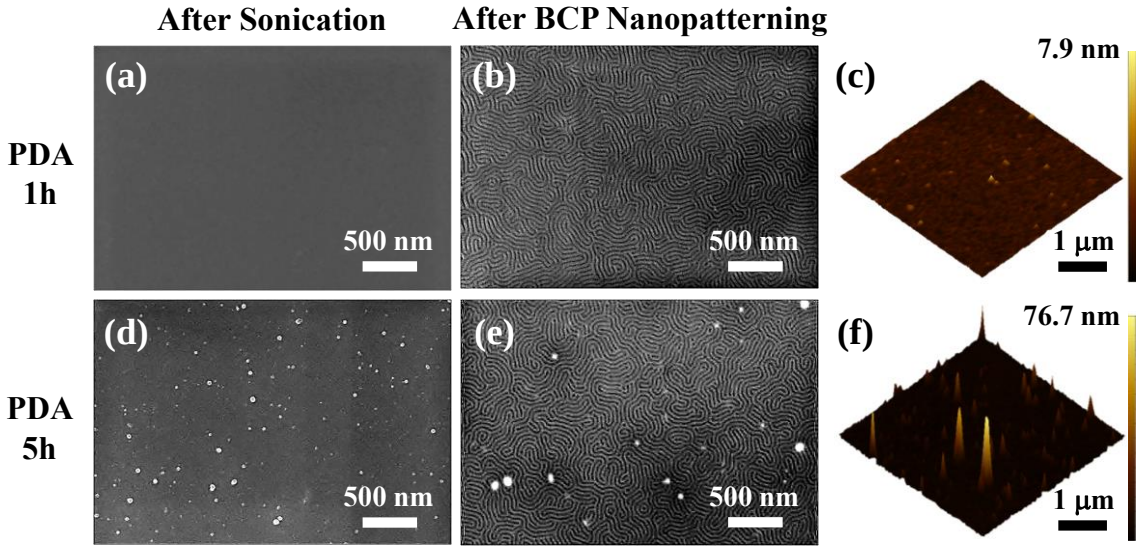

Figure 5.9: SEM images of PDA coating for (a) 1 h and (d) 5 h after sonication and after subsequent BCP nanopatterning (second column; b, e). AFM images (third column, 3μm × 3μm) of Si wafers that were PDA-coated for (c) 1 h and (f) 5 h after sonication.

This BCP lithography technique was employed on a variety of polymer surfaces, some currently used as roll-to-roll substrates as well as potentially useful for soft lithography. Commercial polymer films such as Teflon, Kapton, and polyethylene terephthalate (PET) are inexpensive and soft enough to easily bend and deform. However, they are not ideally suited for BCP nanopatterning due to thermal shrinkage and difficulty in introducing chemical functionalities to their surfaces. These challenges suggest the need for a new, simple, and facile surface modification technique, one that is insensitive to the surface roughness of substrates, applicable to virtually all kinds of surfaces, and has suitable thermal stability.

As shown in **Figure 5.10**, BCP lithography was successfully achieved on not only smooth organic and inorganic surfaces but also on flexible commercial polymer films regardless of surface chemistry/energy of the substrates. For example, this BCP lithography

approach readily generated unifirm and periodic fingerprint BCP nanodomains on diverse substrates from an extremely hydrophilic Si surface (θ_w = ~5°) to an exceptionally hydrophobic surface of Teflon (θ_w = 113°; **Table 5.1**). Furthermore, perpendicular lamellar orientation of PS-*b*-PMMA was successfully fabricated on not only a smooth polytetrafluoroethylene (PTFE) brush self-assembled monolayers (SAM) (**Figure 5.10a**) but also on commercial Teflon tape with a highly wrinkled surface texture (**Figure 5.10b**). This is in spite of it being well-known that chemical surface modifiers can rarely be anchored to a Teflon surface.[16] This successful fabrication demonstrates that our surface engineering approach depends neither on surface energy/chemistry nor the physical topography of the substrates. Moreover, self-assembled nanopatterning was also successfully introduced onto widely used elastomers of polyimide (**Figure 5.10c**) and its commercial relative Kapton (**Figure 5.10d**) as well as onto one of the most popular roll-to-roll materials of PET (**Figure 5.10e**). The implication of these successes is the approach's wide applicability to a variety of commercially attractive polymer substrates for soft lithography.

BCP spin-coated thin film on Si was thermally annealed at 250 °C for 5 min and BCP self-assembled nanopatterning was readily achieved (**Figure 5.10f**). The same procedure for BCP lithography was readily applied to Kapton tape, polyimide thin film, and PTFE brush without any modifications. Polyimide is a high glass transition temperature (T_g) material well-known for its remarkable thermal stability. The 3 nm-thick PTFE brush layer was covalently linked to a Si surface and thus its mobility was highly restrained, leading to reasonable stability at high temperature. However, most of the soft polymeric roll-to-roll films such as Teflon and PET can change shape/shrink substantially at an annealing temperature of 250 °C, which caused fracture and dewetting of the BCP film due to significant thermal shrinkage of underlying substrates. As a result, vertically

oriented BCP nanopatterns were successfully fabricated on Teflon tape and PET film by annealing the BCP thin film at reduced temperature of 160-185 °C, which is well-above the glass transition temperature of PS and PMMA. However, the heating times were prolonged to 3 h, to compensate for the lower temperature (**Figure 5.10b** and **Figure 5.10e**). Ultimately, this slight modification to the annealing conditions was successful in stabilizing the film substrate and enabled high quality micro-phase separation of PS-*b*-PMMA into vertically oriented domains.

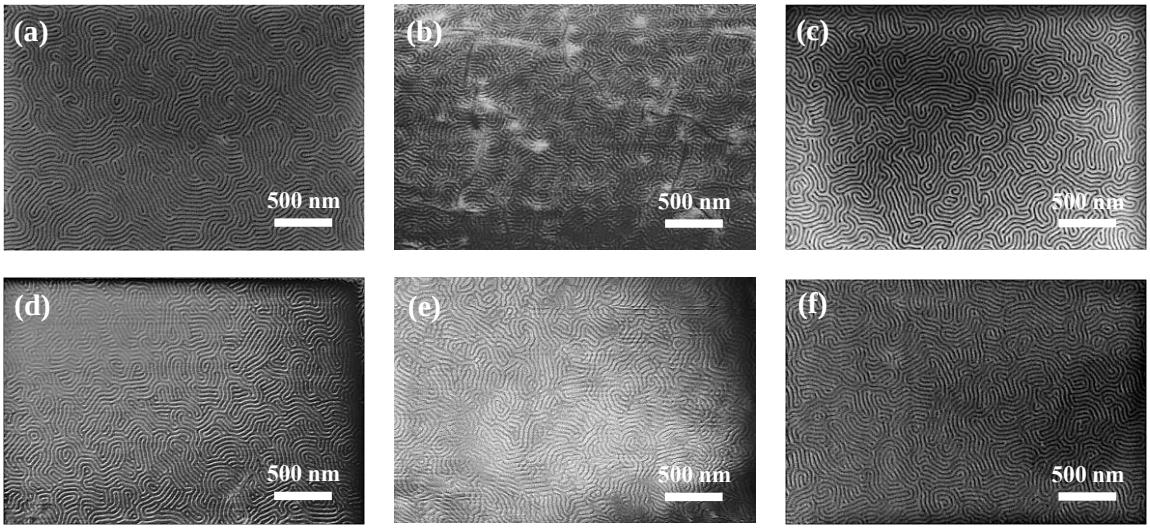

Figure 5.10: SEM images of perpendicularly oriented PS-*b*-PMMA domains on (a) PTFE brush self-assembled monolayer (SAM), (b) Teflon tape, (c) polyimide thin film, (d) Kapton tape, (e) polyethylene terephthalate (PET) film, and (f) Si.

5.5 CONCLUSIONS

A mussel-inspired universal strategy for surface treatment resulted in vertically oriented BCP domains on a variety of demanding but technologically relevant surfaces, including flexible organic materials. Sonication of the initially grown PDA deposition (< 1 h) in mild alkaline water (pH 8.5) prepared smooth (RMS roughness < 0.6 nm) and conformal functional PDA ad-layers with dense functionality available for secondary

reactions. PDA quickly grew on a wide spectrum of polymeric substrates with varying hydrophilicity (θ_w = 0°-113°) to converge in 1 h to that consistent with pure PDA (θ_w = 52°-68°). This demonstrates a fast, efficient, and universal surface engineering method. This biomimetic universally adhesive surface modification approach added a significant processing tool to current BCP lithography procedures by allowing simple functionalization of any surface that is compatible with conventional thermal annealing. This allowed nanopatterns to be created on mass-produced, flexible, and thick polymer films, such as Kapton, Teflon, and PET. This new bioinspired strategy overcame the limitations of current substrate-specific chemical modification approaches, opening possible routes to unprecedented practical realizations for electronics, nanotechnology, and biomedical engineering.[5-6, 29]

5.6 EXPERIMENTAL

5.6.1 MATERIALS

Dopamine-HCl and osmium tetroxide were purchased from Sigma-Aldrich. Tris (tris(hydroxymethyl)aminomethane) base was obtained from Fisher Scientific. Polyethylene terephthalate (PET) film (Melinex® ST505) was kindly provided by Dupont Teijin Films™ and used as received. Kapton® polyimide film tape (3M 5413) and Teflon tape (3M 5180) were purchased from 3M. Polyimide P84® was kindly provided by Evonik Industries. (Tridecafluoro-1,1,2,2,-tetrahydrooctyl) methyldichlosilane was purchased from Gelest, Inc. Si wafers were obtained from NOVA Electronic Materials, LLC. Ultrapure water (18.2 MΩ-cm) was obtained from a Thermo Scientific Barnstead E-pure water purification system. Symmetric PS-*b*-PMMA was purchased from Polymer Source, Inc. and each block has a molecular weight of 37 kDa. The domain spacing of this lamellae-forming BCP was reported as ~ 42 nm.[37] GL51 and GL57 refer to two random copolymers

of poly(styrene-*co*-methyl methacrylate-*co*-glycidyl methacrylate) (P(S-*r*-MMA-*r*-G)), which were synthesized by free radical polymerization according to the reported procedure.[38] The M_n of GL51 and GL57 were 26.7 kDa (PDI = 1.6) and 23.6 kDa (PDI = 1.6), respectively. The molecular weight and polydispersity data were determined using a Viscotek GPC Max VE 2001 size exclusion chromatography (SEC) equipped with a Viscotek Model 270 dual detector of viscometer/light scattering detector, a Viscotek VE 3580 refractive index detector, and two I-Series mixed bed low MW columns. The molar ratio between styrene, methyl methacrylate, and glycidyl methacrylate in the resultant random copolymers of GL51 and GL57 were 71:28:1 and 77:22:1, respectively, as measured by ^{1}H NMR. ^{1}H NMR spectra were recorded in $CDCl_3$ solution with a Varian Unity Plus 400 MHz spectrometer.

5.6.2 SUBSTRATE PREPARATION

PTFE brush SAM (~ 1 nm) was grafted onto the Si wafer surface using silane chemistry. 0.1 mL of (tridecafluoro-1,1,2,2, - tetrahydrooctyl) methyldichlosilane was added to 100 mL of toluene. A piranha cleaned Si wafer was immersed in this solution, which was subsequently heated to 75^{o}C and kept at this temperature overnight. After the grafting reaction, the treated Si wafer was thoroughly washed several times with deionized water and isopropanpol, then dried under vacuum. Besides, thin films (540 nm) of polyimide in a *n*-metyl-2-pyrrolidone (NMP) solution (10 wt%) were spin-coated (3000 rpm, 180s) on Si wafers at 70 ^{o}C, then annealed at 160 ^{o}C for 4 h under vacuum to completely remove residual solvent. The thickness of the polyimide thin films was determined by a spectroscopic ellipsometer (VB-400 VASE Ellipsometer, J. A. Woollam Co., Inc.) using wavelengths from 382 to 984 nm with a 65° angle of incidence.

5.6.3 PDA COATING

Si wafers were thoroughly cleaned by immersion in a piranha solution (80% H_2SO_4: 20% H_2O_2) at 100 °C for 30 min, and polymer substrates were rinsed with isopropanol before use. Dopamine-HCl (2 mg/mL) was completely dissolved in 10mM Tris-HCl (pH 8.5) for one minute, and substrates were then quickly immersed in this solution for the designated time. During dopamine polymerization, the substrates were vertically oriented in the solution while the solution was vigorously stirred to prevent macroscopic aggregation of PDA on the substrate surface. After PDA deposition, the coated substrates were rinsed with DI water, then quickly immersed in 10mM Tris-HCl (pH 8.5), followed by sonication for 100 min (Branson 2510 Ultrasonic Cleaner). Finally, the samples were dried with air from the in-house air supply line, thoroughly rinsed with DI water, then dried under vacuum for one day.

Between the PDA coating and sonication procedures, the coated samples were kept wet. Otherwise, once the polydopamine deposition solidified, the adhesion between the PDA particles and the sublayer became too strong for the aggregates to be separated from the substrate by sonication. The adhesion is due to the hydrogen bonding, charge transfer, and π-π interaction among catechols on the interface between the PDA particles and the sublayer. This process also explains the insolubility of PDA as well as its notable stability as a coating.[21, 39-40] In addition, the samples were steeply tilted or vertically oriented in basic water during sonication so that PDA grains could roll down the surface due to gravity. The thickness of the PDA thin films were measured using a spectroscopic ellipsometer.

5.6.4 BCP NANO-PATTERNING PROCESS

A 0.4 wt% solution in cyclopentanone of two random copolymers of P(S-*r*-MMA-*r*-G), GL51 and GL57, mixed at a 1:1 weight ratio was prepared. This solution was spin-coated onto PDA-coated substrates at 1500 rpm for 40 s, and the resulting films were

annealed in vacuum at 160°C for 48 hours to crosslink the XST layer over the underlying PDA coating. The annealed films were then thoroughly washed with tetrahydrofuran several times to completely remove unreacted GL51 and GL57. Consequently, a 7-8 nm thick XST ad-layer was obtained on the PDA sublayer, as measured by ellipsometry. Subseqeuntly, thin films of PS-*b*-PMMA (44 nm) were spin-coated (2000 rpm, 40 s) onto the XST layer. These systems were then thermally annealed under vacuum at the different temperatures and for different lengths of time, depending on the substrate. The annealing temperatures were chosen with the thermal stability of each substrate in mind. For example, PS-*b*-PMMA films on Si wafer, polyimide thin film, and Kapton tape were annealed at 250 °C for 5 min while PS-*b*-PMMA films on Teflon tape and PET film were annealed at 185°C for 3 h and 160 °C for 3 h, respectively. Before imaging, all samples were oxygen plasma etched for 45 s to selectively remove the PMMA domain to enhance SEM imaging contrast.

5.6.5 CHARACTERIZATION

5.6.5.1 SCANNING ELECTRON MICROSCOPY

BCP self-assembly images were acquired by SEM (Zeiss Supra 40 VP). Samples were scanned at a voltage of 1 kV with an in-lens detector and a working distance of 3-6 mm. Prior to imaging, self-assembled BCP thin films on thick polymer substrates such as PET film and Teflon tape were coated with osmium tetroxide for 23-28 h to prevent charging.

5.6.5.2 ATOMIC FORCE MICROSCOPY

Phase images of samples were recorded using an Asylum Research MFP-3D AFM in tapping mode. AFM images were taken using 300 series tapping mode AFM tips (tip radius < 10nm, Ted Pella) with a resonant frequency of 300 kHz and a force constant of 42 N/m.

5.6.5.3 CONTACT ANGLE GONIOMETRY

Static water contact angles (θ_w) were measured using a Ramé-Hart, Inc. NRL C.A. goniometer (model #100-00). A 6 μL drop of deionized water was placed on the sample for the measurement, and the image was taken within 15 s of placing the drop on the sample.

5.7 REFERENCES

1. Warren, S. C.; Messina, L. C.; Slaughter, L. S.; Kamperman, M.; Zhou, Q.; Gruner, S. M.; DiSalvo, F. J.; Wiesner, U. *Science* **2008,** *320*, 1748-1752.
2. Jeong, B.; Bae, Y. H.; Lee, D. S.; Kim, S. W. *Nature* **1997,** *388*, 860-862.
3. Kataoka, K.; Harada, A.; Nagasaki, Y. *Adv. Drug Delivery Rev.* **2001,** *47*, 113-131.
4. Bates, C. M.; Maher, M. J.; Janes, D. W.; Ellison, C. J.; Willson, C. G. *Macromolecules* **2014,** *47*, 2-12.
5. Rogers, J. A.; Someya, T.; Huang, Y. G. *Science* **2010,** *327*, 1603-1607.
6. Xia, Y.; Whitesides, G. M., *Angew. Chem. Int. Ed.* **1998,** *37*, 550-575.
7. Lee, H.; Dellatore, S. M.; Miller, W. M.; Messersmith, P. B. *Science* **2007,** *318*, 426-430.
8. Ye, Q.; Zhou, F.; Liu, W. M., *Chem. Soc. Rev.* **2011,** *40*, 4244-4258.
9. d'Ischia, M.; Napolitano, A.; Pezzella, A.; Meredith, P.; Sarna, T. Angew. Chem.-Int. Edit. 2009, 48, 3914.
10. Dreyer, D. R.; Miller, D. J.; Freeman, B. D.; Paul, D. R.; Bielawski, C. W. Chem. Sci. 2013, 4, 3796-3802.
11. Kang, S. M.; Ryou, M. H.; Choi, J. W.; Lee, H. *Chem. Mater.* **2012,** *24*, 3481-3485.
12. Shultz, M. D.; Reveles, J. U.; Khanna, S. N.; Carpenter, E. E. *J. Am. Chem. Soc.* **2007,** *129*, 2482-2487.
13. Lee, H.; Rho, J.; Messersmith, P. B. *Adv. Mater.* **2009,** *21*, 431-434.
14. Chien, H. W.; Kuo, W. H.; Wang, M. J.; Tsai, S. W.; Tsai, W. B. *Langmuir* **2012,** *28*, 5775-5782.
15. Ku, S. H.; Ryu, J.; Hong, S. K.; Lee, H.; Park, C. B. *Biomaterials* **2010,** *31*, 2535-2541.
16. Kim, B. H.; Lee, D. H.; Kim, J. Y.; Shin, D. O.; Jeong, H. Y.; Hong, S.; Yun, J. M.; Koo, C. M.; Lee, H.; Kim, S. O. *Adv. Mater.* **2011,** *23* , 5618-5622.
17. McCloskey, B. D.; Park, H. B.; Ju, H.; Rowe, B. W.; Miller, D. J.; Freeman, B. D. *J. Membrane Sci.* **2012,** *413*, 82-90.
18. McCloskey, B. D.; Park, H. B.; Ju, H.; Rowe, B. W.; Miller, D. J.; Chun, B. J.; Kin, K.; Freeman, B. D. *Polymer* **2010**, *51*, 3472-3485.
19. Zhang, L.; Wu, J. J.; Wang, Y. X.; Long, Y. H.; Zhao, N.; Xu, J. *J. Am. Chem. Soc.* **2012,** *134*, 9879-9881.

20. Cho, J. H.; Shanmuganathan, K.; Ellison, C. J. *ACS Appl. Mater. Interfaces* **2013**, *5*, 3794-3802.
21. Dreyer, D. R.; Miller, D. J.; Freeman, B. D.; Paul, D. R.; Bielawski, C. W. *Langmuir* **2012**, *28*, 6428-6435.
22. Postma, A.; Yan, Y.; Wang, Y. J.; Zelikin, A. N.; Tjipto, E.; Caruso, F. *Chem. Mater.* **2009,** *21*, 3042-3044.
23. Klosterman, L.; Riley, J. K.; Bettinger, C. J. *Langmuir* **2015,** *31,* 3451-3458.
24. Ball, V.; Del Frari, D.; Toniazzo, V.; Ruch, D. *J. Colloid. Interface Sci.* **2012,** *386*, 366-372..
25. Lee, H.; Scherer, N. F.; Messersmith, P. B. *Proc. Natl. Acd. Sci. U. S. A.* **2006**, *103*, 12999-13003.
26. Wei, Q.; Zhang, F. L.; Li, J.; Li, B. J.; Zhao, C. S. *Polym. Chem.* **2010,** *1*, 1430-1433.
27. Guardingo, M.; Esplandiu, M. J.; Ruiz-Molina, D. *Chem. Commun.* **2014,** *50*, 12548-12551.
28. Bao, Z. N.; Feng, Y.; Dodabalapur, A.; Raju, V. R.; Lovinger, A. J. *Chem. Mater.* **1997,** *9*, 1299-1301.
29. Rogers, J. A.; Bao, Z.; Baldwin, K.; Dodabalapur, A.; Crone, B.; Raju, V. R.; Kuck, V.; Katz, H.; Amundson, K.; Ewing, J.; Drzaic, P. *Proc. Natl. Acd. Sci. U. S. A.* **2001,** *98*, 4835-4840.
30. Garnier, F.; Hajlaoui, R.; Yassar, A.; Srivastava, P. *Science* **1994,** *265*, 1684-1686.
31. Gelinck, G. H.; Huitema, H. E. A.; Van Veenendaal, E.; Cantatore, E.; Schrijnemakers, L.; Van der Putten, J.; Geuns, T. C. T.; Beenhakkers, M.; Giesbers, J. B.; Huisman, B. H.; Meijer, E. J.; Benito, E. M.; Touwslager, F. J.; Marsman, A. W.; Van Rens, B. J. E.; De Leeuw, D. M. *Nat. Mater.* **2004,** *3*, 106-110.
32. Jackman, R. J.; Wilbur, J. L.; Whitesides, G. M. *Science* **1995,** *269*, 664-666.
33. Xia, Y. N.; Qin, D.; Whitesides, G. M. *Adv. Mater.* **1996,** *8*, 1015-1017.
34. Janes, D. W.; Thode, C. J.; Willson, C. G.; Nealey, P. F.; Ellison, C. J. *Macromolecules* **2013,** *46*, 4510-4519.
35. Ju, K.-Y.; Lee, Y.; Lee, S.; Park, S. B.; Lee, J.-K. *Biomacromolecules* **2011,** *12*, 625-632.
36. Bernsrnann, F.; Ersen, O.; Voegel, J. C.; Jan, E.; Kotov, N. A.; Ball, V. *Chemphyschem* **2010,** *11*, 3299-3305.
37. Liu, G.; Stoykovich, M. P.; Ji, S.; Stuen, K. O.; Craig, G. S. W.; Nealey, P. F. *Macromolecules* **2009**, 42, 3063-3072.
38. Han, E.; Stuen, K. O.; La, Y. H.; Nealey, P. F.; Gopalan, P. *Macromolecules* **2008,** *41*, 9090-9097.
39. Hong, S.; Na, Y. S.; Choi, S.; Song, I. T.; Kim, W. Y.; Lee, H. *Adv. Funct. Mater.* **2012,** *22*, 4711-4717.
40. Liebscher, J.; Mrowczynski, R.; Scheidt, H. A.; Filip, C.; Hadade, N. D.; Turcu, R.; Bende, A.; Beck, S. *Langmuir* **2013,** *29*, 10539-10548.

Chapter 6: Bioinspired Catecholic Flame Retardant Nanocoating for Flexible Polyurethane Foams

6.1 INTRODUCTION

The National Fire Protection Association (NFPA) reported that in 2013 the United States had 1.24 million fires, resulting in 3,240 civilian deaths, 15,925 injuries, and $11.5 billion of direct property loss.[1] The issues and concerns associated with such statistics has highlighted the need to develop flame retardant materials. Flame retardant materials can be used to protect property as well as to reduce the risk of fires and the threat to human life. One material that calls especially for effective flame resistance combined with minimal environmental impact is flexible PU foams. PU foams are highly flammable and used widely in furniture, bedding, mattresses, and automotive seating.[2-3] Even as the use of flame retardants dramatically grows, their end uses of saving lives and reducing economic loss are governed by strict safety regulations.[4] However, environmental concerns continue to grow regarding the most common flame retardant chemistries like halogenated small molecule compounds.[5-6] Toxic halogenated flame retardants have been found to bioaccumulate even in isolated locations on earth, raising environmental concerns. Hence, the need is undeniable to develop flame retardant materials that combine efficiency with environmentally friendly aspects. Recently, so as to impart flame retardancy to flexible PU foam, the method of layer-by-layer (LbL) assembly has been introduced[4, 7-8]; LbL assembly constructs a fire-resistant barrier coating on the foam surface. All flame retardants are placed on the foam's surface, precisely where they are needed, and the coating of the surface flame retardant is carried out efficiently, with no compromise to the foam's mechanical properties; in contrast, the simple mixing of small molecule flame-retardant additives into foams often results in adverse changes to the mechanical properties of PU

foams. The flame-retardant coating is a unique approach and, for flexible PU foams, quite efficient.

This chapter will focus on polydopamine (PDA) coatings as a nontoxic and environmentally friendly flame retardant. PDA is an excellent mimic of adhesive proteins present, in significant quantities, in the feet of *Mytilus edulis*. In fact, this accounts for mussels' ability to strongly tether themselves to a variety of surfaces. Indeed, PDA has been extensively exploited as a universal surface modification agent for a wide range of applications in biomedical engineering,[9-12] electrochemistry,[13-14] membrane technology,[15-16] nanotechnology,[17-18] and more. Researchers have studied the interaction of other catechols, such as synthetic melanins, with specifically generated oxidizing and reducing free radicals and reported that synthetic melanins are powerful scavengers of carbon-centered radicals.[19-20] Recently, Ju et al. synthesized PDA nanoparticles and demonstrated the catechols' strong radical-scavenging activity.[21] In addition, we have previously reported that melanins display a significant thermal and thermooxidative stabilization effect on commercial polymers[22] and that PDA substantially delayed the peak decomposition of PMMA in copolymer architectures.[23] This radical scavenging capability of PDA along with its universal adhesive nature strongly suggests that PDA could be useful for a flame retardant surface coating system, which is exceptionally suitable for highly flammable foamed materials with low densities, complicated geometries, and large surface areas. Moreover, given its biological origin (in living animals), PDA is intrinsically nontoxic and biocompatible.[24] This biomimetic coating could serve as an effective and an environmentally friendly flame retardant system for flexible PU foams.

6.2 PDA COATING GROWTH AND MICROSTRUCTURE

Since Lee et al. developed the first mussel-inspired surface coating protocol,[25] PDA coatings have been extensively exploited in a variety of fields, while recently much effort has been devoted to fundamental study of the film growth mechanism.[26] Attachment of this bioinspired coating is understood to be universal, but its thickness, adhesion force, deposition kinetics, and surface morphology are highly varied depending on many parameters like coating time, pH and dopamine concentration of the solution, surface chemical composition of substrates, and kinds of oxidants used.[26-31] Moreover, it has been interestingly noted that PDA films grow continually without any slowing in growth kinetics by consecutive immersion into freshly prepared dopamine solutions[29] or increased dopamine concentration higher than 2mg/mL.[26] However, the investigation into PDA growth kinetics has been focused on bare or chemically modified silicon surfaces with a planar geometry. Less effort has been devoted to investigating its growth kinetics on polymer surfaces as well as surfaces with complicated geometries. Here, we investigate conformal PDA coating evolution on open-cell PU flexible foam and used this catecholic functional nanocoating to impart flame retardancy to the highly flammable foam material.

PDA-coated PU foams were prepared using an established procedure with simple modifications. A dopamine solution (2 mg/mL) in 10mM Tris-HCl (tris(hydroxymethyl)aminomethane-hydrogen chloride) (pH 8.5) buffer was prepared and open cell PU foams were immersed in the solution. The solution was stirred continuously for the designated period and the solution color was blackened by alkaline pH-induced oxidative polymerization of dopamine. This simple dip-coating procedure resulted in a conformal nanolayer on the complicated geometry of an open cell foam. The foam color darkened and the % mass PDA of the coated foams showed linear growth as a function of PDA deposition time while the PDA coating looked consistent over the entire foam surface

(**Figure 6.1a, b**). For example, % mass PDA was 5.3%, 10.5%, and 15.9% for PU flexible foams PDA-coated for 1 day (PDA1D), for 2 days (PDA2D) and for 3 days (PDA3D). Cross-sections of PDA-coated foams also showed uniform color all through the cut surface without any gradation, demonstrating uniform PDA growth on the foam surface regardless of location (**Figure 6.1a**). A cross-sectional SEM image of a strut of PDA3D is shown in **Figure 6.1c** and the PDA coating on the PU surface was further magnified in **Figure 6.1d**. These images clearly demonstrate uniform and complete coverage of the PDA along with its globular surface topography after PDA coating for 3 days on the foam.

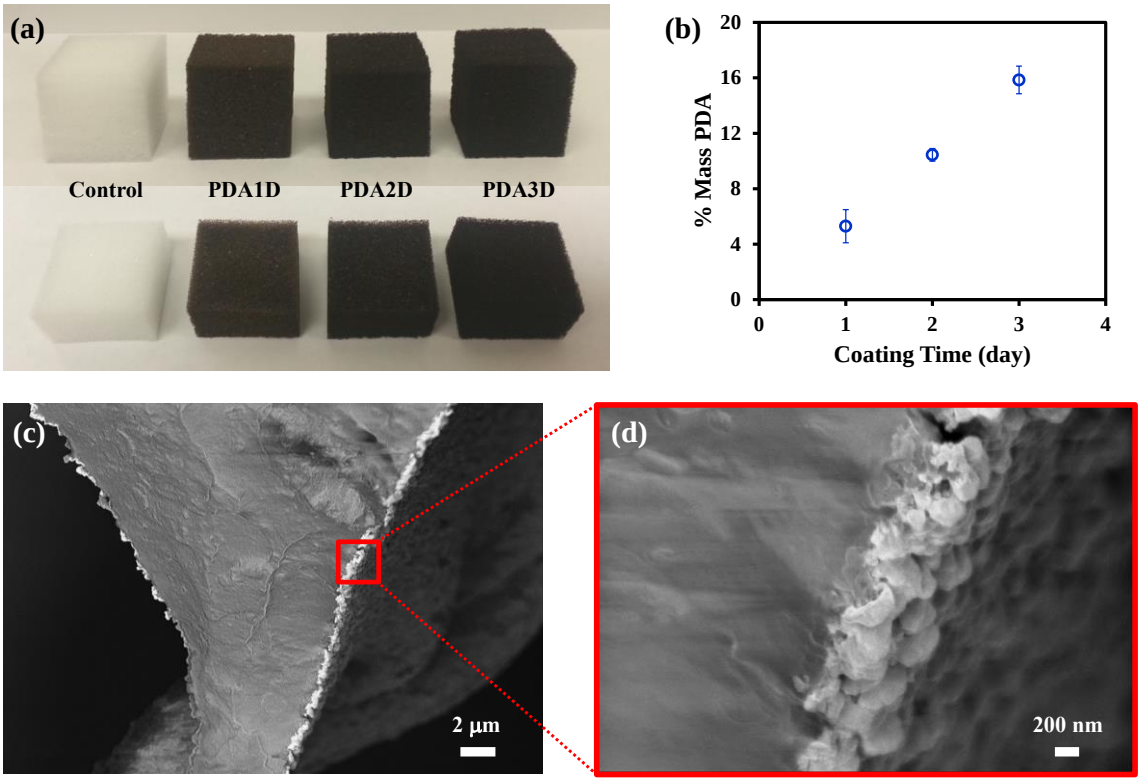

Figure 6.1: (a) Pictures of 1×1×1 in^3 control and PDA-coated foam cubes (top row) and their respective cross-sections (bottom row). (b) % Mass PDA of coated foams as a function of coating time. SEM images of (c) cross-section of a strut of PDA3D foam and (d) its magnified image of PDA coating deposited on PU.

Figure 6.2 displays the evolution of surface topography of the PDA coating on PU foam with increasing coating time. In contrast to the smooth surface of the control foam (**Figure 6.2a**), a PDA film grown for 1 day on PU foam was composed of small islets on top of a thin film (**Figure 6.2b**) and displayed a uniform nanotexture that confirmed the conformal nature of the PDA deposition. Furthermore, the SEM cross-section of PDA1D in **Figure 6.3** is a representative image of the PDA coating throughout the entire surface of the PU foam, demonstrating a conformal and coherent PDA film without any significant pores or cracks. Interestingly, the PDA coating consists of a planar and smooth sublayer, along with a distinct heterogeneous secondary-layer of large granules; the significant morphological discordance between a planar sublayer and the attached protruding large grains reasonably implies that the bulk solution and surface have different growth mechanisms.[31-32] With additional PDA deposition, surface grains became larger as well as greater in number while the nanotexture of the sublayer was also growing (**Figure 6.2c**). The large grains (i.e., PDA nanoparticles) are grown in solution and can attach themselves to the PDA film on the foam surface, by virtue of the mussel-inspired strong wet adhesion of PDA; eventually, they grow together with the PDA coating on the surface of the foam. These growing nanostructures on the surface eventually coalesce into a grainy, yet integrated, film with additional deposition of PDA (**Figure 6.2d**).

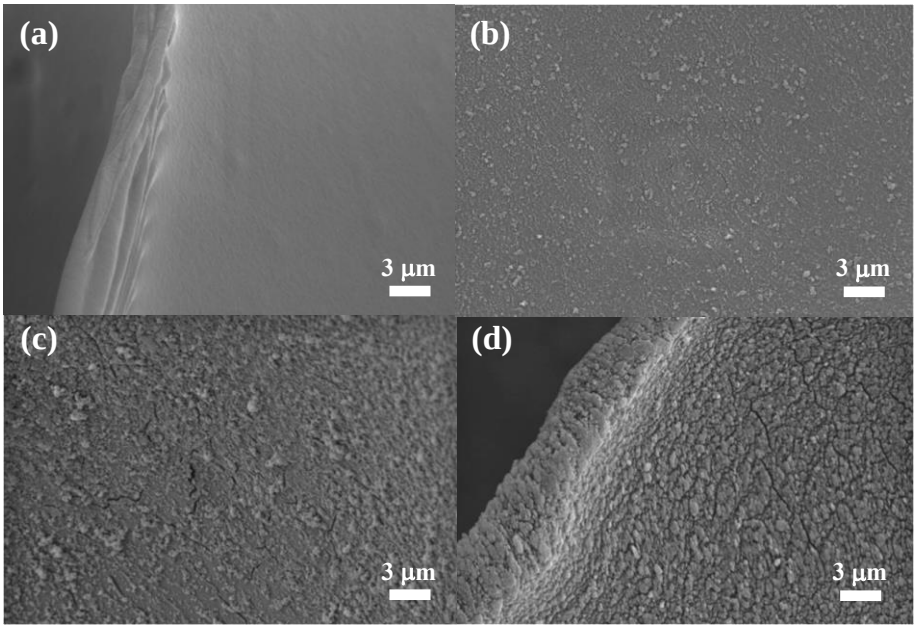

Figure 6.2: SEM images of surface of (a) control, (b) PDA1D, (c) PDA2D and (d) PDA3D PU foams.

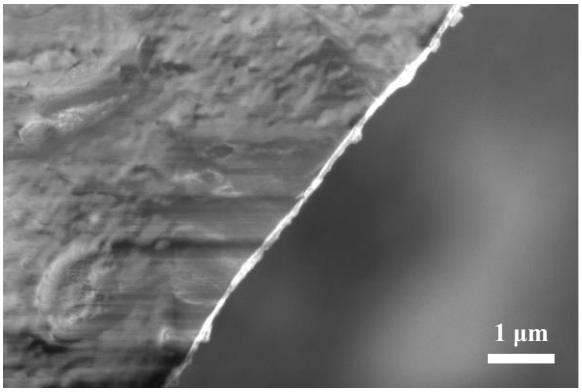

Figure 6.3: SEM cross-sections of PDA layer deposited on PU foam struts for 1 day.

Cross-sections of the PDA layers on PU were explored with deposition time. Findings strongly supported the aforementioned PDA coating growth mechanism (**Figure 6.4**). Consequently, the PDA thin film composed of a smooth surface and a few particles turned into a bumpy and consistently thick film after undergoing an intermediate stage of

combination of growing planar sublayer and incorporated grains. Incidentally, dip-coating PU foam in dopamine solution for 24 h and 48 h resulted in 55 and 91 nm thick planar PDA sublayers, respectively, suggesting that the PDA sublayer gradually grew and, even after 24 h, never reached saturation. The thicker PDA deposition and prolonged PDA growth kinetics on this open-cell PU foam compared to those on more extensively studied Si surfaces might be due to PU's more hydrophobic surface.[31, 33] However, further investigation of substrate geometry effects on PDA growth is needed. The secondary layer granular structure and the underlying planar sublayer gradually grew together and were eventually integrated into a consolidated globular thick layer (241 nm) after 3 days of deposition, as shown in **Figure 6.4c**. The PDA deposition on PU appeared to be quite robust and was not delaminated, in contrast to that on Si.[27] In addition, the PDA layers look continuous and compact in **Figure 6.4**; others have reported such layers to be dense enough to be impermeable to electroactive ions.[29] This simple, facile, and spontaneous deposition technique and its resulting conformal and dense physical structure of the surface layer could be suitable as an flame retardant system for flexible PU foam, which is highly flammable due to its open-celled porous structure, large surface area, and low density.[34]

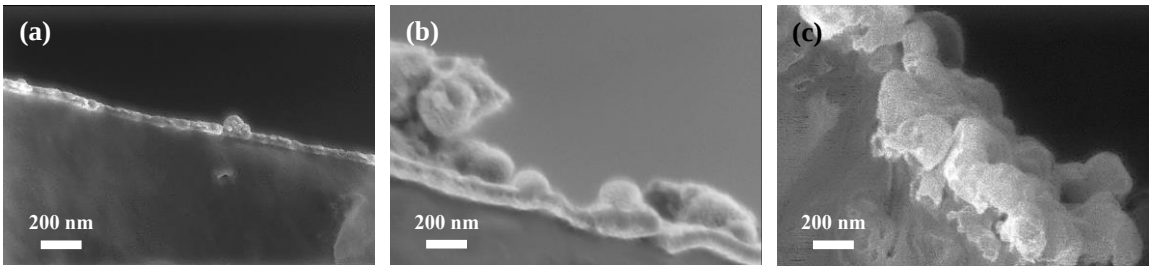

Figure 6.4: SEM cross-sections of PDA coating, deposited on PU foam struts, for (a) PDA1D, (b) PDA2D, and (c) PDA3D PU foams.

6.3 THERMAL ANALYSIS AND MICRO-COMBUSTION CALORIMETER

The thermal properties and flammability of pure PDA and PU foam were initially measured using thermogravimetric analysis (TGA) and a micro-combustion calorimeter (MCC). Upon being heated to 600 °C in TGA under N_2, the PU flexible control foam exhibited no residue. It has been classified as one of the most flammable polymeric materials, as represented by the large peaks in a MCC plot (**Figure 6.5**). In the MCC test, the peak heat release rate (P-HRR) and total heat release (HR) of a control foam were 498.3 W/g and 22.7 kJ/g, respectively. On the other hand, pure PDA had 63.6 wt% residue left after a TGA run and showed an undetectable peak heat release rate (P-HRR) and 2.4 kJ/g of total HR in a MCC test, demonstrating it's a char forming and nonflammable material. Interestingly, the original shape and cellular structure of a small MCC sample (~ 4 mg) of PDA3D were largely retained after the MCC test, although the weight was reduced. Formation of a consolidated carbonaceous char on the surface of each foam strut from high heat or fire would isolate the fuel/molten polymer and prevent the foam from collapsing into a liquid so as to significantly delay pyrolysis of PU decomposition products. In addition, given the radical scavenging effect of catecholic compounds of melanin and PDA,[21-22] it is simply deduced that a PDA coating could inhibit radicals, lowering the heat release values such as the average and peak heat release rates during MCC testing. The removal of radicals from flammable gases could slow the burning process and reduce the spread of fire during an actual fire.

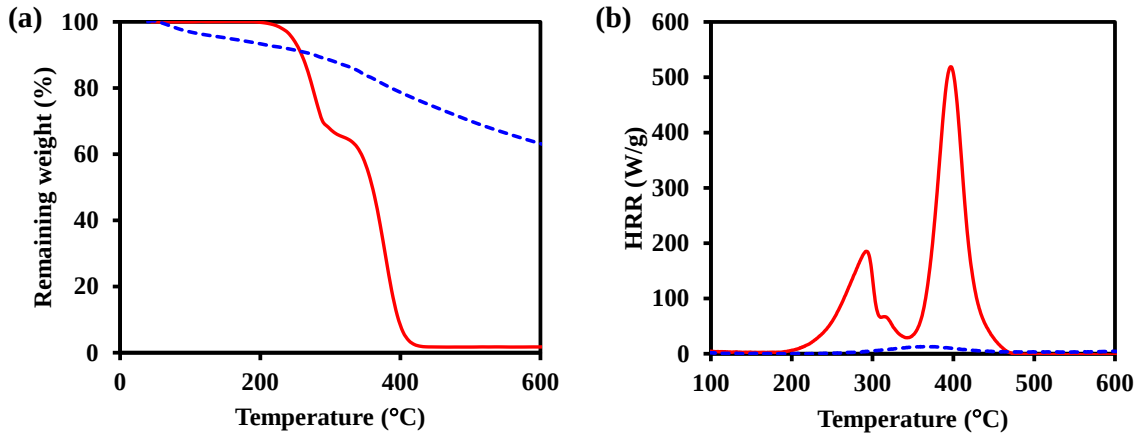

Figure 6.5: (a) Thermogravimetric analysis in nitrogen and (b) micro-combustion calorimetry (MCC) of uncoated PU foam control (red solid line) and preformed PDA (blue dashed line).

6.4 FLAME RETARDANT BEHAVIOR

PU foams ($50 \times 50 \times 25$ mm^3) were subjected to a direct flame from a butane torch for 10 s and the foam flammability was qualitatively investigated. Upon exposure to direct flame, the control foam immediately ignited, formed a melt pool, and was completely consumed while the fire was transferred to underlying materials by melt dripping. On the other hand, no melt dripping was exhibited by any of the PDA coated foams and the PDA layer performed better as a flame retardant shield when increasing its thickness. Consequently, PDA3D retained its original shape upon exposure to flame and the flame self-extinguished the quickest among the coated samples, leaving a part of the foam unburned, while PDA1D collapsed and was severely damaged (**Figure 6.6a** and **Figure 6.6b**). This implies that a heavier coating resulted in a better shielding effect. A cross-section of the post-burn PDA3D revealed undamaged foam beneath the char. In addition, the cellular structure was well-preserved throughout all of the foam although the surface that was directly scorched by the torch flame displayed a contracted and dehydrated foam char structure. The surface char morphology, examined at higher magnification as shown

in **Figure 6.6f**, revealed a consolidated and grainy surface which closely resembles a pristine PDA coating, indicating a largely retained PDA coating structure during exposure to the torch flame. Furthermore, flame spread was substantially delayed upon exposure of PDA3D to the torch flame, which is likely due to the radical scavenging capability of catechols. On the other hand, after immediate ignition of PDA1D, the flame quickly spread over the entire surface with strong heat generation, which caused substantial thermal shrinkage (**Figure 6.6b**). However, a conformal PDA thin film completely encapsulating the entire PU surface during PDA dip-coating left a highly consolidated char residue on the foam surface struts after the fire, which resulted in its underlying preserved cellular structure as well as no melt dripping during fire. The surface char of PDA1D revealed leather-like features with a few grains, indicating the existence of PDA residue on the surface. Also, PDA2D did not collapse, upon exposure to flame, and burned much less aggressively than PDA1D. In summary, PDA3D displayed the best flame retardant effect among the three coated foams, which could be attributed to the increased thickness of the catecholic surface coating. Also, as the coating weight increased, the coated foams retained greater weight (up to 40 wt%) after the torch burn test (**Figure 6.7**).

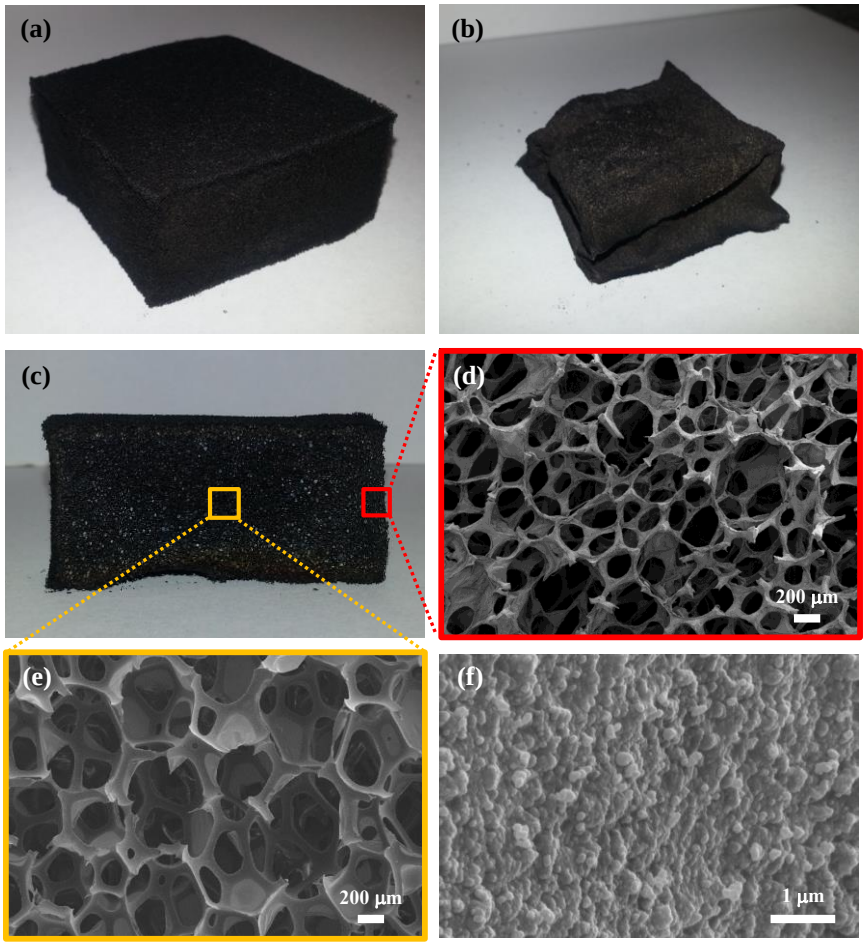

Figure 6.6: Pictures of post-burn foams of (a) PDA3D and (b) PDA1D, and (c) a cross-section of post-burn PDA3D foam. Boxes of the same color represent the area that were further magnified in a cross-section of post-burn PDA3D foam (d and e). (f) SEM image of char surface of post-burn PDA3D foam.

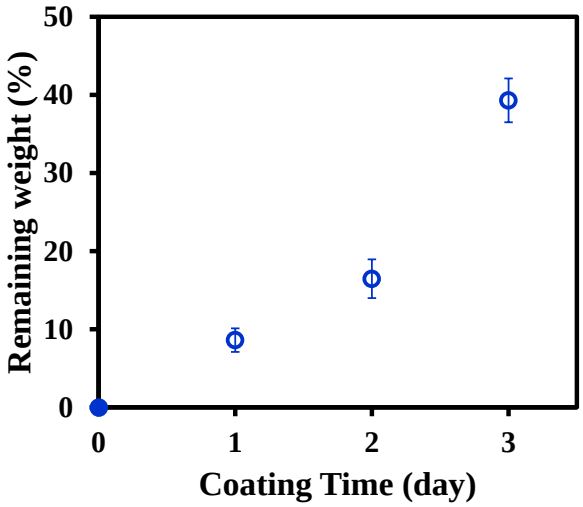

Figure 6.7: Remaining weight of control (blue solid circle) and PDA-coated foams (blue open circles) such as PDA1D, PDA2D, and PDA3D after torch burn test.

For a detailed investigation of flame retardancy, samples were tested in a cone calorimeter, as shown in **Figure 6.8**, according to a standard protocol (ASTM E-1354/ISO 5660). This test is an advanced method for assessing the fire behavior of materials; it is widely employed to examine the performance of fire retardant materials, but requires significantly larger sample sizes than TGA or MCC. The gases evolved during the combustion of samples are sent to a detection system and the test provides a range of information on the flammability behavior like mass loss, P-HRR, average heat release rate (A-HRR), etc. Two overlapped peaks were seen from the trace of a control PU foam. The first peak rose quickly once ignited, attributable to rapid foam collapse. The foam immediately transformed into a liquid pool, followed by the quick decomposition of volatile products. This process promoted rapid fire propagation and resulted in a second larger peak, which dramatically decayed after the foam was nearly consumed completely. The PDA coating added a flame-resistant surface on the PU foam and the coated foams exhibited enhanced flame retardancy. The HRR curve of PDA1D looked quite similar to

the control, although the PDA coating caused a marginal reduction in P-HRR. On the other hand, PDA2D and PDA3D showed a significant reduction in key flammability parameters such as P-HRR and A-HRR, implying the PDA coating substantially altered the inherent burning behavior of the PU foam. Eventually, the PDA coating totally eliminated the second peak and induced a prolonged burn time due to the delayed prolysis of the PU decomposition products. As a result, PDA3D revealed a sharp reduction in P-HRR (67%) and A-HRR (69%) along with a dramatic decrease in mass loss (79.6%), as listed in **Table 6.1**. P-HRR has been found to be the most important parameter to evaluate fire safety and represents the point in a fire where the heat generation is sufficient to propagate the flame or ignite adjacent material. Therefore significant reduction in P-HRR by the PDA coating indicates inhibition of the combustion process and factors associated with rapid flame spread. The PDA2D coating also substantially reduced the flammability of the foam, represented by a dramatic reduction in P-HRR (50%) and A-HRR (45%) compared to the control foam. Meanwhile, the HRR curve of PDA2D showed a significantly delayed second pyrolysis peak relative to the control foam. The thicker the PDA coating the better fire retarding performance. The PDA nanocoating acted to interrupt the self-sustained combustion cycle and to inhibit and suppress the combustion process. This unique protective nanobarrier is envisioned to perform at the physical and chemical level, in both the condensed phase and gas phase. First, the combustion process was physically retarded by forming a consolidated protective carbon residue on the PU surface, which prevented the foam from collapsing during fire and consequently led to the absence of a second peak in the HRR curve of PDA3D. Second, catechol functional groups of the PDA coating scavenged flammable free radicals during the fire and the fuel supply was considerably suppressed. These aforementioned synergistic physical and chemical actions of the PDA

nanocoating during the fire resulted in a new efficient and environmentally friendly flame-retardant system.

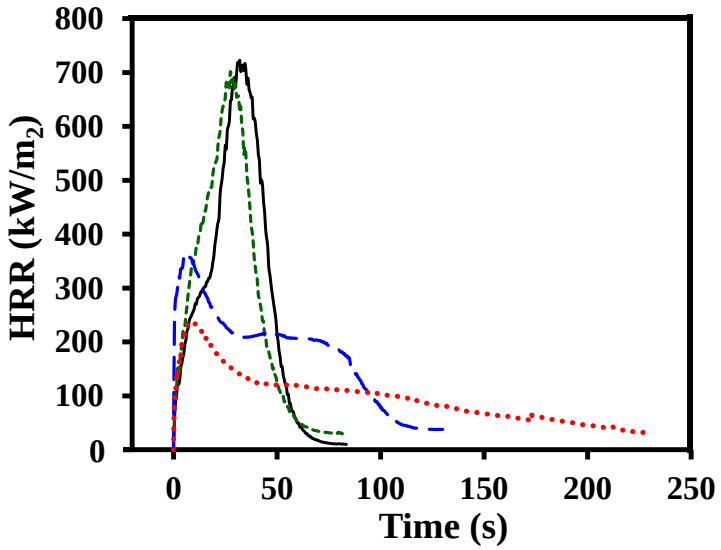

Figure 6.8: Heat release rate (HRR) of control (black solid line), PDA1D (green short-dashed line), PDA2D (blue long-dashed line), and PDA3D (red dotted line), as a function of time during cone calorimeter testing.

Sample	P-HRR (kW/m^2)	A-HRR (kW/m^2)	Total HR (MJ/m^2)	Time to Ignition (s)	Mass Loss (wt%)
Control	734	732	23	1.95	99.4
PDA1D	709	697	22	1.92	99.2
PDA2D	368	403	21	1.88	95.9
PDA3D	239	230	21	1.43	79.6

Table 6.1: Cone calorimeter results for control, PDA1D, PDA2D, and PDA3D. The samples were tested in triplicates and the values of measured parameters were averaged.

The literature has reported cone calorimetric analysis on flexible PU foams modified with commercial flame retardant additives. The results are summarized in **Table 6.2**. Comparing PDA coatings with conventional flame retardant systems for % reduction of P-HRR, it can be seen that PDA2D and PDA3D showed significantly higher reductions in the P-HRR than the best-performing conventional flame retardant systems with a lower loading of PDA.

Additive Type	**Flame retardants in flexible PU foam (wt%)**	**Commercial product / Supplier**	**P-HRR Reduction (%)**
Non-Halogen Additive	Zn Stearate (10)	Synpro® Zinc stearate / Ferro	17
Halogen Additive	Pentabromodiphenyl oxide blend (20)	DE-60F / Great Lakes Chemical	37
Halogen-Phosphorus Additive	Tris(1.3-dichloro isopropyl) phosphate (20)	Fyrol® FR2 / Akzo Nobel Chemicals	21
Halogen-Phosphorus + Non-Halogen Additives	Halogenated phosphate ester (28) + Sb_2O_3 (7)	Firemaster® HP-36 / Great Lakes Chemical + Antimony Oxide / Laurel Industries	43

Table 6.2: Cone calorimeter results reported in literature for flexible PU foams with commercial flame-retardants.[35]

6.5 CONCLUSIONS

A green flame-retardant nanocoating was deposited, via a simple dip-coating process, on the surface of flexible PU foam. As a function of coating time, % mass PDA linearly increased up to 15.9 %, corresponding to a 241 nm thick layer, derived from

simultaneous evolution of a planar sublayer and a secondary grainy structure. This layer appeared compact, continuous, and uniform over the entire foam surface and was strongly adhered to the PU surface. Preformed PDA revealed an unquantifiably weak HRR signal in MCC and large char yields of 63.6 wt% in TGA under N_2. The control foam exhibited strong P-HRR of 498.3 W/g in MCC and was totally consumed during a TGA run in N_2, demonstrating advantageous thermal and fire-related characteristics of PDA as a flame retardant. In the torch burn test, the PDA coating largely remained on the surface with a high level of integrity, which also prevented melt-dripping and retarded the pyrolysis process by preventing the foam from collapsing into a liquid pool. In addition, the catecholic surface barrier effectively interrupted the radical mechanism of the combustion process as well as substantially quenched flammable free-radicals during fire. As a result, in the torch burn test of the best-performing PDA3D, self-extinguishing occurred, leaving a portion of foam undamaged, and its cellular structure and original appearance were mostly preserved along with 40 wt% remaining weight. Cone calorimetry showed that the PDA coating resulted in dramatic reduction (by up to 67%) in P-HRR of flexible PU foam compared to that of an uncoated foam, verifying that the PDA coating has a stronger and more efficient fire-retarding effect than does the conventional additive approach of commercial flame retardants. This synergistic combination of physical and chemical actions resulted in a reduction in flammability of PDA-coated foams, which is directly aligned with % mass PDA coating applied.

6.6 EXPERIMENTAL

6.6.1 MATERIALS

Dopamine-HCl and melamine were purchased from Sigma-Aldrich. Tris base was obtained from Fisher Scientific. Ultrapure water (18.2 MΩ-cm) was obtained from a

Thermo Scientific Barnstead E-pure water purification system. Polyether-based polyurethane foam (type 1850, Future Foams, High Point, NC) without flame-retardant additives has a density of 28 kg/m^3 and was used as received.

6.6.2 PDA COATING

PU foam was immersed into dopamine solution (2 mg/mL) in 10mM Tris-HCl (pH 8.5). During the initial stage of dopamine polymerization, the foam was wrung out several times in the solution to draw the solution into the foams. The solution was then aggressively stirred, continuously, for 1-3 days. The solution color turned black by the alkaline pH-induced oxidative polymerization of dopamine. To facilitate the homogeneous circulation of dopamine and growing polydopamine in the solution, the foam was shaken in the solution every 2 h during the first 10 h until the solution color darkened and became consistent. PDA-coated foams were rinsed with ultrapure water and then immersed in deionized water under mild stirring for 3 days to remove unbound PDA while the deionized water continuously changed during the purification. Subsequently, these foams were dried with a mild air stream for 2 days and then under vacuum for one day until a constant weight was reached. Finally, foam samples were dried at 70 °C under vacuum for 2 h before testing. The foam weight was measured before and after the coating to determine the % mass PDA of each sample. In addition, the weight of a control foam decreased upon immersion in the 10mM Tris-HCl (pH 8.5) because some small molecules (e.g., residual unreacted monomers and chemicals) leached out of the foam. The weight loss leveled out after 1 day of immersion in the buffer, reaching a steady state. Since the weight loss from a control foam upon immersion in buffer was about 4.8 wt%, this weight loss was taken into account when % mass PDA was calculated.

6.6.3 TORCH BURN TEST

Foam flammability was qualitatively evaluated through 10 s of exposure to direct flame from a butane torch on the foam's surface.[4, 8] A blue flame from a butane torch implied that the flame temperature was approximately 1300 °C. The burning behaviors of samples (e.g., flame spread, dripping, charring, and receding away from flame) were evaluated visually and videos were recorded. To ascertain the flammability of the material, observations from the torch burn test were analyzed in correlation with the combustion tests.

6.6.4 COMBUSTION TESTS

To evaluate flame retardancy, samples were tested in both a MCC and a cone calorimeter. Microscale combustibility was assessed using a Govmark MCC-2 according to ASTM D7309 method A. The sample size was 4 mg and samples were tested at a heating rate of 1 °C/s under nitrogen, from 80 to 900 °C. The cone calorimeter investigation was performed with a FTT Dual Cone calorimeter at a radiant flux of 35 kW/m^2 with an exhaust flow of 24 L/s based on ASTM E 1354 "Standard Test Method for Heat and Visible Smoke Release rates for Materials and Products using an Oxygen Consumption Calorimeter." The sample dimensions used were 100 × 100 mm^2 with a thickness of 25 mm. The samples were wrapped in aluminum foil without frame or grid, and for each sample three repetitions were done.

6.6.5 CHARACTERIZATION

6.6.5.1 SCANNING ELECTRON MICROSCOPY

Images of the foam surfaces, cross-sections of the foams, and the char morphology were acquired by SEM (Zeiss Supra 40 VP). For SEM images of foam surface and char morphology, the samples were sputter coated with an Au-Pd target prior to imaging to

prevent charging. In addition, to obtain SEM cross-sectional images of the PDA deposition on the foam, the sliced foam samples were cryo-fractured and then coated with osmium tetroxide for 20 h to prevent charging, followed by grounding the samples with strips of copper tape. SEM cross-sectional images were analyzed by using ImageJ software and the average thickness of PDA coating on PU surface was determined. 10 locations per sample were analyzed to measure the average thickness of the PDA coating.

6.6.5.2 THERMOGRAVIMETRIC ANALYSIS

The thermal stability of the samples was investigated with a thermogravimetric analyzer (DSC/TGA 1, Mettler Toledo). Samples were tested from 30 °C to 800 °C at 10 °C/min in nitrogen gas and air.

6.7 REFERENCES

1. Karter, J. J. M., *Fire loss in the United States during 2013*. National Fire Protection Association: Quincy, Massachusetts, 2014.
2. Flambard, X.; Bourbigot, S.; Kozlowski, R.; Muzyczek, M.; Mieleniak, B.; Ferreira, M.; Vermeulen, B.; Poutch, F. *Polym. Degrad. Stab.* **2005,** *88*, 98-105.
3. Kozlowski, R.; Mieleniak, B.; Muzyczek, M. *Polym. Degrad. Stab.* **1999,** *64*, 511-515.
4. Laufer, G.; Kirkland, C.; Morgan, A. B.; Grunlan, J. C. *ACS Macro Lett.* **2013,** *2*, 361-365.
5. Leu, T. S.; Wang, C. S. *J. Appl. Polym. Sci.* **2004,** *92*, 410-417.
6. Watanabe, I.; Sakai, S. *Environ. Int.* **2003,** *29*, 665-682.
7. Pan, H.; Pan, Y.; Wang, W.; Song, L.; Hu, Y.; Liew, K. M. *Ind. Eng. Chem. Res.* **2014,** *53*, 14315-14321.
8. Laufer, G.; Kirkland, C.; Cain, A. A.; Grunlan, J. C. *ACS Appl. Mater. Interfaces* **2012,** *4*, 1643-1649.
9. Shultz, M. D.; Reveles, J. U.; Khanna, S. N.; Carpenter, E. E. *J. Am. Chem. Soc.* **2007,** *129*, 2482-2487.
10. Lee, H.; Rho, J.; Messersmith, P. B. *Adv. Mater.* **2009,** *21*, 431-434.
11. Chien, H. W.; Kuo, W. H.; Wang, M. J.; Tsai, S. W.; Tsai, W. B.. *Langmuir* **2012,** *28*, 5775-5782.
12. Ku, S. H.; Ryu, J.; Hong, S. K.; Lee, H.; Park, C. B. *Biomaterials* **2010,** *31*, 2535-2541.
13. Luczak, T.. *Electrochim. Acta* **2008,** *53*, 5725-5731.

14. Zhang, Y.; Wang, H.; Nie, J.; Zhou, H.; Shen, G.; Yu, R. *Electrochem. Commun.* **2009,** *11*, 1936-1939.
15. McCloskey, B. D.; Park, H. B.; Ju, H.; Rowe, B. W.; Miller, D. J.; Freeman, B. D. *J. Membr. Sci.* **2012,** *413*, 82-90.
16. McCloskey, B. D.; Park, H. B.; Ju, H.; Rowe, B. W.; Miller, D. J.; Chun, B. J.; Kin, K.; Freeman, B. D.,*Polymer* **2010,** *51*, 3472-3485.
17. Kim, B. H.; Lee, D. H.; Kim, J. Y.; Shin, D. O.; Jeong, H. Y.; Hong, S.; Yun, J. M.; Koo, C. M.; Lee, H.; Kim, S. O. *Adv. Mater.* **2011,** *23* , 5618-5622.
18. Fei, B.; Qian, B. T.; Yang, Z. Y.; Wang, R. H.; Liu, W. C.; Mak, C. L.; Xin, J. H. *Carbon* **2008,** *46*, 1795-1797.
19. Dunford, R.; Land, E. J.; Rozanowska, M.; Sarna, T.; Truscott, T. G.. *Free Radical Biol. Med.* **1995,** *19* (6), 735-740.
20. Rozanowska, M.; Sarna, T.; Land, E. J.; Truscott, T. G. *Free Radical Biol. Med.* **1999,** *26*, 518-525.
21. Ju, K. Y.; Lee, Y.; Lee, S.; Park, S. B.; Lee, J. K. *Biomacromolecules* **2011,** *12*, 625-632.
22. Shanmuganathan, K.; Cho, J. H.; Iyer, P.; Baranowitz, S.; Ellison, C. J. *Macromolecules* **2011,** *44*, 9499-9507.
23. Cho, J. H.; Shanmuganathan, K.; Ellison, C. J., Bioinspired Catecholic Copolymers for Antifouling Surface Coatings. *ACS Appl. Mater. Interfaces* **2013,** *5*, 3794-3802.
24. Postma, A.; Yan, Y.; Wang, Y. J.; Zelikin, A. N.; Tjipto, E.; Caruso, F. *Chem. Mater.* **2009,** *21*, 3042-3044.
25. Lee, H.; Dellatore, S. M.; Miller, W. M.; Messersmith, P. B. *Science* **2007,** *318*, 426-430.
26. Ball, V.; Del Frari, D.; Toniazzo, V.; Ruch, D. *J. Colloid. Interface Sci.* **2012,** *386*, 366-372.
27. Bernsmann, F.; Ball, V.; Addiego, F.; Ponche, A.; Michel, M.; Gracio, J. J. D.; Toniazzo, V.; Ruch, D. *Langmuir* **2011,** *27*, 2819-2825.
28. Bernsmann, F.; Frisch, B.; Ringwald, C.; Ball, V. *J. Colloid Interface Sci.* **2010,** *344*, 54-60.
29. Bernsmann, F.; Ponche, A.; Ringwald, C.; Hemmerle, J.; Raya, J.; Bechinger, B.; Voegel, J. C.; Schaaf, P.; Ball, V. *J. Phys. Chem. C* **2009,** *113*, 8234-8242.
30. Bernsrnann, F.; Ersen, O.; Voegel, J. C.; Jan, E.; Kotov, N. A.; Ball, V. *Chemphyschem* **2010,** *11*, 3299-3305.
31. Klosterman, L.; Riley, J. K.; Bettinger, C. J. *Langmuir* **2015,** *31*, 3451-3458
32. Wei, Q.; Zhang, F. L.; Li, J.; Li, B. J.; Zhao, C. S. *Polym. Chem.* **2010,** *1*, 1430-1433.
33. Jiang, J. H.; Zhu, L. P.; Zhu, L. J.; Zhu, B. K.; Xu, Y. Y. *Langmuir* **2011,** *27*, 14180-14187.
34. Chen, M. J.; Shao, Z. B.; Wang, X. L.; Chen, L.; Wang, Y. Z. *Ind. Eng. Chem. Res.* **2012,** *51*, 9769-9776.
35. Gordon, L. N., Charles, A. W. (eds.), *Fire and Polymers: Materials and Solutions for Hazard Prevention*. ACS Symposium Series 797 ed.; Washington DC: American Chemical Society, 2001.

Chapter 7: Effect of Catechol Functionality on Flammability of PU Foams

7.1 INTRODUCTION

Polyurethanes (PUs) have a wide range of applications as coatings, foams, adhesives, sealants, synthetic leather, and more. PU is, however, a highly flammable material. For instance, once ignited, PU foam is capable of setting a room to flashover in less than 10 minutes.[1] Hence, researchers have shown great interest in imparting flame retardancy to PUs, particularly as a foam, so as to reduce fire-related deaths and property loss.[2-3] In the previous chapter, we demonstrated that polydopamine (PDA) coatings served as a flame retardant in PU foam. A key functional unit for the flame retardancy is catechol and PDA coatings on flexible PU foams contain a high content of catechol functionality. Since the repeating unit in PUs is the urethane linkage produced from the reaction of an isocyanate (–N=C=O, NCO) with an alcohol (–OH), an alternative approach to coating is to form PUs by reacting catecholic precursors (L-dopa, LD) as polyol with diisocyanates. This reactive incorporation approach might minimize leaching issues encountered with other small molecule flame-retardant additives. To compare the two approaches, we investigated the effect of catechol functionality on the flammability of PU foams by conducting cone calorimetric analysis of PDA-coated flexible PU foam and LD-containing rigid PU foam (LD-PU).

7.2 SYNTHESIS OF L-DOPA CONTAINING RIGID PU FOAM

LD-PU was synthesized by reacting methylene diphenyl diisocyanate (MDI) and a polyol blend of a polyether polyol and a catecholic monomer, such as LD, which has functional groups such as -OH, -NH_2, and -COOH that can react with NCOs to yield urethane, urea, and amide linkages, respectively (**Scheme 7.1**). In addition, the reaction of carboxylic acid and NCO releases carbon dioxide, which can assist in foaming PU during

the reaction.

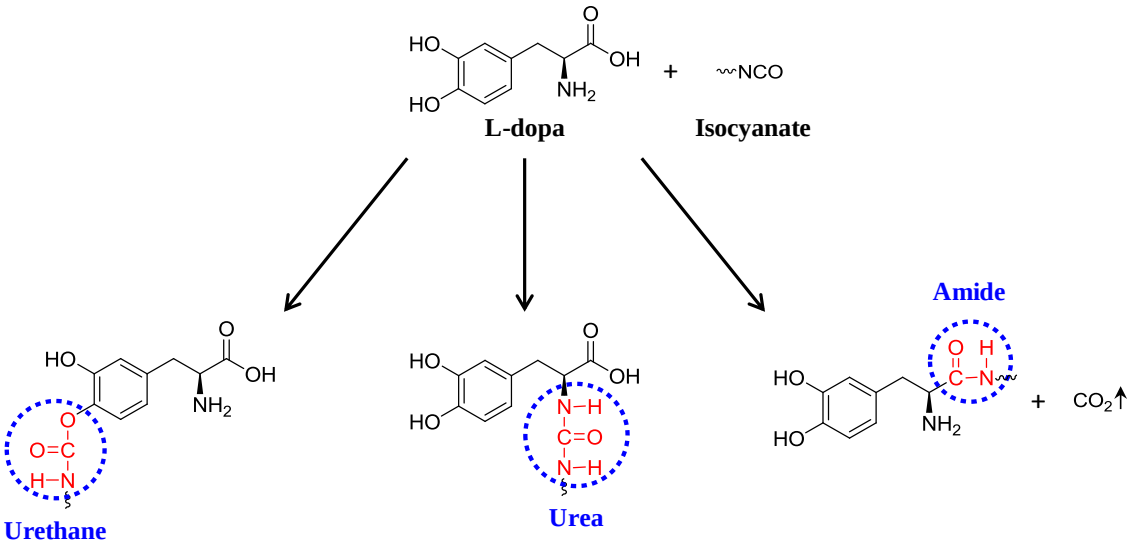

Scheme 7.1: Reaction of L-dopa (LD) and isocyanate (NCO) to produce urethane, urea, and amide linkages.

During the foaming process, NCOs react with distilled water to form CO_2. Water, along with cyclopentane, act as foam-blowing agents. Gelling and blowing catalysts like Polycat® 8 and Polycat® 5 (Air Products) were added in appropriate amounts as outlined in Harikrishnan et al.'s procedure.[4-5] In a typical procedure shown in **Figure 7.1**, a calculated quantity of LD was added to polyol; this was then aggressively stirred for 2 h, using a homogenizer, in a closed container at a temperature of 65 °C. This blend was ultrasonicated for 5 h and allowed to cool for 24 h before foaming and then moderately stirred at 65 °C for 1 h before use. Except for MDI, all the ingredients (catalysts, surfactants, and blowing agents etc.) were weighed into the polyol blend using a 12-ounce paper cup. This solution was mixed manually for 30 s and then with a mechanical stirrer at 2500 rpm for 30 s. At the end of the mixing period, the pre-measured MDI was added to the cup and the mixing was continued at 2500 rpm until the mixture looked uniform and bubbles had started to appear. The contents were then quickly transferred to an aluminum-

lined rectangular mold (6 × 6 × 4 in^3) and the mold was quickly closed. The foam was allowed to rise for 1 h and then demolded. Subsequently, the rigid PU foams were cut into precisely measured 2.5 × 2.5 × 2.5 in^3 cubes. By measuring the weight of the foams, their respective densities were determined. The density was measured from five specimens per sample and then averaged.

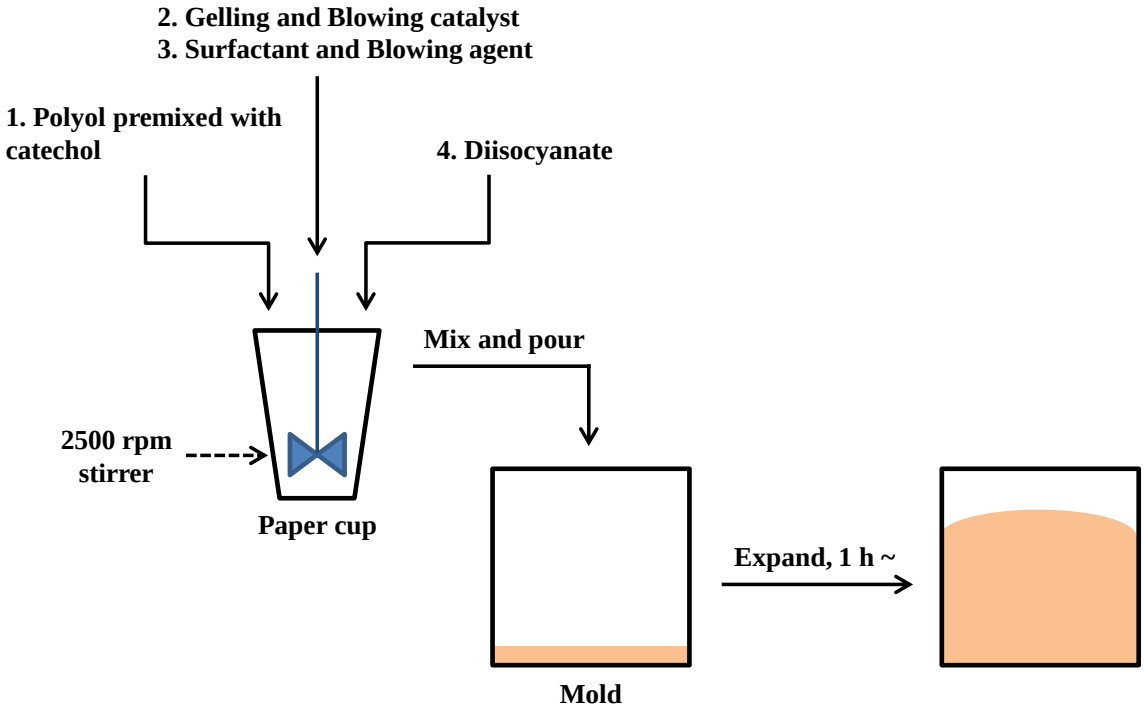

Figure 7.1: Lab-scale batch-foaming procedure. The components are added in the sequence of 1 to 4 while stirring. The mixture is poured quickly into a mold for foaming.

$$\text{NCO Index} = \frac{\text{Actual amount of NCO used}}{\text{Theoretical amount of NCO required}} \times 100 \qquad \text{Eq. 7.1}$$

The amount of NCO used relative to the theoretical equivalent amount is known as the NCO index (**Eq. 7.1**). The NCO index varied from 60 to 105, and 105 is a typical NCO index for industrial rigid PU foams; 0 to 40 wt% of the polyol was replaced by LD. The amount of NCO required to react with the polyol and any other reactive additives was calculated in terms of stoichiometric equivalents. Foam samples were labeled with two numbers separated by a dash; the first number represents the NCO index and the second number represents the wt% of polyol replaced by LD (e.g., 105-40).

7.3 CELL MORPHOLOGY STUDY OF RIGID PU FOAM

Rigid PU foams were synthesized according to a reported procedure[6] and the formulations are listed in **Table 7.1**, while varying the NCO index from 60 to 105 and replacing polyol by LD up to 40 wt%. Subsequently, the rigid PU foams were cut into 2.5 × 2.5 × 2.5 in^3 cubes (**Figure 7.2**), which were then used for foam morphology studies.

Component		Description	Supplier	Part by weight
Monomer	Polyol	Jeffol® SD361 Polyol	Huntsman	100
		L-dopa (LD)	Sigma-Aldrich	
	MDI	Rubinate® M	Huntsman	
Gelling catalyst		Polycat® 8	Air Products	1.19
Blowing catalyst		Polycat® 5	Air Products	0.13
Silicone surfactant		Tegostab® 8404	Evonik industries	0.88
Cyclopentane		95% purity	Sigma-Aldrich	3.96
Water		Distillated water	UT Austin	1.01

Table 7.1: Typical formulation of rigid PU foam.

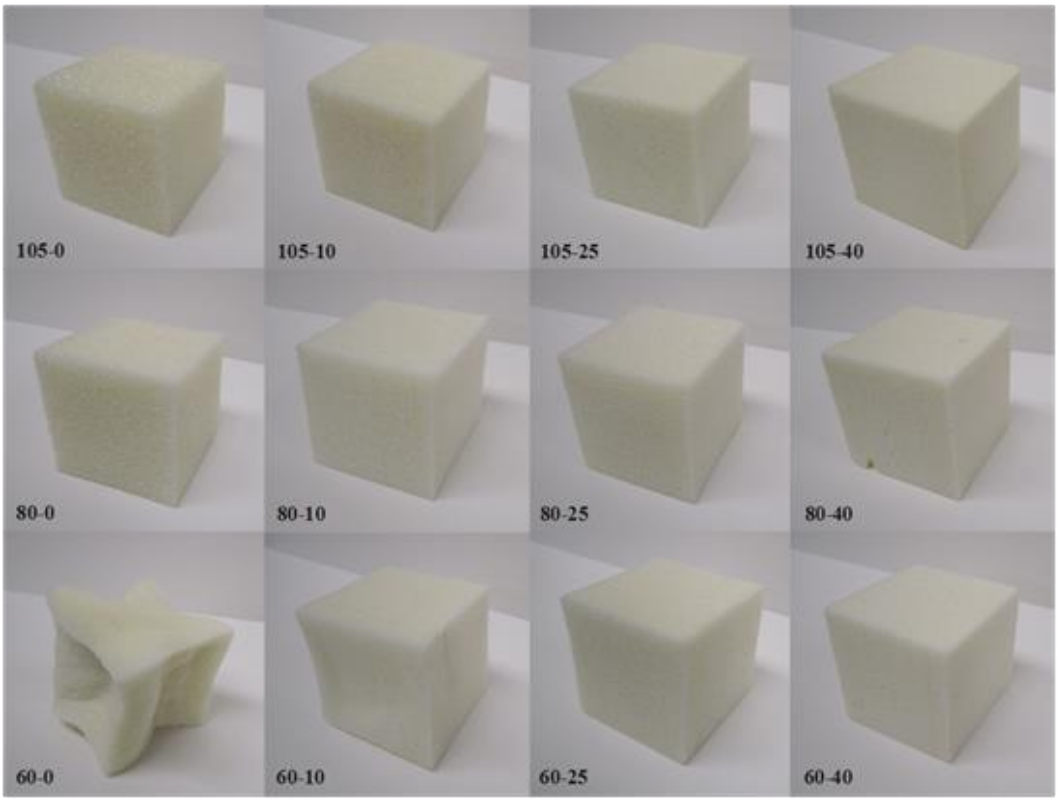

Figure 7.2: Pictures of rigid PU foams with different NCO index (60, 80, 105) and wt% of polyol replaced by LD (0, 10, 25, 40).

LD served to reinforce the foams and replaced the ductile polyether-based polyol, which resulted in enhanced dimensional stability of the rigid foams containing excess polyol (NCO index = 60, 80). For example, shrinkage of foams with the NCO index of 60 diminished with the addition of LD, as shown in the bottom row of **Figure 7.2**. Also, the LD addition neither compromised the foam color (**Figure 7.2**) or the uniformity of foam cellular structure (**Figure 7.3**) nor reduced the foam density (**Table 7.2**). The properties of all produced foams containing LD were comparable to those of commercial products. The foams had average cell diameters ranging from 0.29 to 0.60 mm and average densities of 28-49 kg/m^3, corresponding to the cell size and foam density of typical industrial rigid PU foams.[6] On the other hand, it has been noted that PU foam density can be reduced by

incorporating other natural molecules such as lignin as a partial replacement of polyol.[7] The reduction in density was attributed to the formation of larger cells and voids, which result in a less uniform cell structure, but lignin also negatively altered the foam color.

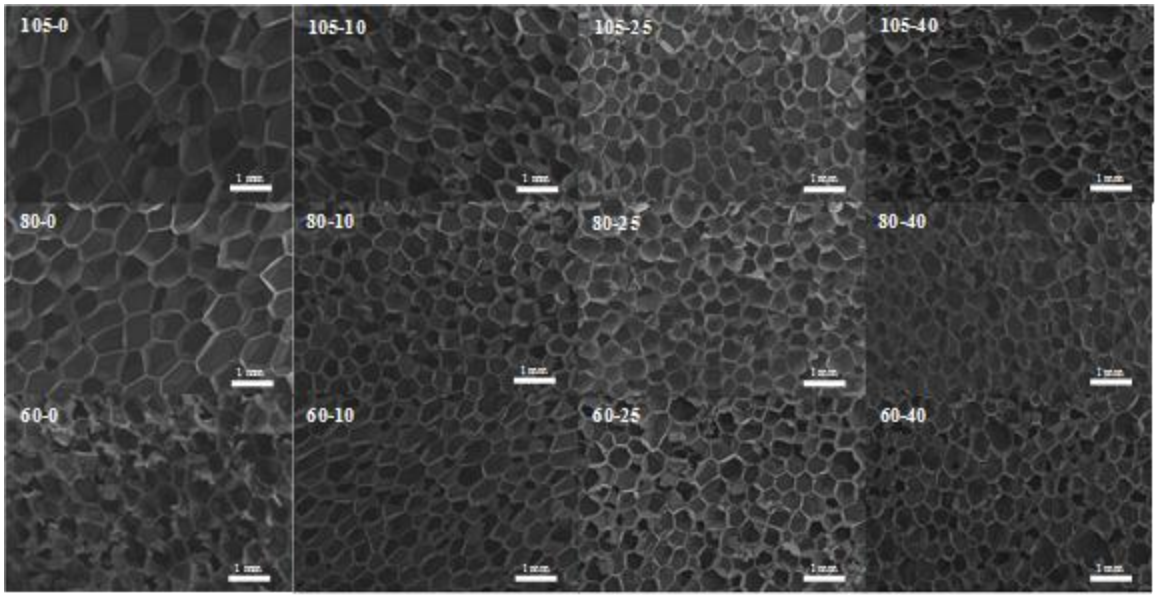

Figure 7.3: Scanning electron micrographs (SEMs) of rigid PU foams with varied NCO index (60, 80, 105) and wt% of polyol replaced by LD (0, 10, 25, 40).

Foam	Foam Density (kg/m^3)	Cell diameter (mm)	LD content (wt%) [a)]
Typical rigid PU foam	20-50	0.25-0.5	
105-0 (control)	29	0.60	0
105-10	32	0.43	4.0
105-25	33	0.39	8.8
105-40	49	0.32	12.5
80-0	29	0.55	0
80-10	28	0.38	4.8
80-25	28	0.35	11.3
80-40	34	0.31	15.4
60-0	N.A.	N.A.	0
60-10	31	0.38	5.6
60-25	30	0.35	12.6
60-40	31	0.29	18.5

[a)] wt% of LD relative to total weight of the foam

Table 7.2: Property comparison of produced foams compared to typical industrial rigid PU foam.[6]

The scanning electron micrographs (SEMs) of **Figures 7.3** show the cell morphology of the produced rigid PU foams. Comparison of the first and second columns of **Figure 7.3** imply that incorporating LD resulted in a significant reduction of cell size at the same NCO index. The LD particles may have reduced the free energy of nucleation followed by generating numerous bubble-nucleating sites.[4] However, comparing LD-PU

foams at the same NCO index, the cell size was roughly maintained or decreased slightly with increasing LD concentration (**Figure 7.4**). Meanwhile, LD did not induce cell opening and aggregation of LD was not seen in cell windows, even for 105-40, which had the highest loading of LD (12.5 wt% relative to total weight of foam, see **Table 7.2**) among PU foams with NCO index of 105 (**Figure 7.5**). This indicates that LD is not antifoaming by nature but compatible with the polyol and the PU liquid matrix. Hence, LD does not result in film drainage and rupture, unlike fillers such as clay nanoparticles that are incompatible with the PU liquid matrix resulting in a rupturing effect on the cell window.[5] This uniform and intact closed cellular structure of the rigid PU foams would be beneficial in thermal insulation applications.[6]

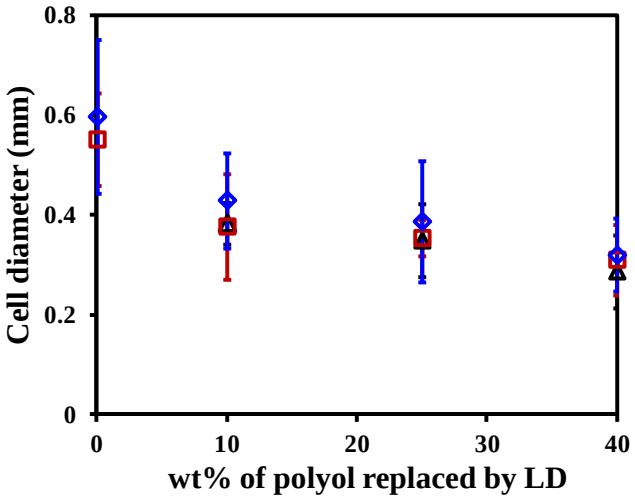

Figure 7.4: Cell diameter according to wt% of polyol replaced by LD of PU foams at the NCO index of 60 (black triangle), 80 (red square), and 105 (blue diamond). Error bars indicate standard deviation from fifteen measurements.

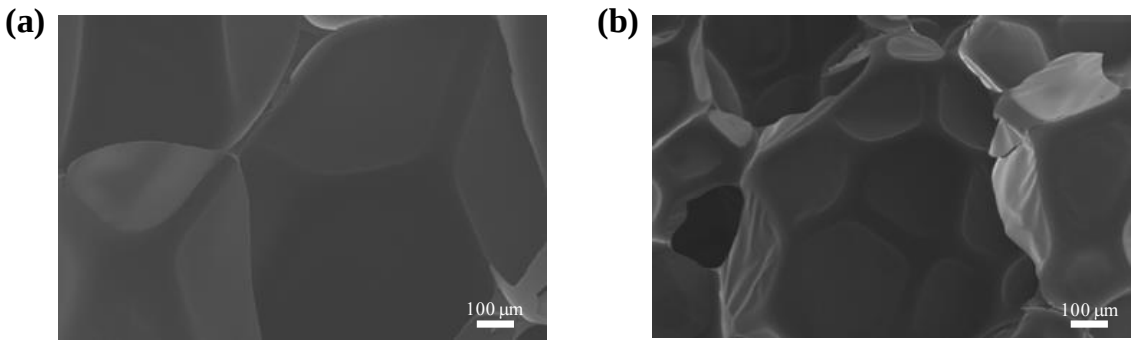

Figure 7.5: SEM images of cell windows of (a) neat PU foam (105-0) and (b) LD-PU foam (105-40).

7.4 QUANTIFICATION OF L-DOPA COVALENTLY LINKED TO PU MATRIX USING LC-MC

To quantify how much LD was covalently bound to the foam matrix, the PU foam with the highest concentration of LD at the NCO index of 105 (105-40) was immersed in ultrapure water at a concentration of 10 mg/mL; it was shaken aggressively during the designated time, up to 2 weeks. This was followed by an analysis of the aqueous solutions by liquid chromatography equipped with mass spectrometry (LC-MS). The wt% of LD leaching out of the foam relative to the original weight of LD in the foam plateaued after 10 days of immersion in water **(Figure 7.6**).

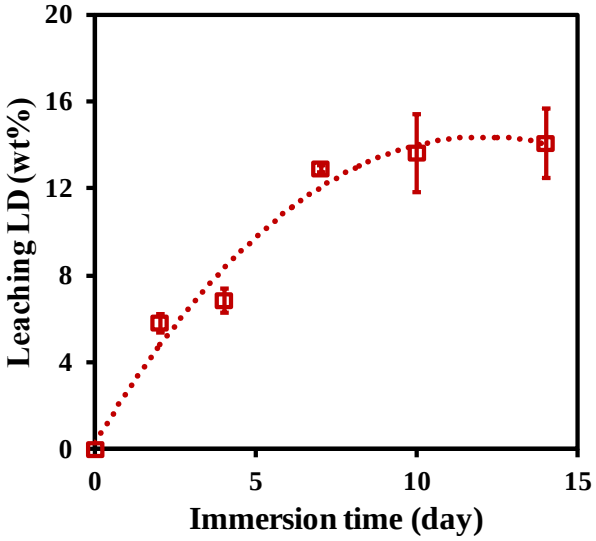

Figure 7.6: The wt% of LD leaching out of foam relative to original weight of LD in the foam upon immersion of the foam in pure water (10 mg/mL, the concentration of the foam in pure water) under aggressive shaking for the designated time, up to 2 weeks. Error bars indicate standard deviation from three measurements.

Of the original weight of LD in the foam (105-40), ~14.1 wt% was extracted, corresponding to a 1.8% weight loss from the total weight of the foam. The wt% of LD leaching out of the foam relative to its original weight was identical to that of a natural macromolecular polyol of lignin in rigid PU foam, reported by Pan et al.,[7] despite the small molecular weight of LD. In sum, the majority of the LD was not physically trapped but chemically bound to the PU foam network, implying that the functional groups of LD were largely depleted during the PU-foaming reaction.

7.5 THERMAL STABILIZATION EFFECT OF L-DOPA IN RIGID PU FOAM

Thermal stability was investigated using thermogravimetric analysis (TGA). As shown in **Figure 7.7**, the thermal decomposition of PU foams under nitrogen and air showed one- and two-step processes, respectively. The second decomposition peak significantly increased for the TGA running in air due to the accelerated char oxidation in

the presence of oxygen. In both nitrogen and air, a small weight loss of neat PU foam was observed at low temperatures between 100 and 200 °C, which is dominated by the evaporation of water and small molecules while most chemical bonds have yet to decompose.[8] In contrast, regardless of LD content, LD-PU foams displayed no weight loss at temperatures lower than 200 °C. Thermal decomposition of PU foam was delayed by the addition of LD such that the peak decomposition temperature shifted up to 63 °C in nitrogen (**Table 7.3**). This indicates a significant thermooxidative stabilization effect of LD on rigid PU foams that could potentially be useful to extend the use temperature of this commercial polymer. This thermal stabilization effect is ascribed to the radical-scavenging capability of catechols as displayed in melanin and polydopamine.[9-10] Although catechols were largely depleted during PU foaming, LD performed well as a thermal stabilizer in PU foams. The enhanced thermal stability of the PU foams implies uniform dispersion of LD during the foaming process and suggests that thermal stabilization of PU can be achieved with a small quantity of catechols.

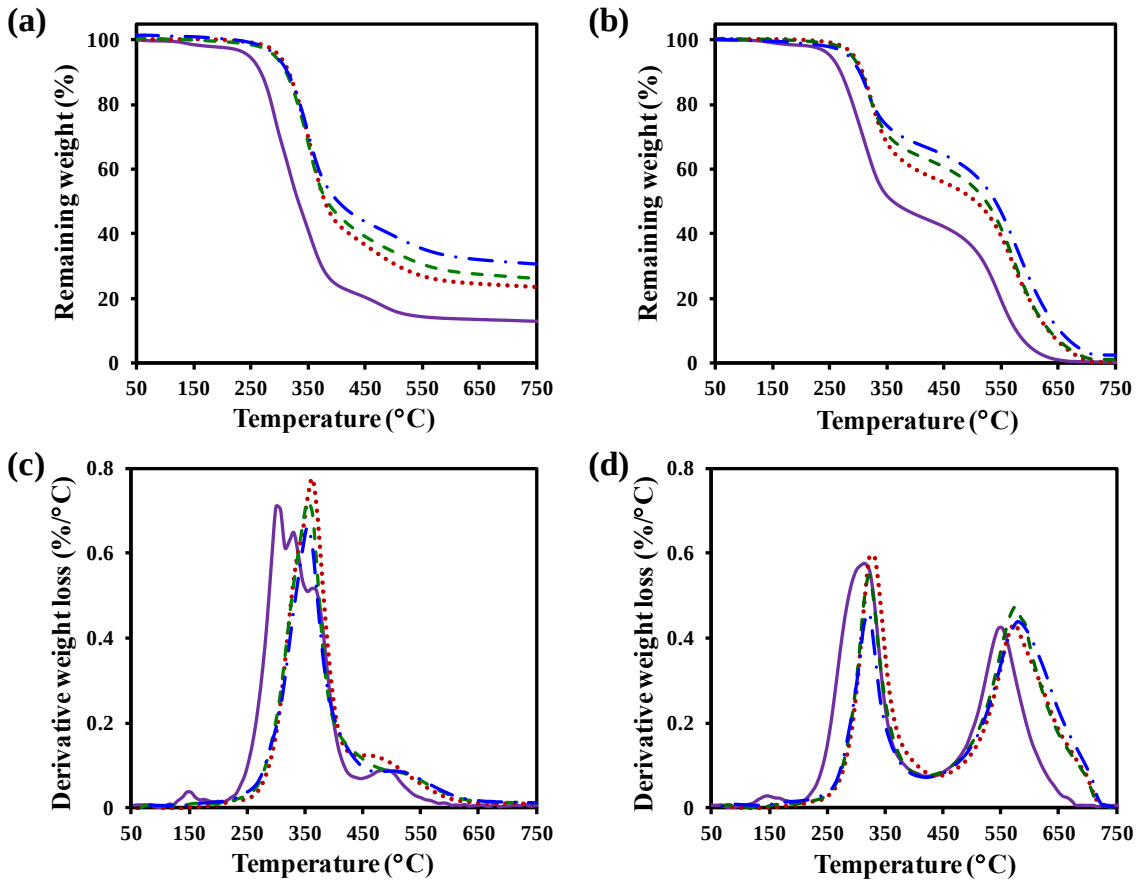

Figure 7.7: Thermogravimetric analysis (TGA) of rigid PU foams of 105 NCO index in (a) nitrogen and (b) air. Derivative thermogravimetric analysis plots of rigid PU foams of 105 NCO index in (c) nitrogen and (d) air: 105-0 (purple solid line), 105-10 (red dotted line), 105-25 (green dashed line) and 105-40 (blue dash-dotted line). All samples were heated at 10 °C/min in a nitrogen or air atmosphere.

Sample	TGA in Nitrogen		TGA in Air	
	Peak Decomp. Temp. (°C)	Remaining Weight at 800 °C (%)	Peak Decomp. Temp. (°C)	Remaining Weight at 800 °C (%)
105-0	300	12	308	0
105-10	363	23	323	0
105-25	355	26	323	0
105-40	355	31	324	0

Table 7.3: TGA result of control and LD-PU foams at a NCO index of 105.

7.6 CONE CALORIMETER RESULTS

As shown in **Figure 7.8** and summarized in **Table 7.4** and **Table 7.5**, LD-containing rigid PU foams exhibited no enhancement in flammability compared to the control rigid PU foam while PDA-coated flexible PU foam achieved a sharp reduction in peak-heat release rate (P-HRR) relative to the control flexible foam (Chapter 6). This huge difference in flammability enhancement between the two distinct approaches was derived from preserving the catechol functionality in the foam coatings. Catechols of LD were largely consumed as a polyol during the PU-foaming reaction and not preserved sufficiently to perform any flame-retardant function. On the other hand, a majority of the catechols in the PDA coating were not consumed and could serve as a radical scavenger upon exposure to flame so that the PDA-coated foam might show significant flame retardancy. As a result, the P-HRR of PDA-coated foams exhibited a reduction by up to 67% while no enhancement in flammability of the rigid PU foams was achieved by replacement of polyol by LD for rigid PU foam. This result demonstrated that catechol functionality provides a powerful flame-retardant effect and should be preserved during incorporation for enhanced flammability of PU foams.

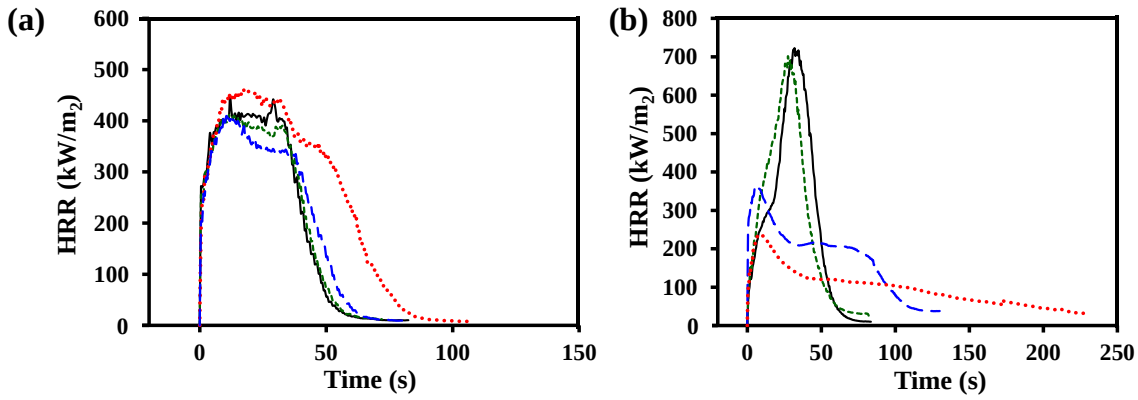

Figure 7.8: (a) Heat release rate (HRR) of 105-0 (black solid line), 105-10 (green dashed line), 105-25 (blue long-dashed line) and 105-40 (red dotted line) as a function of time during cone calorimeter testing. (b) HRR of control (black solid line), PDA1D (flexible PU foam PDA-coated for 1 day, green dashed line), PDA2D (flexible PU foam PDA-coated for 2 day. blue long-dashed line), and PDA3D (flexible PU foam PDA-coated for 3 day, red dotted line) as a function of time during cone calorimeter testing (topic of Chapter 6).

Sample	P-HRR (kW/m^2)	A-HRR (kW/m^2)	Total HR (MJ/m^2)	Time to Ignition (s)	Mass Loss (wt%)
105-0 (Control)	444	285	17	2.02	10.3
105-10	422	298	17	1.92	15.7
105-25	434	282	16	1.63	20.4
105-40	467	333	24	2.30	22.8

Table 7.4: Cone calorimeter results for rigid PU foams of 105-0 (control), 105-10, 105-25, and 105-40.

Sample	P-HRR (kW/m^2)	A-HRR (kW/m^2)	Total HR (MJ/m^2)	Time to Ignition (s)	Mass Loss (wt%)
Control	734	732	23	1.95	99.4
PDA1D	709	697	22	1.92	99.2
PDA2D	368	403	21	1.88	95.9
PDA3D	239	230	21	1.43	79.6

Table 7.5: Cone calorimeter results for flexible PU foams of control, PDA1D (flexible PU foam PDA-coated for 1 day), PDA2D (flexible PU foam PDA-coated for 2 day), and PDA3D (flexible PU foam PDA-coated for 3 day) (topic of Chapter 6).

7.7 CONCLUSIONS

LD-PU foams were synthesized by replacing up to 40 wt% polyether polyol with LD in the PU foam formulation and the flame retardancy of the foams was investigated by cone calorimetry. LD-PU showed uniform cell structure and average foam density, comparable to those of typical industrial rigid PU foams, regardless of LD concentration. LD was compatible with the PU liquid matrix which resulted in an intact closed cellular foam structure, which is beneficial for thermal insulation. Catechols of LD reacted with NCOs of MDI and were largely consumed during PU foaming. This depleted catecholic functionality resulted in no enhancement in flame retardancy of LD-PUs while PDA coatings on flexible PU foams (subject of Chapter 6) led to a sharp reduction in flammability of the coated foams. This work demonstrates that catechol is a key functional unit for flame retardancy and the functionality should be preserved during incorporation for enhanced flame retardancy of PU foams.

7.8 EXPERIMENTAL

7.8.1 MATERIALS

LD was purchased from AK Scientific (Union City, CA). Cyclopentane were obtained from Sigma-Aldrich. Huntsman kindly provided polyether polyol (Jeffol® SD361, Huntsman) with a functionality of 4.2, polymethylenepolyphenyl polyisocyanate (MDI, Rubinate® M, Huntsman) with a functionality of 2.7, silicone surfactant (Tegostab® 8404), gelling catalyst (Polycat® 8, Air Products) and a blowing catalyst (Polycat® 5, Air Products) and these were used as received. Ultrapure water (18.2 MΩ-cm) was obtained from a Thermo Scientific Barnstead E-pure water purification system and used as a chemical blowing agent.

7.8.2 CHARACTERIZATION

7.8.2.1 SCANNING ELECTRON MICROSCOPY

Images of the cellular microstructure of PU foams and char morphology were acquired by SEM (Zeiss Supra 40 VP). To prevent charging, all samples were sputter coated with an Au-Pd target prior to imaging. SEM images were analyzed by using ImageJ software and the average cell diameter of PU foams was determined. To measure the cell size, 15 closed cells per sample were analyzed.

7.8.2.2 THERMOGRAVIMETRIC ANALYSIS

The thermal stability of PU foams was determined using a thermogravimetric analyzer (DSC/TGA 1, Mettler Toledo). PU samples were heated from 30 °C to 800 °C at a ramp rate of 10 °C/min under nitrogen gas and air, respectively. Onset and peak decomposition temperatures were determined while monitoring weight loss in samples as a function of temperature.

7.8.2.3 LD EXTRACTION TEST

Foam sample was immersed into degassed ultrapure water at a concentration of 10 mg/mL and the container of the solution was filled with Ar to prevent the oxidation of LD. The solutions were aggressively shaken during the designated time for up to two weeks. Then to quantify the concentration of LD in the aqueous solutions, a liquid chromatography (Dionex Ultimate 3000) equipped with mass spectrometry (Thermo Finnigan TSQ Quantum; LC-MS) was used.

7.8.2.4 COMBUSTION TEST

To evaluate flame retardancy, samples were tested in a cone calorimeter. The cone calorimeter investigation was performed with an FTT Dual Cone calorimeter at a radiant flux of 35 kW/m^2 with an exhaust flow of 24 L/s based on ASTM E 1354 "Standard Test Method for Heat and Visible Smoke Release rates for Materials and Products using an Oxygen Consumption Calorimeter." The sample dimensions used were 100 × 100 mm^2 with a thickness of 25 mm. The samples were wrapped in aluminum foil without frame or grid, and for each sample three repetitions were done.

7.9 REFERENCES

1. Kramer, R. H.; Zammarano, M.; Linteris, G. T.; Gedde, U. W.; Gilman, J. W.*Polym. Degrad. Stab.* **2010,** *95*, 1115-1122.
2. Laufer, G.; Kirkland, C.; Morgan, B. A.; Grunlan, C. J. *ACS Macro Letters* **2013,** *2*, 361-365.
3. Chattopadhyay, D. K.; Webster, D. C. *Prog. Polym. Sci.* **2009,** *34*, 1068-1133.
4. Harikrishnan, G.; Lindsay, C. I.; Arunagirinathan, M. A.; Macosko, C. W. *ACS Appl. Mater. Interfaces* **2009,** *1*, 1913-1918.
5. Harikrishnan, G.; Singh, S. N.; Kiesel, E.; Macosko, C. W. *Polymer* **2010,** *51*, 3349-3353.
6. Widya, T.; Macosko, W. C., Nanoclay-Modified Rigid Polyurethane Foam. *J. Macromol. Sci. Phys.* **2005,** *44*, 897-908.
7. Pan, X. J.; Saddler, J. N. *Biotechnol Biofuels* **2013,** *6*, 12
8. Jiao, L. L.; Xiao, H. H.; Wang, Q. S.; Sun, J. H. *Polym. Degrad. Stab.* **2013,** *98*, 2687-2696.

9. Cho, J. H.; Shanmuganathan, K.; Ellison, C. J.*ACS Appl. Mater. Interfaces* **2013,** *5*, 3794-3802.
10. Shanmuganathan, K.; Cho, J. H.; Iyer, P.; Baranowitz, S.; Ellison, C. J. *Macromolecules* **2011,** *44*, 9499-9507.

Chapter 8: Future Work

8.1 Introduction

As evidenced in the previous chapters of this dissertation, significant progress has been made regarding catecholic polymers such as melanin and polydopamine (PDA). Still, the are opportunities for future research that could forge a variety of interesting directions. In this chapter, I offer a glimpse of some of these possibilities as they relate to the specific work I completed during my graduate study.

Many properties of melanins and PDA remain largely unexplored and their exact polymeric chemical structure remains elusive. However, the functional aspects of their catecholic chemistries have begun to be exploited and actively studied for a variety of applications over the last decade. This was motivated by Lee et al. renewing interest in catechols by suggesting a mussel-inspired versatile coating system connected to the polymerized catecholic amine known as PDA.[1] Catechols and their derivatives attach to various inorganic and organic materials including metals, polymers and oxides. This universal attachment strategy can impart catechols' useful, multiple functions to the surface while the catecholic sublayers may serve as a platform for secondary reactions. By forming a wide range of ad-layers on top of the PDA adhesive sublayer, the surface properties of materials could be highly tailored enabling future application of catechols in biomedical research, nanotechnology, electronics, flame retardancy, and so on.

8.2 PDA Flame Retardant Surface Coating System

We have demonstrated that PDA can serve as an efficient and environmentally friendly flame retardant due to its strong radical scavenging and char forming capability along with its universal adhesive nature. In particular, this catecholic flame-retardant surface coating approach is exceptionally suitable for highly flammable foamed materials

having low densities with complicated geometries and associated large surface area to volume ratios. All flame retardants are placed on the foam's surface precisely where they are needed, and the coating of the surface flame retardant is carried out efficiently, without compromising the foam's mechanical properties. This advanced fire-retarding approach can be applied to other kinds of foamed materials such as rigid PU (polyurethane) foams and PS (polystyrene) foams, which have been widely used in construction and insulation, where flame retardancy is also a critical issue. Moreover, it might also be fruitful to explore the grafting of flame retardant ad-layers onto PDA coatings for further enhancement of flame retardancy. The PDA layer containing catechol groups is a versatile platform for further modification; the functionalization of the PDA sublayer with additional organic layers could be accomplished through the use of amine-functionalized phosphate or sulfate molecules in a secondary reaction step, giving rise to multifunctional flame-retardant surfaces (**Figure 8.1**).[1]

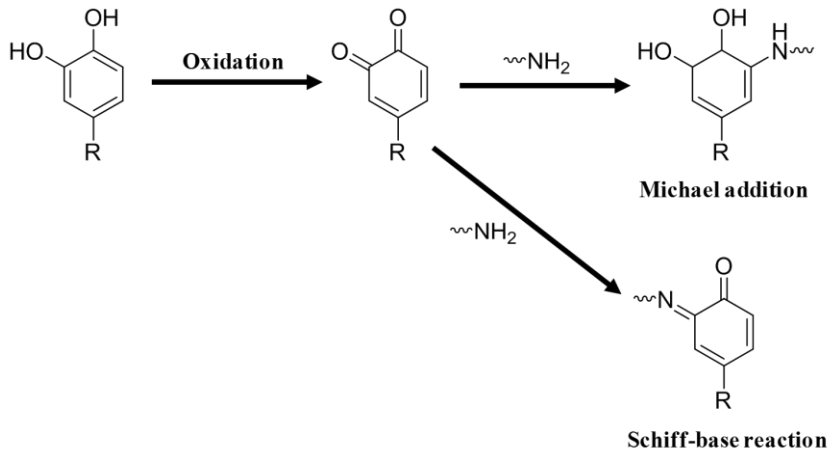

Figure 8.1: Catechol oxidative chemistry for attachment of amine-functionalized molecules to dopamine coatings

Through different mechanisms, phosphorous and sulfur species can play a pivotal

role in retarding flames. Phosphorus species are able to react upon heating to generate a swollen multicellular insulating layer that protects the underlying material from heat and flame while PDA itself serves as a carbon source.[2-5] In addition, as sulfur species degrade, they release nonflammable gases, which may dilute oxygen on the burning surface and scavenge flammable radicals during a fire.[6] The removal of radicals from flammable gasses can slow the burning process and reduce fire spread.[7]

For example, phosphorus-based flame resistant surfaces could be prepared by grafting phosphorylethanolamine [PO_4H_2-C_2H_4-NH_2 in 10 mM tris, pH 8.5, 50°C] onto PDA-coated substrates (**Figure 8.2**).[1] The surface modification can be confirmed by X-ray photoelectron spectroscopy (XPS) and contact angle measurements.[1] This flame-resistant bi-layer nanocoating can be applied to almost any surface with complex structure (i.e., foam, fabric, etc.). A sulfur-containing ad-layer could also be formed in the same way.

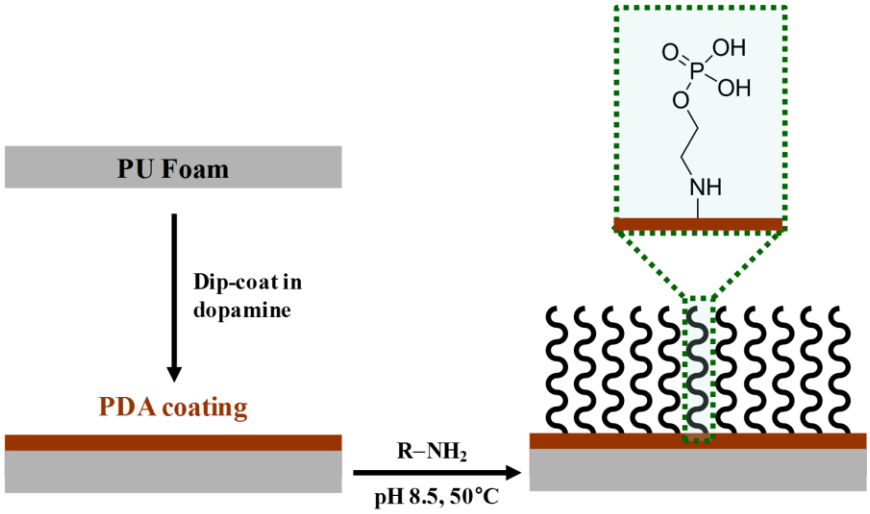

Figure 8.2: PDA-phosphorylethanol bilayer flame retardant nanocoating. R represents the phosphorylethanol chain.

8.3 Antimicrobial and Antifungal Functions of PDA Coatings

In regard to both processing and applications, one of the most versatile polymeric

materials is PU foam. From automotive seating, furniture, to bedding/cushioning, PU foams can be found in almost all aspects of life.[8-9] However, PU biodegradation by microorganisms has become an important issue in the study of foam degradation mechanisms and PU aging, as well as for their end uses. PU biodegradation is hypothesized to be due to microorganisms' utilization of this material as carbon or nitrogen sources or fortuitous biodegradation in the presence of other nutrients and substrates.[10] Moreover, due to their widespread use in our daily lives, the growth and attachment of microorganisms like bacteria and fungi onto the PU foams have become a critical human health issue.

Common herbs such as tarragon and thyme both contain caffeic acid, which is a catecholic derivative that is effective at rejecting viruses, bacteria and fungi.[11] Catechol consists of multiply hydroxylated phenols, which have been shown to be toxic to many microorganisms. The sites and number of hydroxyl groups on the phenol group are thought to be related to their relative toxicity to microorganisms, with evidence that increased hydroxylation results in increased toxicity. In addition, another catecholic molecules such as eugenol are considered bacteriostatic against both fungi and bacteria.[12] If a catechol is oxidized, it becomes a quinone, which is known to react irreversibly with nucleophilic amino acids in proteins,[13] often leading to inactivation of proteins and loss of their function. For that reason, the potential range of quinone antimicrobial effects are many. Quinones may also render substrates unavailable to a microorganism. Given the antimicrobial and antifungal effects of catechols and quinones, it's reasonably deduced that a PDA coating could also prevent microorganisms and fungi from attaching and growing on the PU foams. PDA can act as an effective surface anchor via catechol by itself as well as directly create antimicrobial and antimolding surfaces. To start, simple standard tests for antifungal and antimicrobial activity would be useful in demonstrating the utility of PDA coatings on foams.

8.4 REFERENCES

1. Lee, H.; Dellatore, S. M.; Miller, W. M.; Messersmith, P. B. *Science* **2007**, *318*, 426-430.
2. Wang, J. Q.; Chow, W. K. *J. Appl. Polym. Sci.* **2005,** *97*, 366-376.
3. Li, Y. C.; Mannen, S.; Morgan, A. B.; Chang, S. C.; Yang, Y. H.; Condon, B.; Grunlan, J. C. *Adv. Mater.* **2011,** *23*, 3926-3931.
4. Laufer, G.; Kirkland, C.; Morgan, A. B.; Grunlan, J. C. *Biomacromolecules* **2012**, 13, 2843-2848.
5. Bourbigot, S.; Duquesne, S. *J. Mater. Chem.* **2007,** *17*, 2283-2300.
6. Laufer, G.; Kirkland, C.; Morgan, A. B.; Grunlan, J. C. *ACS Macro Lett.* **2013,** *2*, 361-365.
7. van der Veen, I.; de Boer, J. *Chemosphere* **2012,** *88*, 1119-1153.
8. Flambard, X.; Bourbigot, S.; Kozlowski, R.; Muzyczek, M.; Mieleniak, B.; Ferreira, M.; Vermeulen, B.; Poutch, F. *Polym. Degrad. Stabil.* **2005,** *88*, 98-105.
9. Kozlowski, R.; Mieleniak, B.; Muzyczek, M., *Polym. Degrad. Stabil.* **1999,** *64*, 511-515.
10. Urgun-Demirtas, M.; Singh, D.; Pagilla, K. *Polym. Degrad. and Stabil.* **2007,** *92*, 1599-1610.
11. Cowan, M. M., Plant products as antimicrobial agents. *Clin. Microbiol. Rev.* **1999,** *12*, 564-582.
12. Thomson, W. A. R. (ed.), *Medicines from the Earth* ; McGraw-Hill Book Co.: Maidenhead, UK, 1978.
13. Stern, J. L.; Hagerman, A. E.; Steinberg, P. D.; Mason, P. K. *J. Chem. Ecol.* **1996,** *22*, 1877-1899.

References

1. Faure, E.; Falentin-Daudre, C.; Jerome, C.; Lyskawa, J.; Fournier, D.; Woisel, P.; Detrembleur, C. *Prog. Polym. Sci.* **2013,** *38*, 236-270.
2. Sedo, J.; Saiz-Poseu, J.; Busque, F.; Ruiz-Molina, D. *Adv. Mater.* **2013,** *25*, 653-701.
3. Borman, S. *Chem. Eng. News* **1992,** *70*, 26-26.
4. http://www.rhodia.com/en/binaries/GPS_2011_09_v1_Catechol_gb.pdf. (04/14/2015)
5. http://monographs.iarc.fr/ENG/Monographs/vol71/mono71-18.pdf. (04/14/2015)
6. Schweigert, N.; Zehnder, A. J. B.; Eggen, R. I. L. *Environ. Microbiol.* **2001**, *3*, 81-91.
7. Heo, J.; Kang, T.; Jang, S. G.; Hwang, D. S.; Spruell, J. M.; Killops, K. L.; Waite, J. H.; Hawker, C. J. *J. Am. Chem. Soc.* **2012**, *134*, 20139-20145.
8. Ye, Q.; Zhou, F.; Liu, W. M. *Chem. Soc. Rev.* **2011**, *40*, 4244-4258.
9. d'Ischia, M.; Napolitano, A.; Pezzella, A.; Meredith, P.; Sarna, T. *Angew. Chem. Int. Ed.* **2009**, *48*, 3914-3921.
10. Watt, A. A. R.; Bothma, J. P.; Meredith, P. *Soft Matter* **2009**, *5*, 3754-3760.
11. Liu, Y.; Simon, J. D. *Pigm. Cell. Res.* **2003**, *16*, 72-80.
12. Zeise, L.; Murr, B. L.; Chedekel, M. R. *Pigm. Cell. Res.* **1992**, *5*, 132-142.
13. Chen, S.-R.; Jiang, B.; Zheng, J.-X.; Xu, G.-Y.; Li, J.-Y.; Yang, N. *Food Chem.* **2008**, *111*, 745-749.
14. Tu, Y. G.; Xie, M. Y.; Sun, Y. Z.; Tian, Y. G. *Pigm. Cell. Melanoma R.* **2009**, *22*, 134-136.
15. Cubo, M. T.; Buendia-Claveria, A. M.; Beringer, J. E.; Ruiz-Sainz, J. E. *Appl. Environ. Microbiol.* **1988**, *54*, 1812-1817.
16. Lee, H.; Dellatore, S. M.; Miller, W. M.; Messersmith, P. B. *Science* **2007**, *318*, 426-430.
18. Deziderio, S. N.; Brunello, C. A.; da Silva, M. I. N.; Cotta, M. A.; Graeff, C. F. O. *J. Non-Cryst. Solids* **2004**, *338*, 634-638.
19. Ling, D.; Park, W.; Park, Y. I.; Lee, N.; Li, F.; Song, C.; Yang, S.-G.; Choi, S. H.; Na, K.; Hyeon, T. *Angew. Chem. Int. Ed.* **2011**, *50*, 11360-11365.
20. Postma, A.; Yan, Y.; Wang, Y.; Zelikin, A. N.; Tjipto, E.; Caruso, F. *Chem. Mater.* **2009**, *21*, 3042-3044.
21. Zhang, X.; Wang, S.; Xu, L.; Feng, L.; Ji, Y.; Tao, L.; Li, S.; Wei, Y. *Nanoscale* **2012**, *4*, 5581-5584.
22. McGinnes.J; Corry, P.; Proctor, P. *Science* **1974,** *183*, 853-855.
23. Ito, S.; Wakamatsu, K. Chemistry of Melanin. In The Pimentary System; Nordlund, J.J; Boissy, R.E; Hearing, V.J.; King, R.A.; Oetting, W.S.; Ortonne, J. Eds.; Blackwell Publishing Ltd: Malden, 2006; Second ed, pp 282-310.
24. Rozanowska, M.; Sarna, T.; Land, E. J.; Truscott, T. G. Free Radic. Biol. Med. 1999, 26, 518.
25. Meredith, P.; Sarna, T. Pigm. Cell. Res. 2006, 19, 572-594.

26. Bernsmann, F.; Ponche, A.; Ringwald, C.; Hemmerle, J.; Raya, J.; Bechinger, B.; Voegel, J. C.; Schaaf, P.; Ball, V. *J. Phys. Chem. C* **2009,** *113*, 8234-8242.
27. Shalev, T.; Gopin, A.; Bauer, M.; Stark, R. W.; Rahimipour, S. *J. Mater. Chem.* **2012,** *22*, 2026-2032.
28. Hong, S.; Na, Y. S.; Choi, S.; Song, I. T.; Kim, W. Y.; Lee, H. *Adv. Funct. Mater.* **2012,** *22*, 4711-4717.
29. Liebscher, J.; Mrowczynski, R.; Scheidt, H. A.; Filip, C.; Hadade, N. D.; Turcu, R.; Bende, A.; Beck, S. *Langmuir* **2013,** *29*, 10539-10548.
30. Sarna Tadeusz, Swartz, H. A. The Physical Properties of Melanins. In *The Pimentary System;* Nordlund, J.J; Boissy, R.E; Hearing, V.J.; King, R.A.; Oetting, W.S.; Ortonne, J. Eds.; Blackwell Publishing Ltd: Malden, 2006; Second ed, pp 311-341.
31. Dunford, R.; Land, E. J.; Rozanowska, M.; Sarna, T.; Truscott, T. G. *Free Radical Biol. Med.* **1995,** *19*, 735-740.
32. Ju, K. Y.; Lee, Y.; Lee, S.; Park, S. B.; Lee, J. K. *Biomacromolecules* **2011**, *12*, 625-632.
33. Shanmuganathan, K.; Cho, J. H.; Iyer, P.; Baranowitz, S.; Ellison, C. J. *Macromolecules* **2011**, *44*, 9499-9507.
34. Cho, J. H.; Shanmuganathan, K.; Ellison, C. J. *ACS Appl. Mater. Interfaces* **2013**, *5*, 3794-3802.
35. Meredith, P.; Powell, B. J.; Riesz, J.; Nighswander-Rempel, S. P.; Pederson, M. R.; Moore, E. G. *Soft Matter* **2006,** *2*, 37-44.
36. Kim, B. H.; Lee, D. H.; Kim, J. Y.; Shin, D. O.; Jeong, H. Y.; Hong, S.; Yun, J. M.; Koo, C. M.; Lee, H.; Kim, S. O. *Adv. Mater.* **2011,** *23*, 5618-5622.
37. Xu, L. Q.; Yang, W. J.; Neoh, K.-G.; Kang, E.-T.; Fu, G. D. *Macromolecules* **2010,** *43*, 8336-8339.
38. Wu, J. J.; Zhang, L.; Wang, Y. X.; Long, Y. H.; Gao, H.; Zhang, X. L.; Zhao, N.; Cai, Y. L.; Xu, J. *Langmuir* **2011,** *27*, 13684-13691.
39. Janes, D. W.; Thode, C. J.; Willson, C. G.; Nealey, P. F.; Ellison, C. J. *Macromolecules* **2013,** *46*, 4510-4519.
40. Kang, S. M.; Ryou, M. H.; Choi, J. W.; Lee, H. *Chem. Mater.* **2012,** *24*, 3481-3485.
41. Shultz, M. D.; Reveles, J. U.; Khanna, S. N.; Carpenter, E. E. *J. Am. Chem. Soc.* **2007,** *129*, 2482-2487..
42. Lee, H.; Rho, J.; Messersmith, P. B. *Adv. Mater.* **2009,** *21*, 431-434.
43. Chien, H. W.; Kuo, W. H.; Wang, M. J.; Tsai, S. W.; Tsai, W. B. *Langmuir* **2012,** *28*, 5775-5782.
44. Ku, S. H.; Ryu, J.; Hong, S. K.; Lee, H.; Park, C. B., General functionalization route for cell adhesion on non-wetting surfaces. *Biomaterials* **2010,** *31* (9), 2535-2541.
45. McCloskey, B. D.; Park, H. B.; Ju, H.; Rowe, B. W.; Miller, D. J.; Freeman, B. D. *J. Membrane Sci.* **2012,** *413*, 82-90.
46. McCloskey, B. D.; Park, H. B.; Ju, H.; Rowe, B. W.; Miller, D. J.; Chun, B. J.; Kin, K.; Freeman, B. D. *Polymer* **2010**, *51*, 3472-3485.
47. Zhang, L.; Wu, J. J.; Wang, Y. X.; Long, Y. H.; Zhao, N.; Xu, J. *J. Am. Chem. Soc.* **2012,** *134*, 9879-9881.

48. Yu, B.; Liu, J. X.; Liu, S. J.; Zhou, F. *Chem. Commun.* **2010,** *46*, 5900-5902.
49. Mendez, J.; Annamalai, P. K.; Eichhorn, S. J.; Rusli, R.; Rowan, S. J.; Foster, E. J.; Weder, C. *Macromolecules* **2011,** *44*, 6827.
50. Pei, A.; Malho, J.-M.; Ruokolainen, J.; Zhou, Q.; Berglund, L. A. *Macromolecules* **2011,** *44*, 4422.
51. Capadona, J. R.; Van Den Berg, O.; Capadona, L. A.; Schroeter, M.; Rowan, S. J.; Tyler, D. J.; Weder, C. *Nat. Nano* **2007,** *2*, 765.
52. Morin, A.; Dufresne, A. *Macromolecules* **2002,** *35*, 2190.
53. Madihally, S. V.; Matthew, H. W. T. *Biomaterials* **1999,** *20*, 1133.
54. Yeo, I.-S.; Oh, J.-E.; Jeong, L.; Lee, T. S.; Lee, S. J.; Park, W. H.; Min, B.-M. *Biomacromolecules* **2008,** *9*, 1106.
55. Brenner, M.; Hearing, V. J. *Photochem. Photobiol.* **2008,** *84*, 539.
56. Clancy, C. M. R.; Simon, J. D. *Biochemistry* **2001,** *40*, 13353.
57. Lawrie, K. J.; Meredith, P.; McGeary, R. P. *Photochem. Photobiol.* **2008,** *84*, 632.
58. Abbas, M.; D'Amico, F.; Morresi, L.; Pinto, N.; Ficcadenti, M.; Natali, R.; Ottaviano, L.; Passacantando, M.; Cuccioloni, M.; Angeletti, M.; Gunnella, R. *Eur. Phys. J. E* **2009,** *28*, 285.
59. Bothma, J. P.; de Boor, J.; Divakar, U.; Schwenn, P. E.; Meredith, P. *Adv. Mater.* **2008,** *20*, 3539.
60. Bettinger, C. J.; Bruggeman, P. P.; Misra, A.; Borenstein, J. T.; Langer, R. *Biomaterials* **2009,** *30*, 3050.
61. Kim, E.; Liu, Y.; Baker, C. J.; Owens, R.; Xiao, S.; Bentley, W. E.; Payne, G. F. *Biomacromolecules* **2011,** *12*, 880.
62. Ju, K.-Y.; Lee, Y.; Lee, S.; Park, S. B.; Lee, J.-K. *Biomacromolecules* **2011,** *12*, 625-632.
63. Goncalves, P. J.; Baffa, O.; Graeff, C. F. O. *J. Appl. Phys.* **2006,** *99*, 104701-104705.
64. Simonovic, B.; Vucelic, V.; Hadzi-Pavlovic, A.; Stepien, K.; Wilczok, T.; Vucelic, D. *J. Therm. Anal. Calorim.* **1990,** *36*, 2475-2482.
65. Gómez-Marín, A. M.; Sánchez, C. I. *J. Non-Cryst. Solids* **2010,** *356*, 1576-1580.
66. Hong, L.; Simon, J. D. *J. Phys. Chem. B* **2007,** *111*, 7938-7947.
67. Holland, B. J.; Hay, J. N. *Polym. Degrad. Stabil.* **2002,** *77*, 435-439.
68. Hu, Y.-H.; Chen, C.-Y. *Polym. Degrad. Stabil.* **2003,** *82*, 81-88.
69. Kashiwagi, T.; Inaba, A.; Brown, J. E.; Hatada, K.; Kitayama, T.; Masuda, E. *Macromolecules* **1986,** *19*, , 2160-2168.
70. Manring, L. E.; Sogah, D. Y.; Cohen, G. M. *Macromolecules* **1989,** *22*, 4652-4654.
71. Hirata, T.; Kashiwagi, T.; Brown, J. E. *Macromolecules* **1985,** *18*, 1410-1418.
72. Ozawa, T. *J. Therm. Anal. Calorim.* **1970,** *2*, 301-324.
73. Flynn, J. H.; Wall, L. A. *J. Polym. Sci. Part B: Polym. Lett.* **1966,** *4*, 323-328.
74. Waldman, W. R.; De Paoli, M. A. *Polym. Degrad. Stabil.* **1998,** *60*, 301-308.
75. Peterson, J. D.; Vyazovkin, S.; Wight, C. A. *Macromol. Chem. Phys.* **2001,** *202*, 775-784.
76. McGinness, J.; Corry, P. *Science* **1974,** *183*, 853-855.

77. Stark, K. B.; Gallas, J. M.; Zajac, G. W.; Eisner, M.; Golab, J. T. *J. Phys. Chem. B 2* **2003,** *107*, 11558-11562.
78. Kim, B. G.; Kim, S.; Lee, H.; Choi, J. W. *Chem. Mater.* **2014,** *26*, 4757-4764.
79. Hill, H. Z.; Li, W.; Xin, P.; Mitchell, D. L. *Pigment cell res.* **1997,** *10*, 158-161.
80. Bertrand, P.; Jonas, A.; Laschewsky, A.; Legras, R. *Macromol. Rapid Comm.* **2000,** *21*, 319-348.
81. Lvov, Y.; Decher, G.; Mohwald, H., Assembly. *Langmuir* **1993,** *9*, 481-486.
82. Cain, A. A.; Nolen, C. R.; Li, Y.-C.; Davis, R.; Grunlan, J. C. *Polym. Degrad. Stab.* **2013,** *98*, 2645-2652.
83. Priolo, M. A.; Gamboa, D.; Holder, K. M.; Grunlan, J. C. *Nano Lett.* **2010,** *10*, 4970-4.
84. Yang, Y. H.; Bolling, L.; Priolo, M. A.; Grunlan, J. C. *Adv. Mater.* **2013,** *25*, 503-8.
85. Joshi, M.; Khanna, R.; Shekhar, R.; Jha, K. *J. Appl. Polym. Sci.* **2011,** *119*, 2793-2799.
86. Nuraje, N.; Asmatulu, R.; Cohen, R. E.; Rubner, M. F. *Langmuir* **2011,** *27*, 782-91.
87. Shimomura, H.; Gemici, Z.; Cohen, R. E.; Rubner, M. F. *ACS Appl. Mater. Interfaces* **2010,** *2*, 813-20.
88. Pitts, D. G.; Cullen, A. P.; Hacker, P. D. *Invest. Ophthalmol. Vis. Sci.* **2003,** *16*, 932-939.
89. Picart, C.; Lavalle, P.; Hubert, P.; Cuisinier, F. J. G.; Decher, G.; Schaaf, P.; Voegel, J.-C. *Langmuir* **2001,** *17*, 7414-7424.
90. Wünsche, J.; Cicoira, F.; Graeff, C. F. O.; Santato, C. *J. Mater. Chem. B* **2013,** *1*, 3836.
91. Gandini, S.; Autier, P.; Boniol, M. *Prog. Biophys. Mol. Biol.* **2011,** *107*, 362-6.
92. Wu, J.; Zhang, L.; Wang, Y.; Long, Y.; Gao, H.; Zhang, X.; Zhao, N.; Cai, Y.; Xu, J. *Langmuir* **2011,** *27*, 13684-91.
93. Alemu, D.; Wei, H.-Y.; Ho, K.-C.; Chu, C.-W. *Energy Environ. Sci.* **2012,** *5*, 9662.
94. Dawidczyk, T. J.; Walton, M. D.; Jang, W.-S.; Grunlan, J. C. *Langmuir* **2008,** *24*, 8314-8318.
95. Dalsin, J. L.; Messersmith, P. B. *Mater. Today* **2005**, *8*, 38-46.
96. Statz, A. R.; Meagher, R. J.; Barron, A. E.; Messersmith, P. B. *J. Am. Chem. Soc.* **2005**, *127*, 7972-7973.
97. Gao, C. L.; Li, G. Z.; Xue, H.; Yang, W.; Zhang, F. B.; Jiang, S. Y. *Biomaterials* **2010**, *31*, 1486-1492.
98. Chambers, L. D.; Stokes, K. R.; Walsh, F. C.; Wood, R. J. K. *Surf. Coat. Technol.* **2006**, *201*, 3642-3652.
99. Yebra, D. M.; Kiil, S.; Dam-Johansen, K. *Prog. Org. Coat.* **2004**, *50*, 75-104.
100. Lee, H.; Lee, B. P.; Messersmith, P. B. *Nature* **2007**, *448*, 338-U334.
101. Yu, M. E.; Deming, T. J. *Macromolecules* **1998**, *31*, 4739-4745.
102. Huang, Z. X.; Zhang, Y. M.; Li, H.; Luan, Y. H.; Liu, Y. G. *J. Polym. Sci., Part A: Polym. Chem.* **2008**, *46*, 1416-1426.
103. Kwak, Y.; Matyjaszewski, K. *Polym. Int.* **2009**, *58*, 242-247.
104. Min, K.; Gao, H. F.; Matyjaszewski, K. *Macromolecules* **2007**, *40*, 1789-1791.
105. Jakubowski, W.; Matyjaszewski, K. *Angew. Chem., Int. Ed.* **2006**, *45*, 4482-4486.
106. Jakubowski, W.; Min, K.; Matyjaszewski, K. *Macromolecules* **2006**, *39*, 39-45.

107. Hiemenz, P. C.; Lodge,T. P. *Polymer Chemistry*, 2nd ed.; CPC Press: Boca Raton, FL, 2007.
108. Moad, G.; Solomon, D. H. *The Chemistry of Free Radical Polymerization*, 1st ed.; Pergamon: Tarrytown, NY, 1995.
109. Pop-Georgievski, O.; Popelka, S.; Houska, M.; Chvostova, D.; Proks, V.; Rypacek, F. *Biomacromolecules* **2011**, *12*, 3232-3242.
110. da Silva, M. I. N.; Deziderio, S. N.; Gonzalez, J. C.; Graeff, C. F. O.; Cotta, M. A. *J. Appl. Phys.* **2004**, *96*, 5803-5807.
111. Wei, Q.; Zhang, F. L.; Li, J.; Li, B. J.; Zhao, C. S. *Polym. Chem.* **2010**, *1*, 1430-1433.
112. Hu, Y. H.; Chen, C. Y. *Polym. Degrad. Stab.* **2003**, *82*, 81-88.
113. Dreyer, D. R.; Miller, D. J.; Freeman, B. D.; Paul, D. R.; Bielawski, C. W. *Langmuir* **2012**, *28*, 6428-6435.
114. Wang, H.; Li, L. L.; Tong, Q.; Yan, M. D. *ACS Appl. Mater. Interfaces* **2011**, *3*, 3463-3471.
115. Lee, H.; Scherer, N. F.; Messersmith, P. B. *Proc. Natl. Acd. Sci. U. S. A.* **2006**, *103*, 12999-13003.
116. Fu, G. D.; Xu, L. Q.; Yao, F.; Zhang, K.; Wang, X. F.; Zhu, M. F.; Nie, S. Z. *ACS Appl. Mater. Interfaces* **2009**, *1*, 239-243.
117. Taylor, M.; Urquhart, A. J.; Anderson, D. G.; Williams, P. M.; Langer, R.; Alexander, M. R.; Davies, M. C. *Macromol. Rapid Commun.* **2008**, *29*, 1298-1302.
118. Zhu, B. C.; Edmondson, S. *Polymer* **2011**, *52*, 2141-2149.
119. Warren, S. C.; Messina, L. C.; Slaughter, L. S.; Kamperman, M.; Zhou, Q.; Gruner, S. M.; DiSalvo, F. J.; Wiesner, U. *Science* **2008,** *320*, 1748-1752.
120. Jeong, B.; Bae, Y. H.; Lee, D. S.; Kim, S. W. *Nature* **1997,** *388*, 860-862.
121. Kataoka, K.; Harada, A.; Nagasaki, Y. *Adv. Drug Delivery Rev.* **2001,** *47*, 113-131.
122. Bates, C. M.; Maher, M. J.; Janes, D. W.; Ellison, C. J.; Willson, C. G. *Macromolecules* **2014,** *47*, 2-12.
123. Rogers, J. A.; Someya, T.; Huang, Y. G. *Science* **2010,** *327*, 1603-1607.
124. Xia, Y.; Whitesides, G. M., *Angew. Chem. Int. Ed.* **1998,** *37*, 550-575.
125. Dreyer, D. R.; Miller, D. J.; Freeman, B. D.; Paul, D. R.; Bielawski, C. W. Chem. Sci. 2013, 4, 3796-3802.
126. Klosterman, L.; Riley, J. K.; Bettinger, C. J. *Langmuir* **2015,** *31*, 3451-3458.
127. Ball, V.; Del Frari, D.; Toniazzo, V.; Ruch, D. *J. Colloid. Interface Sci.* **2012,** *386*, 366-372.
128. Guardingo, M.; Esplandiu, M. J.; Ruiz-Molina, D. *Chem. Commun.* **2014,** *50*, 12548-12551.
129. Bao, Z. N.; Feng, Y.; Dodabalapur, A.; Raju, V. R.; Lovinger, A. J. *Chem. Mater.* **1997,** *9*, 1299-1301.
130. Rogers, J. A.; Bao, Z.; Baldwin, K.; Dodabalapur, A.; Crone, B.; Raju, V. R.; Kuck, V.; Katz, H.; Amundson, K.; Ewing, J.; Drzaic, P. *Proc. Natl. Acd. Sci. U. S. A.* **2001,** *98*, 4835-4840.
131. Garnier, F.; Hajlaoui, R.; Yassar, A.; Srivastava, P. *Science* **1994,** *265*, 1684-1686.

132. Gelinck, G. H.; Huitema, H. E. A.; Van Veenendaal, E.; Cantatore, E.; Schrijnemakers, L.; Van der Putten, J.; Geuns, T. C. T.; Beenhakkers, M.; Giesbers, J. B.; Huisman, B. H.; Meijer, E. J.; Benito, E. M.; Touwslager, F. J.; Marsman, A. W.; Van Rens, B. J. E.; De Leeuw, D. M. *Nat. Mater.* **2004,** *3*, 106-110.
133. Jackman, R. J.; Wilbur, J. L.; Whitesides, G. M. *Science* **1995,** *269*, 664-666.
134. Xia, Y. N.; Qin, D.; Whitesides, G. M. *Adv. Mater.* **1996,** *8*, 1015-1017.
135. Liu, G.; Stoykovich, M. P.; Ji, S.; Stuen, K. O.; Craig, G. S. W.; Nealey, P. F. *Macromolecules* **2009**, 42, 3063-3072.
136. Han, E.; Stuen, K. O.; La, Y. H.; Nealey, P. F.; Gopalan, P. *Macromolecules* **2008,** *41*, 9090-9097.
137. Karter, J. J. M., *Fire loss in the United States during 2013*. National Fire Protection Association: Quincy, Massachusetts, **2014**.
138. Flambard, X.; Bourbigot, S.; Kozlowski, R.; Muzyczek, M.; Mieleniak, B.; Ferreira, M.; Vermeulen, B.; Poutch, F. *Polym. Degrad. Stab.* **2005,** *88*, 98-105.
139. Kozlowski, R.; Mieleniak, B.; Muzyczek, M. *Polym. Degrad. Stab.* **1999,** *64*, 511-515.
140. Laufer, G.; Kirkland, C.; Morgan, A. B.; Grunlan, J. C. *ACS Macro Lett.* **2013,** *2*, 361-365.
141. Leu, T. S.; Wang, C. S. *J. Appl. Polym. Sci.* **2004,** *92*, 410-417.
142. Watanabe, I.; Sakai, S. *Environ. Int.* **2003,** *29*, 665-682.
143. Pan, H.; Pan, Y.; Wang, W.; Song, L.; Hu, Y.; Liew, K. M. *Ind. Eng. Chem. Res.* **2014,** *53*, 14315-14321.
144. Laufer, G.; Kirkland, C.; Cain, A. A.; Grunlan, J. C. *ACS Appl. Mater. Interfaces* **2012,** *4*, 1643-1649.
145. Luczak, T. *Electrochim. Acta* **2008,** *53*, 5725-5731.
146. Zhang, Y.; Wang, H.; Nie, J.; Zhou, H.; Shen, G.; Yu, R. *Electrochem. Commun.* **2009,** *11*, 1936-1939.
147. Fei, B.; Qian, B. T.; Yang, Z. Y.; Wang, R. H.; Liu, W. C.; Mak, C. L.; Xin, J. H. *Carbon* **2008,** *46*, 1795-1797.
148. Bernsmann, F.; Ball, V.; Addiego, F.; Ponche, A.; Michel, M.; Gracio, J. J. D.; Toniazzo, V.; Ruch, D. *Langmuir* **2011,** *27*, 2819-2825.
149. Bernsmann, F.; Frisch, B.; Ringwald, C.; Ball, V. *J. Colloid Interface Sci.* **2010,** *344*, 54-60.
150. Jiang, J. H.; Zhu, L. P.; Zhu, L. J.; Zhu, B. K.; Xu, Y. Y. *Langmuir* **2011,** *27*, 14180-14187.
151. Chen, M. J.; Shao, Z. B.; Wang, X. L.; Chen, L.; Wang, Y. Z. *Ind. Eng. Chem. Res.* **2012,** *51*, 9769-9776.
152. Gordon, L. N., Charles, A. W. (eds.), *Fire and Polymers: Materials and Solutions for Hazard Prevention*. ACS Symposium Series 797 ed.; Washington DC: American Chemical Society, 2001.
153. Kramer, R. H.; Zammarano, M.; Linteris, G. T.; Gedde, U. W.; Gilman, J. W.*Polym. Degrad. Stab.* **2010,** *95*, 1115-1122.
154. Chattopadhyay, D. K.; Webster, D. C. *Prog. Polym. Sci.* **2009,** *34*, 1068-1133.

155. Harikrishnan, G.; Lindsay, C. I.; Arunagirinathan, M. A.; Macosko, C. W. *ACS Appl. Mater. Interfaces* **2009,** *1*, 1913-1918.
156. Harikrishnan, G.; Singh, S. N.; Kiesel, E.; Macosko, C. W. *Polymer* **2010,** *51*, 3349-3353.
157. Widya, T.; Macosko, W. C., Nanoclay-Modified Rigid Polyurethane Foam. *J. Macromol. Sci. Phys.* **2005,** *44*, 897-908.
158. Pan, X. J.; Saddler, J. N. *Biotechnol Biofuels* **2013,** *6*, 12
159. Jiao, L. L.; Xiao, H. H.; Wang, Q. S.; Sun, J. H. *Polym. Degrad. Stab.* **2013,** *98*, 2687-2696.
160. Wang, J. Q.; Chow, W. K. *J. Appl. Polym. Sci.* **2005,** *97*, 366-376.
161. Li, Y. C.; Mannen, S.; Morgan, A. B.; Chang, S. C.; Yang, Y. H.; Condon, B.; Grunlan, J. C. *Adv. Mater.* **2011,** *23*, 3926-3931.
162. Laufer, G.; Kirkland, C.; Morgan, A. B.; Grunlan, J. C. *Biomacromolecules* **2012**, 13, 2843-2848.
163. Bourbigot, S.; Duquesne, S. *J. Mater. Chem.* **2007,** *17*, 2283-2300.
164. van der Veen, I.; de Boer, J. *Chemosphere* **2012,** *88*, 1119-1153.
165. Flambard, X.; Bourbigot, S.; Kozlowski, R.; Muzyczek, M.; Mieleniak, B.; Ferreira, M.; Vermeulen, B.; Poutch, F. *Polym. Degrad. Stabil.* **2005,** *88*, 98-105.
166. Kozlowski, R.; Mieleniak, B.; Muzyczek, M., *Polym. Degrad. Stabil.* **1999,** *64*, 511-515.
167. Urgun-Demirtas, M.; Singh, D.; Pagilla, K. *Polym. Degrad. and Stabil.* **2007,** *92*, 1599-1610.
168. Cowan, M. M., Plant products as antimicrobial agents. *Clin. Microbiol. Rev.* **1999,** *12*, 564-582.
169. Thomson, W. A. R. (ed.), *Medicines from the Earth* ; McGraw-Hill Book Co.: Maidenhead, UK, 1978.
170. Stern, J. L.; Hagerman, A. E.; Steinberg, P. D.; Mason, P. K. *J. Chem. Ecol.* **1996,** *22*, 1877-1899.